

# **The role of lipid rafts in UVA radiation-induced signal transduction in human keratinocytes**

Inaugural-Dissertation

zur Erlangung des Doktorgrades  
der Mathematisch-Naturwissenschaftlichen Fakultät  
der Heinrich-Heine-Universität Düsseldorf



vorgelegt von

**Rehab Walli**

aus Tripoli-Libyen

Düsseldorf, Dezember 2009

Gedruckt mit der Genehmigung der  
Mathematisch-Naturwissenschaftlichen Fakultät der  
Heinrich-Heine-Universität Düsseldorf

Referent: Priv.-Doz. Dr.rer.nat. S. Grether-Beck  
Koreferent: Uni.-Prof. Dr.rer.nat.P. Proksch

Tag der mündlichen Prüfung:

## Acknowledgements

This Work was carried out at the Institute of Molecular preventive medicine research of Heinrich Heine University, Dusseldorf, under direction of Professor Jean Krutmann, during the years 2006-2009.

It was indeed the teamwork which helped me to finish my work and only the kind help of a number of people made it possible.

I would like to give my loads of thanks to all these people, particularly, my direct supervisor Mrs PD Dr. Susanne Grether-Beck, the head of the cell biology department. I am indebted for her productive criticism and valuable annotations during the preparation of this manuscript. I am also extremely thankful to her for keeping embarrassing mistakes in my thesis away from seeing the light of day.

I would also like to express my thanks to all the staff of the cell biology department especially Mrs Heidi Brenden, Miss Zippora Khone, Miss Katja Nehrenheim, and Mr Ingo Felsner for help, support, and encouragement during the years of study.

I wish to convey my sincere gratitude to Professor Jean Krutmann, for giving me the opportunity to be one member of his institute and for providing excellent research facilities.

My supervisor Professor Peter Proksch deserves my innermost gratitude for all the help, guidance, encouragement and support he has given me during these years. With his enormous amounts of kindness and patience he has gained my greatest approbation and uppermost respect.

I am really indebted to Mrs Angelika Simons at the doctorate office for the kind help and support during the study.

I would also like to thank all the staff of the Biochemistry department at the faculty of pharmacy and at the faculty of science at Al-Fateh University in Libya. My thanks also to Miss Dr. Asma Al-Najjar at the Agriculture faculty in Libya for her valued help.

I am greatly indebted to my father, for encouragement, and persistent support.

I would like to express my appreciation to my husband who has contributed to the success of this thesis through his loving support in thousand and one wonderful ways than a page can hold.

Rehab Walli  
Düsseldorf, 16.12.2009

**To my Teachers, from whom I continue to learn**

**To my Family for its support, encouragement, and love**

# Curriculum Vitae

## Personal data

Name: Rehab Walli  
Gender: Femal (Married, 1 child)  
Actual address: Auf'm Hennekamp Str. 46  
40225 Düsseldorf  
E-Mail address: Rehabwalli2003@yahoo.com  
Rehab.walli@Uni-deuesseldorf.de  
Date of birth: 03.03.1979  
Place of birth: Tripoli, Libya  
Nationality: Libyan

## Academic background

**03.2006 – 09.2009:** PhD student at the environmental medicine research institute, University of Dusseldorf, Germany. Project “UVA radiation signaling in human skin cells”

**10.2005 – 03.2006:** Attending the main pharmaceutical lectures at the faculty of pharmacy at the Dusseldorf University and successfully pass the admittance examinations to start the PhD study in pharmacy.

**11.2004 – 07.2005:** Learning the German language at the Goethe institute, Dusseldorf, including German language for Academic purposes.

**10.2001 – 10.2004:** Working as teaching assistant at the faculty of pharmacy at the University of Al-Fateh, Tripoli, Libya, department of Biochemistry and clinical Biochemistry.  
Part time pharmacist in a private pharmacy.

**10.2000 – 10.2001:** Bachelor’s Project “Diabetes Mellitus in Tripoli area: Prospective and Retrospective study” under the supervision of Prof. Dr. Mustafa Abugila at the department of Biochemistry and clinical Biochemistry, University of Al-Fateh, Tripoli, Libya.

**10.1996 – 10.2000:** Bachelor of Science (Excellent degree) in Pharmaceutical Science, University of Al-Fateh, Tripoli, Libya.

## **Publications**

### **Full research paper:**

Grether-Beck S, Salahshour-Fard M, Timmer A, Brenden H, Felsner I, **Walli R**, Füllekrug J, Krutmann J. Ceramide and raft signaling are linked with each other in UVA radiation-induced gene expression. *Oncogene*. 2008 Aug 14; 27(35):4768-78. Epub 2008 Apr 28

### **Poster presentation:**

Grether-Beck S, Brammertz D, Brenden H, Felsner I, **Walli R**, Füllekrug J, Krutmann J. The UVA response in keratinocytes depends on the ratio of cholesterol (Chol) versus ceramide (Cer) within membrane microdomains. Poster in the annual spring meeting, German Society for Biochemistry and Molecular Biology (GMB), Mosbach (Baden), March 29-31, 2007.

**Walli R**, Salahshour-Fard M, Kohne Z, Brenden H, Felsner I, Füllekrug J, Krutmann J, Grether-Beck S Further analysis of the UVA stress response in human keratinocytes reveals a crucial role for neuraminidase 3 induced ganglioside degradation. Poster in the 15<sup>th</sup> International Congress on Photobiology, Düsseldorf, June 18-23, 2009.

### **Additional Attended Conference:**

The 1<sup>st</sup> international Conference on Dermatotoxicology, Vaalsbroek, Netherlands, October 22-25, 2008.

## **Table of contents**

<b>Abbreviations.....</b>	<b>vii</b>
<b>List of Tables.....</b>	<b>x</b>
<b>List of Figures.....</b>	<b>xii</b>
<b>1. Introduction.....</b>	<b>1</b>
1.1. Structure and function of human skin.....	1
1.2. Effects of UV radiation on human skin.....	3
1.3. The barrier function of epidermis.....	5
1.4. Glycosphingolipids.....	8
1.4.1. The biosynthesis of glycosphingolipids.....	9
1.4.2. The catabolism of glycosphingolipids.....	11
1.5. The cell plasma membrane and lipid rafts.....	14
1.5.1. Plasma membrane-associated neuraminidase (Neu3).....	20
1.5.2. Localization of neuraminidase 3 in caveolae.....	23
1.6. State of the art.....	25
1.7. Aim and scopes of the study.....	27
<b>2. Materials and Methodes.....</b>	<b>28</b>
2.1. Chemicals.....	28
2.1.1. Generally used chemical.....	28
2.1.2. Chemicals used in cell culture.....	29
2.1.3. Pharmacological inhibitors used in this work.....	29
2.1.4. Equipments and materials .....	30
2.2. Cell culture.....	31
2.2.1. Cells and cell lines.....	31
2.2.1.1. Isolation of human keratinocytes from foreskin.....	31
2.2.1.2. Preparation of keratinocytes medium.....	32

2.2.1.3. Culturing of the human cell line HaCaT.....	32
2.2.1.4. Preparation of culture medium of HaCaT cells.....	33
2.2.3. Passaging cells.....	33
2.2.4. Cell culture conditions.....	33
2.2.5. Cryopreservation of cells.....	34
2.2.6. UVA irradiation.....	35
2.3. Preparation of cellular extracts.....	35
2.3.1. Preparation of whole cell extracts for lipid analysis by HPTLC.....	35
2.3.2. Preparation of whole cell extracts for western blot analysis.....	36
2.3.3. Preparation of lipid raft extracts for western blot analysis.....	36
2.3.4. Isolation of plasma membrane microdomains (Lipid rafts).....	37
2.3.5. Preparation of nuclear extracts for band shift assay.....	38
2.3.6. Preparation of cytosolic extracts.....	38
2.3.7. Isolation of cellular membranes fraction.....	39
2.4. Lipid analysis by HPTLC.....	40
2.4.1. Extraction of lipids with hydrolysis.....	40
2.4.2. Extraction of lipids with out hydrolysis.....	41
2.4.3. HPTLC analysis of lipids by AMD2 method from CAMAG.....	41
2.4.4. Plate preparation.....	41
2.4.5. Plate development with AMD2 technique.....	42
2.4.6. Postchromatic plate development and densitometry quantification of lipids...43	
2.5. SDS polyacrylamide gel electrophoresis (Western blot analysis).....	43
2.5.1. Separating protein sample by electrophoresis.....	44
2.5.2. Protein blotting.....	44
2.5.3. Membrane blocking.....	45



2.5.4. Immunological detection of proteins.....	45
2.5.5. Detection of membrane-bound protein by enhanced chemiluminescence (ECL).....	45
2.5.6. Western stripping.....	46
2.6. Identification of lipid rafts by western blot analysis.....	47
2.7. Gene expression analysis by real-time PCR.....	49
2.7.1. RNA isolation.....	49
2.7.2. cDNA-synthesis by RT-PCR.....	49
2.7.3. Quantification of gene expression via real-time PCR analysis.....	51
2.7.4. Determination of primer sequences for real-time PCR.....	54
2.8. Gel electrophoresis mobility shift assay.....	54
2.8.1. Radiolabelling of AP-2 oligonucleotide at 5' end.....	55
2.8.2. Purification of the radiolabelled.....	55
2.8.3. The binding reaction.....	56
2.8.4. Gel retardation electrophoresis.....	56
2.9. Enzymatic activity assay of the plasma membrane-associated neuraminidase (Neu3).....	57
2.10. Protein determination.....	60
2.10.1. Bradford test for quantification of protein.....	61
2.10.2. BCA protein assay.....	61
<b>3. Results.....</b>	<b>63</b>
3.1. UVA radiation leads to a decrease of ganglioside GM3 content in rafts and total cell extracts of human keratinocytes.....	64
3.1.1. UVA induced GM3 decrease is mediated by activation of neuraminidase 3..	65
3.1.2. Alteration of UVA radiation-induced neuraminidase 3 activity by modulation of cholesterol content and by vitamin E pretreatment.....	67
3.1.3. Inhibition of UVA radiation-induced neuraminidase 3 activity with 2-deoxy-2,3-didehydro- <i>N</i> -acetylneuraminic acid (DANA).....	69

3.1.4. Neuraminidase 3 activity partially contributes to UVA radiation-induced gene expression.....	71
3.1.5. UVA radiation-induced GM3 degradation correlates with formation of lactosylceramide and ceramide.....	72
3.2. Impact of caveolin-1 knock down on UVA radiation-induced gene expression.....	76
3.3. Role of caveolin-1 in ceramide-induced gene expression in human keratinocytes..	81
3.4. The link between Src kinase, caveolin-1 and neuraminidase 3 in UVA radiation-induced signal transduction.....	86
3.4.1. Role of Caveolin-1, Src kinase, and neuraminidase 3 in UVA radiation-induced AP-2 activation.....	92
3.4.2. Effects of cholesterol levels on UVA radiation-induced signal transduction..	93
<b>4. Discussion.....</b>	<b>98</b>
4.1. The role of lipid rafts in UVA radiation-induced signal transduction.....	98
4.2. UVA radiation leads to decrease of the ganglioside GM3 content in rafts and total cell extracts of human keratinocytes via activation of neuraminidase 3 enzyme.....	99
4.3. UVA radiation-induced GM3 degradation partially contributes to UVA radiation-induced ceramide formation .....	101
4.4. Neuraminidase 3 partially contributes to UVA radiation-induced gene expression.....	102
4.5. A link between caveolin-1 and neuraminidase 3 in UVA-induced gene expression.....	103
4.6. Role of caveolin-1 in ceramide-induced ICAM-1 expression.....	106
4.7. Cross-talk involving Src kinase, caveolin-1 and neuraminidase 3 in UVA radiation-induced signal transduction.....	109
<b>5. Summary.....</b>	<b>113</b>
<b>6. Reference list.....</b>	<b>114</b>

## Abbreviations

AMD	Automated multiple development
AP-2	Activator protein-2
bp	Base pair
BSA	Bovine serum albumin
BPE	Bovine pituitary extract
C6-Ceramide	N-hexanoyl-D- <i>erythro</i> -sphingosine
cDNS	Complementary deoxyribonucleic acid
Chol	Cholesterol
cpm	radioaktive decay per Minute (counts per minute)
Csk	C-terminale Src-Kinase
CO <sub>2</sub>	Carbon dioxide
DANA	2-Deoxy-2,3-didehydro-N-acetyl neuramnic acid
dd-H <sub>2</sub> O	Double-distilled water
D <sub>2</sub> (vitamin)	Ergocalciferol
D <sub>3</sub> (vitamin)	Cholecalciferol
DMEM	Dulbeccos modified eagle medium
DMSO	Dimethylsulfoxide
DNA	Deoxyribonucleic Acid
DTT	Dithiothreitol
EDTA	Ethylenediaminetetraacetic acid
EGF	Epidermal growth factor
EGFR	EGF-Receptor
ER	Endoplasmic reticulum
EtOH	Ethanol
FCS	Fetal calf serum
Gal	Galactose
GalNac	N-acetylgalactosamine
GAPDH	Glyceraldehyde-3-phosphate dehydrogenase
GEMSA	Gel electrophoresis mobility shift assay
Glc	Glucose
GM3	Neuraminic acid-5-Acetyl(2-3)beta-D-Galactosyl-p-(1-4)beta-D-Gulcosyl-p-(1-1')Ceramide
GM1	Beta-D-Galactosyl-p-(1-3)beta-D-Galactose-N-acetyl-[Neuraminic acide-5-Acetyl(2-3)]beta-D-Galactosyl-p-(1-4)beta-D-Glucosyl-p-(1-1')Ceramide

h	Hour
HPTLC	High Performance Thin Layer Chromotography
HRP	Horse Radish Peroxidase
H <sub>2</sub> O <sub>2</sub>	Hydrogen Peroxide
ICAM-1	Intercellular adhesion molecule-1
IC <sub>50</sub>	Inhibitor concentration producing 50% inhibition of the maximal enzyme velocity
J	Joule
kb	Kilobase
KCl	Potassium chloride
kDa	Kilodalton
K <sub>m</sub>	Substrate concentration producing half-maximal velocity (Michaelis constant)
L	Liter
LacCer	Lactosylceramide (C8 Lactosyl(β) Ceramide (d18:1/8:0) D-lactosyl-β-1,1' N-octanoyl-D- <i>erythro</i> -sphingosine)
ml	Milliliter
mRNA	Messenger ribonucleic acid
min	minutes
M	Molar
MeOH	Methanol
mA	Milliampere
mg	Microgram
MgCl <sub>2</sub>	Magnesium chloride
mJ	Milijoule
mM	Milimolar
nm	Nanometer
nMole	Nanomole
NADH	Reduced nicotinamide adenine dinucleotide
NADPH	Reduced nicotinamide adenine dinucleotide phosphate
Neu3	Neuraminidase3 (Plasma-membrane associated Neuraminidase)
OD	Optical density
O <sub>2</sub>	Molecular oxygen
O <sub>2</sub> <sup>-</sup>	Superoxide radical
O <sub>3</sub>	Ozone
PBS	Phosphate-buffered saline
Pmol	Picomol
RNA	Ribonucleic Acid

RNAi	RNA Interference
RNase	Ribonuclease
Ponceau S	3-Hydroxy-4-[2-sulfo-4(4-sulfophenylazo)phenylazo-]2,7-naphthalene disulfonic acid
ROS	Reactive Oxygen Species
Rpm	Rounds per minute
PP2	4-Amino-5-(4-chlorophenyl)-7-(t-butyl)pyrazolo[3,4- <i>d</i> ]pyrimidine
RT	Room Temperature
RT-PCR	Reverse transcription polymerase chain reaction
SC	Stratum corneum
SDS-PAGE	Sodium dodecyl sulfat-Polyacrylamid gel electrophoresis
Sec	Second
SH2	Src Homology 2 domain
SM	Sphingomyelin
TBS	Tris buffered saline
TE	Tris-EDTA
TEMED	N,N,N',N'-Tetramethylethylenediamin
Tris	Tris(hydroxymethyl)aminomethan
Tyr	L-Tyrosine
U	Unit
UV	Ultraviolet
UVA	Ultraviolet region 320-400nm
UVB	Ultraviolet region 280-320nm
UVC	Ultraviolet region 200-280nm
µg	Mikrograme
µl	Microliter
µM	Micromolar
(v/v)	Volume/volume
(w/v)	Weight/volume

## List of Tables

Table 1.1: Transmission of ultraviolet-radiation through the different layers of the human epidermis.....	5
Table 1.2: Comparison of four types of human neuraminidases.....	22
Table 1.3: Neuraminidase activity toward various substrates in the homogenate of COS-7 cells transfected with plasma membrane-associated sialidase (Neu3) cDNA.....	23
Table 2.1: List of generally used chemicals in this work.....	28
Table 2.2: List of chemicals used in cell culture.....	29
Table 2.3: List of pharmacological inhibitors used in this work.....	29
Table 2.4: List of equipments and materials used in this work.....	30
Table 2.5: Composition of keratinocyte cell culture medium.....	32
Table 2.6: Composition of HaCaT cell culture medium.....	33
Table 2.7: Composition of cell cryopreservation medium.....	34
Table 2.8: Composition of 2x Laemmli sample buffer.....	36
Table 2.9: Composition of TNE buffer.....	37
Table 2.10: Composition of buffers used for preparation of nuclear and cytosolic extracts....	39
Table 2.11: Composition of the lysis buffer used for cellular membranes extraction.....	40
Table 2.12: Composition of the standard used for lipid analysis.....	43
Table 2.13: Recipes for polyacrylamide separating and stacking gels.....	44
Table 2.14: Buffers used in western blot analysis.....	46
Table 2.15: Antibodies used in western blot analysis.....	46
Table 2.16: Composition of SYBR Green pre-mix.....	53
Table 2.17: RT-PCR program.....	53
Table 2.18: Sequences of the primer pairs for real time PCR.....	54
Table 2.19: Composition of the radiolabelling reaction.....	55
Table 2.20: Composition of STE buffer.....	55
Table 2.21: Composition of the binding reaction in EMSA.....	56

Table 2.22: Composition of 5x Ficoll-binding buffer.....	56
Table 2.23: Composition of Non-denaturing TBE-polyacrylamide.....	57
Table 2.24: List of the sources of the substance used in Neuraminidase assay.....	60
Table 3.1: Effect of UVA irradiation on Neu3 activity in total cell extracts prepared from human keratinocytes.....	66
Table 3.2: UVA radiation-induced Neu3 activities in rafts from HaCaT wild type and caveolin-1 knockdown cells.....	78
Table 3.3: Comparison of Neu3 activity in total cell extracts after stimulation with UVA, GM3, or C6-ceramide.....	85
Table 3.4: Molar ratio of sphingomyelin, cholesterol and ceramide in rafts under various conditions and relation to signaling events such as ceramide formation and ICAM-1 upregulation.....	96
Table 3.5: Molar ratio of sphingomyelin, cholesterol and ceramide in rafts after UVA treatment (n=4) and relation to signaling events such as ceramide formation and ICAM-1 upregulation in caveolin-1 knockdown cells.....	97

## List of Figures

Figure 1.1: Diagram of human skin structure, illustrating the principle layers of skin.....	1
Figure 1.2: Schematic diagram of the epidermis: the basal cells change, through differentiation, into flat horny skin cells that have lost their nuclei.....	2
Figure 1.3: Solar spectrum.....	4
Figure 1.4: Structure of the free ceramides of human stratum corneum.....	6
Figure 1.5: Schematic diagram of the epidermis.....	7
Figure 1.6: The de novo biosynthetic pathway for the ceramide backbone of complex sphingolipids.....	9
Figure 1.7: Scheme of ganglioside biosynthesis.....	11
Figure 1.8: Schematic view of the lysosomal degradation pathway of sphingolipids.....	12
Figure 1.9: The fluid mosaic model of the plasma membrane.....	14
Figure 1.10: The lipid rafts.....	15
Figure 1.11: Arrangement of „rafts“ and caveolae in the plasma membrane of eucaryotic cells .....	16
Figure 1.12: The caveolin scaffolding domain and caveolin-binding sequence motifs.....	17
Figure 1.13: The structure and regulation of human Src kinase.....	19
Figure 1.14: Removal of sialic acid residue from glycoconjugate by the action of sialidase...21	
Figure 1.15: Crystal structure of a bacterial neuraminidase shows the same folding pattern as the human neuraminidase.....	24
Figure 1.16: UVA radiation-induced signal transduction leading to gene expression in keratinocytes.....	26
Figure 1.17: UVA-induced signaling in keratinocytes.....	27
Figure 2.1: UV-Spectrum of UVA1 lamp from Sellamed system 2000.....	36
Figure 2.2: Universal gradient for lipid analysis by AMD2 method from CAMAG.....	42
Figure 2.3: Oxidation of luminol by Horseradish peroxidase/hydrogen peroxide in Enhanced chemiluminescence.....	45
Figure 2.4: Distribution of caveolin-1, flotillin-1, transferrin, and nucleoporin across OptiPrep gradient.....	48
Figure 2.5: Distribution of calnexin and GRASP65 receptor protein across OptiPrep gradient.....	49
Figure 2.6: Definition of Ct value.....	53



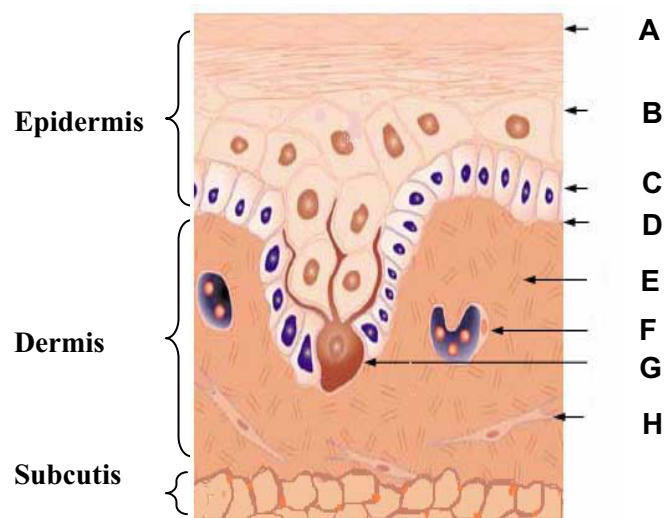
Figure 2.7: Compounds formed during the oxidation step of periodic acid/thiobarbituric acid assay.....	59
Figure 2.8: Chemical structure of Coomassie® Brilliant Blue G-250.....	61
Figure 2.9: Chemical structure of the chelation complex of two molecules of BCA with one cuprous ion.....	62
Figure 3.1: UVA radiation results in a decreased GM3 content in lipid rafts and in total cell extracts.....	64
Figure 3.2: Effect of UVA irradiation on Neu3 activity in total cellular membrane extract and rafts of HaCaT cells.....	67
Figure 3.3: Alteration of UVA radiation-induced Neu3 activity by modulating cholesterol level and by vitamin E pretreatment.....	68
Figure 3.4: Pretreatment with DANA inhibits UVA radiation-induced Neu3 activity in rafts of human keratinocytes.....	69
Figure 3.5: DANA inhibits UVA radiation-induced upregulation of Neu3 mRNA in human keratinocytes.....	70
Figure 3.6: DANA inhibits UVA radiation-induced upregulation of ICAM-1 mRNA expression.....	71
Figure 3.7: UVA radiation-induced GM3 degradation was inhibited by DANA Pretreatment.....	72
Figure 3.8: UVA radiation-induced formation of lactosylceramide.....	73
Figure 3.9: UVA radiation-induced ceramide formation is partially inhibited with DANA pretreatment.....	74
Figure 3.10: UVA radiation-induced GM1 degradation was not inhibited with DANA pretreatment.....	75
Figure 3.11: UVA irradiation results in a significant decrease of sphingomyelin in total extracts and in rafts.....	76
Figure 3.12: Impact of caveolin-1 knockdown on UVA radiation-induced gene expression...77	77
Figure 3.13: Impact of caveolin-1 knockdown on UVA radiation-induced Neu3 activity in human keratinocytes.....	78
Figure 3.14: Effect of caveolin-1 knockdown on UVA radiation-induced changes in lipid composition of human keratinocytes.....	80
Figure 3.15: Role of caveolin-1 knockdown in ceramide-induced ICAM-1 mRNA expression.....	82
Figure 3.16: Role of caveolin-1 in GM3-induced ICAM-1 mRNA expression.....	84

Figure 3.17: Role of Neu3 activity in UVA radiation-induced, ceramide-induced, and GM3-induced phosphorylation of Src kinase at Y416 and caveolin-1 at Y14.....	88
Figure 3.18: Role of caveolin-1 in UVA radiation-induced Src kinase activation.....	89
Figure 3.19: Effect of C6-ceramide, lactosylceramide and GM3 on Src kinase activation in caveolin-1 knockdown cells.....	90
Figure 3.20: Distribution of Src kinase across OptiPrep gradient in primary human keratinocytes.....	91
Figure 3.21: Role of Src kinase and caveolin-1 in UVA radiation-induced AP-2 activation...	92
Figure 3.22: Role of Neu3 in UVA radiation-induced AP-2 activation.....	93
Figure 3.23: Effect of cholesterol content on UVA radiation-induced and ceramide-induced caveolin-1 phosphorylation.....	94
Figure 3.24: Modulating cholesterol content affects UVA radiation-induced Src kinase activation.....	95
Figure 4.1: Chemical structure of some sialidase inhibitors.....	101

# 1. Introduction

## 1.1. Structure and function of human skin

The skin is the heaviest single organ in humans, accounting for about 16% of total body weight, in adults, presenting 1.2-2.3 m<sup>2</sup> of surface to the external environment. The outermost layer of the skin is a stratified epithelium, which protects the body towards the environment. Terrestrial organisms such as vertebrates are protected from dehydration due to evaporation. Moreover, the skin functions as a receptor organ in continuous communication with the environment (Junqueira & Carneiro 2005). Glands of the skin, blood vessels, and adipose tissue participate in thermoregulation, body metabolism, and the excretion of various substances. Skin is a potential organ of oxidative injury because it is continuously exposed to visible and ultraviolet irradiation and high oxygen concentrations and contains a variety of oxidizable structures critical for the maintenance of cellular homeostasis (Fuchs 1992). Vitamin D<sub>3</sub> is formed photochemically when 7-dehydrocholesterol reacts with ultraviolet B radiation in the epidermal layer. The human skin comprises three tissue layers (Figure 1.1): the epidermis, an epithelial layer of ectodermal origin, the underlying dermis, a layer of connective tissue of mesodermal origin and the subcutaneous fat layer (Junqueira & Carneiro 2005).



**Figure 1.1: Diagram of human skin structure, illustrating the principle layers of skin.** A: Cornified layer of keratinocytes (stratum corneum), B: Suprabasal keratinocytes, C: Basal layer of keratinocytes (stratum basale), D: Basement membrane, E: Collagen fibers in dermis, F: Capillary (enclosed by a single microvascular endothelial cell), G: Melanocyte, H: Dermal fibroblast (www.Eucerin.de).

The **subcutaneous tissue** (hypoderm) is a loose connective tissue that may contain a pad of adipose cells providing a mechanical cushion and a thermal barrier. It synthesizes and stores readily available high-energy molecules such as triglycerides.

The **dermis** is composed of the connective tissue that supports the epidermis and binds it to the subjacent subcutaneous layer. The dermis contains two layers, the thin papillary layer which is composed of loose connective tissue made mainly from fibroblasts, mast cells and macrophages and the thick reticular layer which is composed of irregular dense connective tissue and therefore has more fibers (mainly type I collagen) and fewer cells than the papillary layer. This elastic network is responsible for the elasticity of the skin.

The **epidermis** consists mainly of a stratified squamous keratinized epithelium. The keratinocyte is the major constituent of this tissue which also contains three less abundant cell types: melanocytes, Langerhans cells, and Merkel cells.

From the dermis outwards, the epidermis consists of five layers of keratin-producing keratinocytes (Figure 1.2).

**A. Stratum basal (Stratum germinativum):** This layer consists of a single layer of basophilic columnar or cuboidal cells resting on the basal lamina at dermal-epidermal junction. Desmosomes in great quantity join adjacent cells of this layer in their lateral and upper surfaces. The stratum basal is characterized by intense mitotic activity and is responsible, in conjunction with the initial portion of the next layer, for constant renewal of epidermal cells.

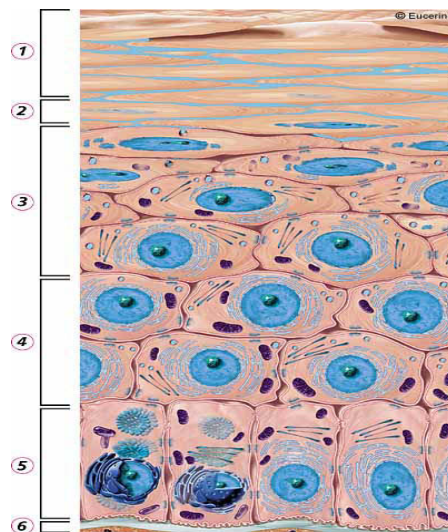


**Figure 1.2: Schematic diagram of the epidermis: the basal cells change, through differentiation, into flat horny skin cells that have lost their nuclei.** 1-Stratum corneum, 2-Stratum lucidum, 3-Stratum granulosum, 4-Stratum spinosum, 5-Stratum basale, and 6-Basal membrane (www.Eucerin.de).

**B. Stratum spinosum:** This layer consists of cuboidal, polygonal, or slightly flattened cells with a central nucleus. The cells of this layer are firmly bound together by the filament-filled cytoplasmic spines and desmosomes.

**C. Stratum granulosum:** This layer is characterized by three to five layers of flattened polygonal cells with the cytoplasm filled with coarse basophilic granules called keratohyalin granules.

**D. Stratum lucidum:** This layer is composed of translucent, thin, extremely flattened eosinophilic cells, where the organelles and nuclei are no longer evident, and the cytoplasm consists of densely packed filaments embedded in an electron-dense matrix. Desmosomes are still evident between adjacent cells.

**E. Stratum corneum:** This layer consists of 15-20 layers of flattened, non-nucleated keratinized cells whose cytoplasm is filled with a scleroprotein called keratin. The composition of this protein changes as epidermal cells differentiate. Basal cells contain polypeptides of lower molecular weight, while more differentiated cells synthesize the higher molecular weight polypeptides.

After keratinization, the cells consist of only fibrillar and amorphous proteins and thickened plasma membranes; they are called horny cells or corneocytes.

## 1.2. Effects of UV radiation on human skin

The solar radiation (Figure 1.3) reaching the surface of Earth is containing (i) UV radiation that makes up about 6.8 % of the electromagnetic radiation human skin is exposed to, (ii) visible light contributing about 38.9 % and (iii) infrared radiation accounting for about 54.3 % of total radiation (Kochevar *et al.* 1999; Schieke *et al.* 2003). UV radiation that reaches the Earth consists of short wavelength UVC (<280 nm), intermediate wavelength UVB (280-320 nm) and long wavelength UVA (320-400 nm). Oxygen formed by photosynthetic activity on Earth constitutes a very effective filter in the outer reaches of our atmosphere that absorbs the most energetic and therefore most harmful short-wave solar UVC radiation. In this process, oxygen molecules split up and recombine to form ozone. This ozone layer in the stratosphere in turn can also absorb UV radiation of higher wavelengths up to about 310 nm. Therefore, a part of the mid wavelength, mid energy UVB is absorbed and the remaining part can reach ground level to interact with human skin. In contrast, the long wavelength, low energy UVA (315-400 nm) completely passes the protective atmosphere (de Gruijl 2000; de Gruijl & van der Leun 2000). The exposure dose of UVB radiation on Earth constitutes about 1-10 % of total UV exposure (Matsui & Deleo 1995). The remaining 90 to 95 % are the long-wave UVA. Accordingly, the amount of UVA radiation reaching the Earth's surface is approximately 20 times greater than that of UVB radiation.

Over the last two decades evidence has been growing that UVA and UVB differ with regards to their effects on human skin. The mid wave UVB penetrates down only to the basal membrane, the deepest layer of the epidermis. UVB was shown to be the main cause

for sunburns (Coles *et al.* 1996), and, finally, the development of skin cancers such as basal cell carcinoma and squamous cell carcinoma (De Gruijl *et al.* 2001). UVB interacts with DNA leading to cyclobutane pyrimidine dimer formation (Ravanat *et al.* 2001).

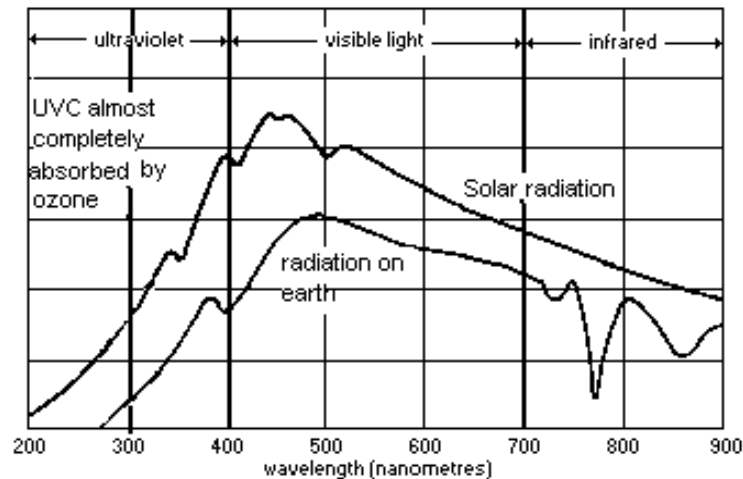


**Figure 1.3: Solar spectrum.** Solar optical radiation alteration by the earth's atmosphere (Environmental Health Criteria 160, WHO 1994).

In contrast, the long-wave UVA can deeply penetrate to the dermal compartments of the skin (Table 1.1). Here, UVA can induce oxidative stress (Tyrrell 1995) leading to oxidative DNA damage and premature aging also called photoaging of the skin (Krutmann 2000). Moreover, phototoxic and photoallergic reactions after UVA irradiation have been observed due to interactions with drugs, plant ingredients, sun screens or skin care products (Epstein 1983). Some epidemiological studies suggest a cause-effect relationship between UVA exposure and the induction of melanoma (Leiter & Garbe 2008). It is known that UV radiation is a potent inducer of oxidative stress leading to changes in gene expression in cells of human skin. The underlying photochemical and photobiological mechanisms are of general interest as UVA induced gene expression is thought to be relevant for photoaging, photocarcinogenesis, and the pathogenesis of the most frequent photodermatosis polymorphic light eruption (Krutmann 2000). Photoaged skin, whose general appearance is termed solar elastosis, is characterized by diffuse yellowish discoloration and deep wrinkles. Following UVA and UVB radiation, there is increased expression and activation of matrix metalloproteinases and other proteases responsible for the degradation of dermal connective tissue. Type I collagen, the main structural protein of dermis is drastically reduced in photoaged skin (Elsner *et al.* 2007).

**Table 1.1: Transmission of ultraviolet-radiation through the different layers of the human epidermis** (Bruls *et al.* 1984).

Transmission in %			
	UVB (290 nm)	UVA (365 nm)	VIS (546 nm)
<b>Stratum corneum</b>	14	64	80
<b>Epidermis</b>	0.27	19	48

Irradiation of cultured cells or human skin with physiological doses of UVA results in the formation of reactive oxygen species (ROS) (Tyrrell 1995; Beak *et al.* 2004). The formation of ROS has been attributed to enzymatic reactions e.g. plasma membrane localized NADPH oxidases after UVA and UVB exposure (Beak *et al.* 2004). Also, a direct formation of singlet oxygen and other reactive oxygen species by photochemical reactions from UVA irradiated lipids and other endogenous chromophores e.g. flavins or NADH / NADPH was observed (Baier *et al.* 2007). Singlet Oxygen ( $^1\text{O}_2$ ) mimics the induction of the expression of genes in human dermal fibroblasts by UVA and has been found to induce the expression of heme oxygenase-1 (HO-1), matrix metalloproteinase-1 (MMP-1), interleukin-6, and intercellular adhesion molecule-1 (ICAM-1) in human skin cells (Klotz *et al.* 1999).

### 1.3. The barrier function of epidermis

The role of the epidermis is to guard against infections, to prevent dehydration, and to undergo re-epithelialization after wound injuries. To accomplish these feats, the epidermis constantly replenishes itself by a process of homeostasis. During this process, dividing cells in the innermost (basal) layer continually execute a program of terminal differentiation, move outwards and are sloughed from the skin surface. The barrier function of the skin is permitted by the stratum corneum (Wertz & Bergh 1998). The average stratum corneum turnover time is about 14 days (Hoath & Leahy 2003).

The stratum corneum is composed of patterned lipid lamellae localized to the extracellular spaces between the corneocytes (Elias *et al.* 1977). Thin layer chromatographic analysis of the stratum corneum solvent extractable lipids reveals a lipid composition consisting of a roughly equimolar mixture of ceramides (40-45% by weight), cholesterol (25%), and fatty acids (10-15%) (Madison *et al.* 1990). Although cholesterol is the major sterol in stratum corneum, cholesterol sulfate is also present there. It is known that excess of cholesterol sulfate due to deficiency of cholesterol sulfatase inhibits corneocyte desquamation as in

ichthyosis (Madison 2003). The free fatty acids in the stratum corneum are predominantly straight chained, with 22 and 24 carbon chain length being the most abundant (Feingold 2007). Stratum corneum ceramides are a heterogeneous complex family of at least nine molecules (designed ceramides 1-9), consisting of sphingoid bases of different alkyl chain length amide-linked with different fatty acids (Figure 1.4). Variations in chain length, type and extent of hydroxylation, saturation etc. are responsible for this heterogeneity of the epidermal sphingolipids (Madison 2003; Wertz & Bergh 1998).

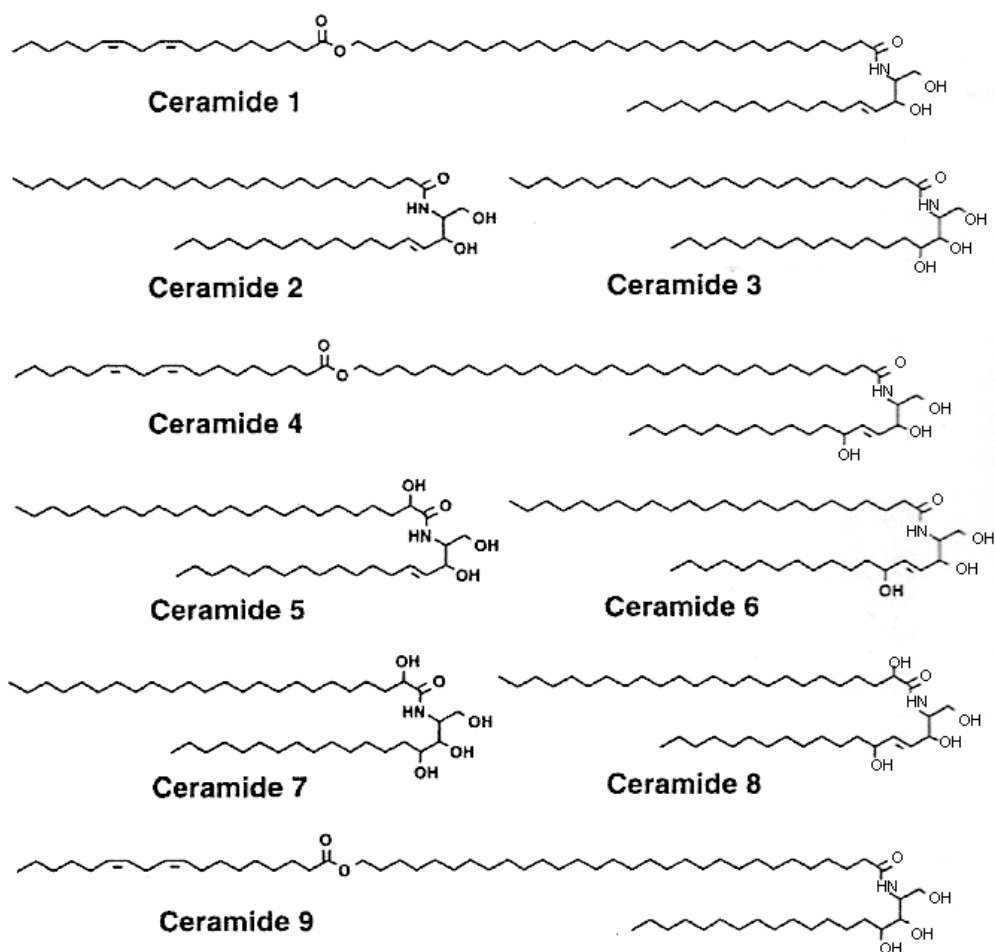


**Figure 1.4: Structure of the free ceramides of human stratum corneum.** Numbers 1 to 8 represent thin layer chromatographic mobility with ceramide 1 being the least polar and ceramide 8 the most polar. Ceramide 9 has a thin layer chromatographic mobility between ceramide 2 and ceramide 4 (Madison 2003).

Prior studies indicate that glucosylceramide and sphingomyelin are important precursors for stratum corneum ceramides (Holleran *et al.* 1993). During keratinocyte differentiation, glucosylceramide synthase is upregulated at the transcriptional level. Various studies indicated that  $\beta$ -glucocerebrosidase- and sphingomyelinase-dependent ceramide production from glucosylceramides and sphingomyelins, respectively, is important for epidermal permeability barrier homeostasis. All ceramide species, including  $\omega$ -hydroxy



fatty-acid-containing ceramides, are derived from glucosylceramide, and ceramide 2 and ceramide 5 may also originate from degradation of sphingomyelin. The importance of sphingomyelin-derived ceramide has been demonstrated in Niemann-Pick patients (acid sphingomyelinase deficiency) following acute barrier disruption. The recovery of barrier function following acute and chronic insults, including skin diseases such as atopic dermatitis, psoriasis, and ichthyosis, may require glucosylceramide and sphingomyelin dependent pathways to compensate the reduction in barrier lipids (Hamanaka *et al.* 2002). Each corneocyte has an approximately 10 nm thick tough peripheral protein envelope, called cornified envelope that is composed of several structural proteins, including involucrin and loricrin, cross-linked by sulfhydryl oxidases and transglutaminases. This envelope is connected to the keratin filaments that fill the intracellular compartment of corneocytes. The multiple layers of corneocytes in the stratum corneum contribute a tough and resilient framework of the intercellular lipid lamella. Lamellar granules are small organelles with a bounding membrane, most prominent in the granular cell layer of the epidermis. They contain stacks of lipid lamellae composed of phospholipids, cholesterol, and glucosylceramides that are precursors of the stratum corneum intercellular lipids. Late in epidermal differentiation, at the transition from granular cells to corneocytes, lamellar granules are thought to fuse with the plasma membrane of the granular cell and discharge their lipid membranes into the intercellular space (Figure 1.5).

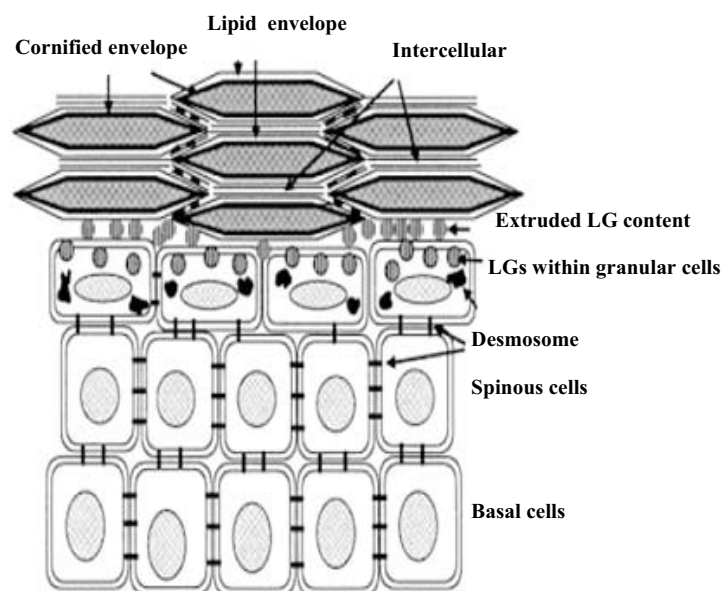


**Figure 1.5: Schematic diagram of the epidermis**, including the transformations of lipid structures that accompany epidermal differentiation, LG indicates lamellar granule (Madison 2003).

In addition to lipids, granular cells secrete a group of acid hydrolases such as  $\beta$ -glucocerebrosidases which degrade phospholipids and convert glucosylceramides to ceramides.  $\beta$ -glucocerebrosidase and an activator protein SAP-C, are required for liberation of ceramides from its precursors (Huwiler *et al.* 2000). Human patients with a complete deficiency of  $\beta$ -glucocerebrosidase, also known as Gaucher disease exhibit ichthyosiform dermatitis and die shortly after birth. Patients suffering from atopic dermatitis possess a markedly reduced content of ceramides (this was suggested due to increased sphingomyelin deacylase activity) in the horny layer of the epidermis which results in an impaired permeability barrier and leads to the characteristic dry and easily antigen-permeable skin of those patients (Madison 2003; Uchida *et al.* 2000). Lamellar granules secrete also acid sphingomyelinase and phospholipase A<sub>2</sub>. These enzymes are also important for the lipid barrier function of the stratum corneum.

More complex glycosphingolipids such as gangliosides, particularly GM3 play a role in many disorders of epidermal hyperproliferation including psoriasis and squamous cell carcinoma (Paller *et al.* 1993). The total amount of epidermal gangliosides is approximately 0.1  $\mu\text{g}/\text{mg}$  dry weight (0.1% of lipids in epidermis). GM3 is the predominant ganglioside of isolated epidermis from all body locations. GM2 and GD3 were also found in significant amount (Paller *et al.* 1992).

Ganglioside content in basal cell carcinomas is markedly increased with regards to overall ganglioside content as compared to normal tissue.

#### **1.4. Glycosphingolipids**

Glycosphingolipids are present on all mammalian cellular plasma membranes. These are amphipathic molecules consisting of a ceramide lipid anchor linked to an oligosaccharide chain of variable length and composition (Sandhoff & Kolter 2003). Glycosphingolipids are classified in different series according to their saccharide portion. In neutral glycosphingolipids this portion may contain glucose, galactose, N-acetylgalactosamine, N-acetylglucosamine or fucose. The term cerebroside is referred to neutral glycosphingolipids containing only galactose or glucose residues. Galactosylceramide is the principal glycosphingolipid in brain amounting 2% of the dry weight of grey matter and 12% of white matter. Glucosylceramides are rare in most tissues but serve as precursor for lactosylceramides and hence most of the complex neutral glycosphingolipids (Proia 2003). In contrast to skin, glucosylceramides are the major constituents of skin lipids.

In acidic glycosphingolipids the saccharide core can be linked to sulfate (sulfatides) or to one or more sialic acid residues (gangliosides). The most widely distributed glycosphingolipids including complex neutral gangliosides contain glucosylceramide as a core structure (Masserini & Ravasi 2001). GM3, a mono-sialylated ganglioside is predominant in the membrane of normal keratinocytes. 65% of the gangliosides found in keratinocyte membranes *in vivo* represent GM3 (Paller *et al.* 1993). Ganglioside mediated signal transduction is based on a non random distribution of glycosyl epitopes and corresponding signal transducing proteins in special microdomains (Hakomori 2000).

#### 1.4.1. The biosynthesis of glycosphingolipids

The biosynthesis of glycosphingolipids takes place in the endoplasmatic reticulum (ER) and in the Golgi complex. It is mediated by membrane bound glycosyltransferases and sialyltransferases, which catalyze the transfer of sugar nucleotide donors to sphingolipid acceptors (d'Azzo *et al.* 2006). *De novo* biosynthesis of the glycosphingolipids occurs at the membrane of the ER with the formation of ceramide (Figure 1.6).

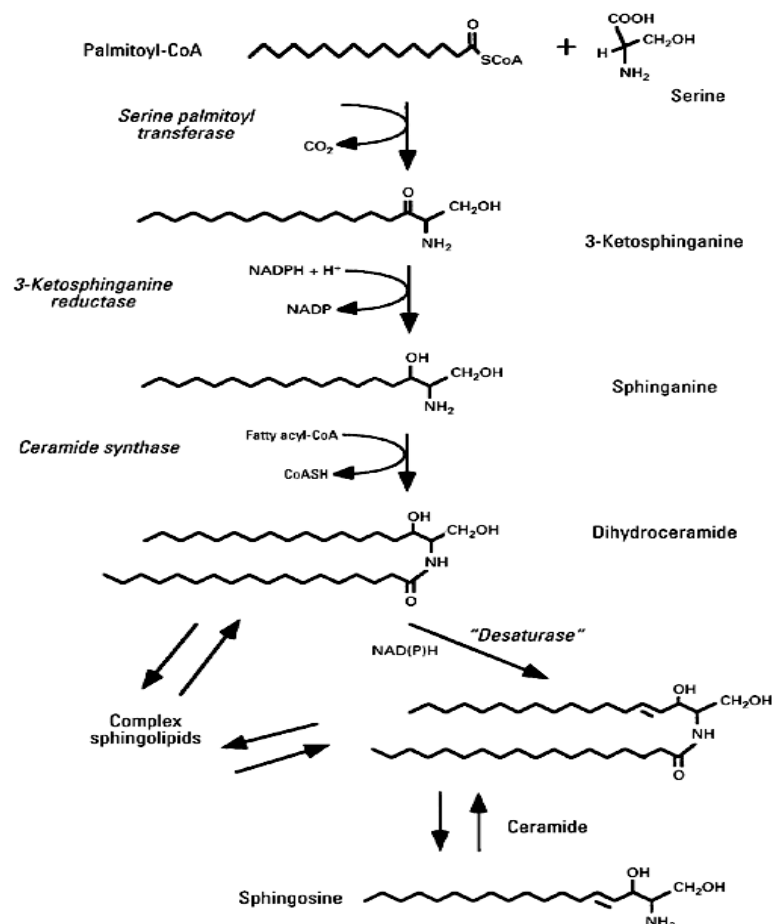


**Figure 1.6: The *de novo* biosynthetic pathway for the ceramide backbone of complex sphingolipids (Merrill *et al.* 2001).**

The condensation of the amino acid L-serine with palmitoyl-coenzyme A to 3-ketosphinganine is catalyzed by the enzyme serine palmitoyl transferase. 3-ketosphinganine is reduced to *D-erythro*-sphinganine by 3-ketosphinganine reductase. Sphinganine is subsequently acylated to dihydroceramide by a ceramide synthase. In the following ceramide desaturase catalysed reaction, dihydroceramide is desaturated to ceramide. Ceramide is also the common precursor of sphingomyelin biosynthesis which occurs in the Golgi apparatus. It is formed by transfer of phosphorylcholine, on the 1-hydroxyl group of ceramide (Sandhoff & Kolter 2003).

For the synthesis of glycosphingolipids, a glucose residue is  $\beta$ -glycosidically linked to the 1-position of ceramide in a reaction catalyzed by glucosylceramide transferase. From the Golgi apparatus glucosylceramide can reach the plasma membrane by direct transport or it can be further modified by additional glycosylation steps in the Golgi apparatus. Lactosylceramide is formed by addition of a galactose residue to glucosylceramide catalyzed by galactosyltransferase I (Sandhoff & Kolter 2003).

Gangliosides are structurally and biosynthetically derived from lactosylceramide. The transferases that catalyze the first steps in ganglioside biosynthesis show high specificity towards their glycolipid substrate, that is the formation of lactosylceramide, GM3, and GD3 (Figure 1.7). The relative amounts of these glycolipids in the steady state seem to determine the amount of 0-series glycolipids, which are derived only from lactosylceramide, a-series gangliosides which are derived from ganglioside GM3, and b-series ganglioside which are derived from gangliosides GD3. Interestingly, the stepwise glycosylation of these precursors is performed by only a few glycosyl transferases of limited specificity. Like on an assembly line, they transfer carbohydrate and sialic acid residues to glycosyl acceptors that differ only in the number of sialic acid residues bound to the inner galactose. Sialyltransferases I and II are much more specific for their glycolipid substrates than sialyltransferase IV and V (Sandhoff & Kolter 2003).

Two enzymes accept lactosylceramide as substrate: sialyltransferase I which forms ganglioside GM3 and GalNAc-transferase (*N*-acetylgalactosaminyl transferase) that forms glycolipid GA2. Owing to the different enzyme-kinetic constants, much more GM3 is formed than GA2. In addition, galactosyltransferase II and GalNAc transferase form a functional enzyme complex that accepts GM3 and finally releases GM1 (Sandhoff & Kolter 2003).

During ontogenesis and cell transformation a correlation between the glycosphingolipid expression and the activity of glycosyltransferases has been observed. Therefore, control

of the glycosyltransferases possibly at the transcription level appears to be a significant regulation point. Moreover, feedback control of several glycosyltransferases either by their respective reaction product or by an end product of the respective ganglioside series has been observed in vitro (Sandhoff & Kolter 2003).

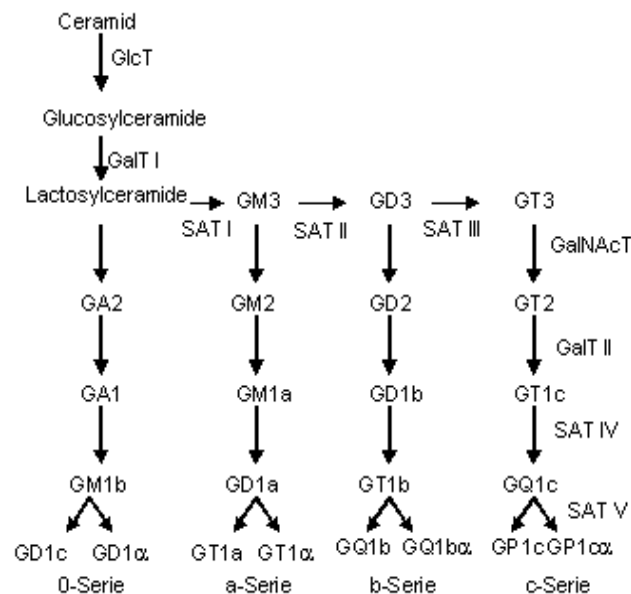


**Figure 1.7: Scheme of ganglioside biosynthesis.** Major gangliosides occurring on neurons in adult mammalian brain are indicated. The enzymes included in this scheme are: GlcT: Glucosyl transferases, GalT: Galactosyltransferases, SAT: Sialyltransferases, GalNAcT: *N*-acetylgalactosaminyl transferases (Kolter *et al.* 2002).

#### 1.4.2. The catabolism of glycosphingolipids

The common way of ganglioside degradation occurs along the endocytic-lysosomal pathway and is controlled by hydrolytic enzymes that function at acidic pH. Plasma membrane gangliosides are internalized and transported in endocytic vesicles to the lysosomes. After endosome-lysosome fusion, gangliosides expose their glycan chains to the luminal face of the lysosome. Initially, a lysosomal neuraminidase converts multisialogangliosides into monosialogangliosides. The enzyme  $\beta$ -galactosidase then removes the  $\beta$ -galactosyl moiety from GM1, thereby giving rise to GM2; and  $\beta$ -*N*-acetylhexosaminidase cleaves the *N*-acetyl galactose residue from GM2 to generate GM3. GM3 is degraded to lactosylceramide by neuraminidase removing the terminal sialic acid residue. Through sequential actions of  $\beta$ -galactosidase and  $\beta$ -glucosidase, lactosylceramide is decomposed to ceramide, and ceramide is further degraded by ceramidase into sphingosine and fatty acids (Figure 1.8).

Under physiological conditions and at steady-state levels, pools of gangliosides are present in different subcellular compartments. Modulation of their concentration at those sites strictly depends on the coordinated regulation of the biosynthetic, degradative, and salvage/recycling pathways.

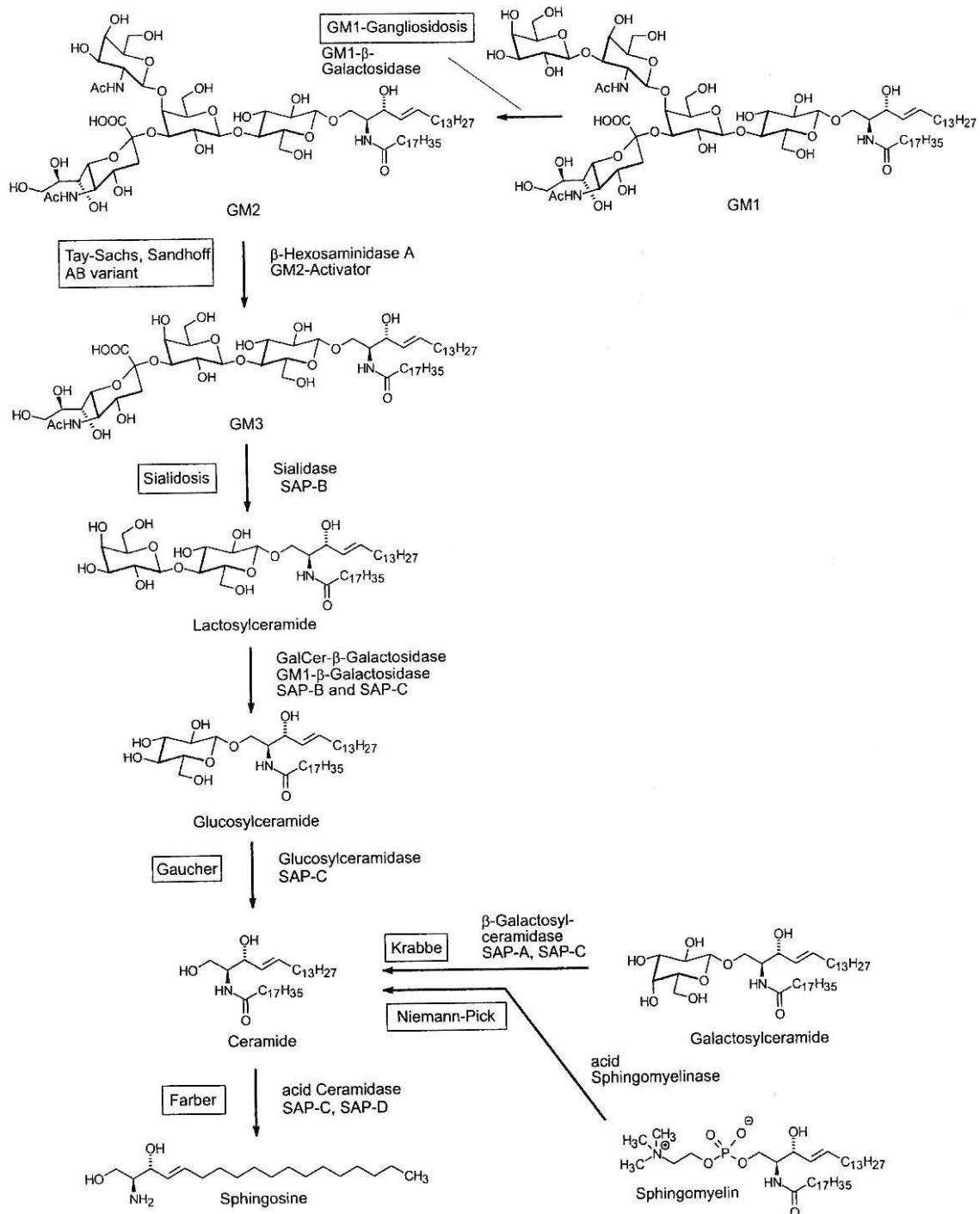


**Figure 1.8: Schematic view of the lysosomal degradation pathway of sphingolipids.** Several inherited sphingolipids storage diseases have been identified presenting defects of the lysosomal degradation pathway of sphingolipids. The names of the diseases are indicated in boxes (Huwiler *et al.* 2000).

The degradation of glycosphingolipids occurs in a stepwise fashion. Every catabolic enzyme in this pathway can be associated with a disease caused by its deficiency. The names of the diseases are indicated within boxes in Figure 1.8.

The lysosomal storage diseases are a group of relatively rare human disorders that are severe in nature and frequently fatal as many of them involve progressive neurodegeneration.

Within the lysosomal storage diseases is a subgroup of biochemically related disorders in which the enzymes required for the catabolism of glycosphingolipids are defective. The accumulated glycosphingolipids form pathological storage bodies in the cells resulting in an increased number and size of lysosomes. It is the storage of the glycosphingolipids that leads to the disease-specific pathologies associated with these disorders. These diseases are a result of mutations in the genes that encode the enzymes required for glycolipid metabolism within lysosomes (Platt & Butters 1998). The therapeutic options for treating these diseases are limited, and for the majority of these disorders there are currently no therapies available. To date most research has focused on correcting the genetic lesion by gene therapy or by augmenting the enzyme activity deficient in these patients by introducing fully functional enzyme. This can be achieved by bone marrow transplantation or intravenous infusion of purified or recombinant enzyme (enzyme replacement). Gene therapy and enzyme replacement therapy are disease specific (Platt & Butters 1998).

Besides the typical biosynthetic and degradative pathways, specialized glycosidases can modify gangliosides at the plasma membrane; gangliosides can be directly recycled to plasma membranes from early endosomes, they can be sorted to the Golgi apparatus from endosomes and subsequently reglycosylated, or they can be fully degraded in lysosomes and reused in the so-called salvage pathway. In the latter process, degradative products leave the lysosomes and are reused for the biosynthesis of new glycosphingolipids.

Neuraminidases play a role in glycosphingolipids degradation. They will be discussed in detail under section 1.5.1.

#### 1.4. The cell plasma membrane and lipid rafts

Our view of the cell membranes has changed from the original fluid mosaic model (Singer & Nicolson 1972) which suggested a random distribution of proteins and lipids across the two bilayer of the membrane (Figure 1.9) to the recent model where membranes are compartmentalized into various microdomains due to an uneven distribution of specific lipids and proteins (Masserini & Ravasi 2001).

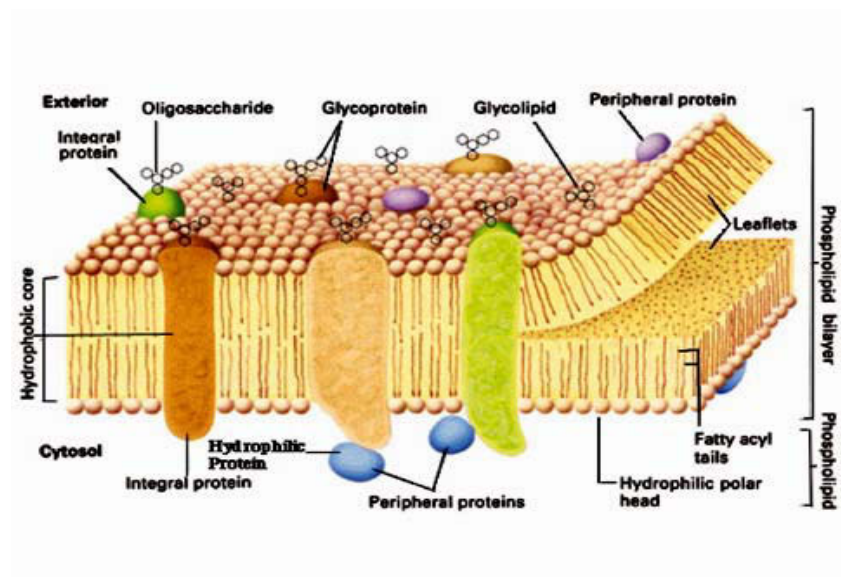
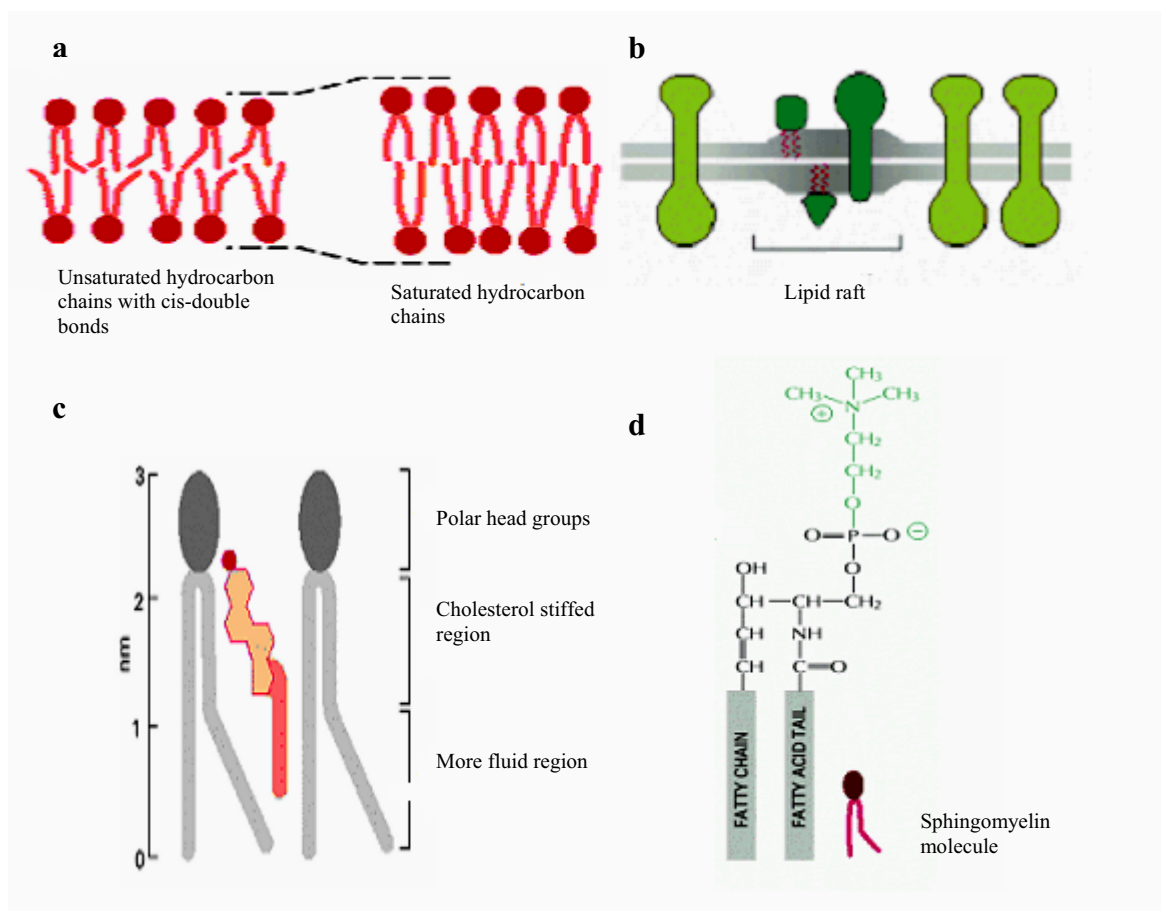


Figure 1.9: The fluid mosaic model of the plasma membrane.

About 50% of the mass of most animal cell membrane is lipid. All of the lipid molecules in cell membranes are amphipathic (that have a polar end and non-polar end). This property of lipids causes them to form bilayer spontaneously in aqueous environment. The most abundant membrane lipids are the phospholipids. However, the cell membrane contains also cholesterol and glycolipids (Alberts *et al.* 2002). Sphingolipids are composed of a hydrophobic moiety, known as ceramide, linked to a polar head constituted either by a phosphorylcholine in sphingomyelin or by carbohydrates such as glucose or galactose in glycosphingolipids. The ceramide portion is formed by a long chain base e.g. sphingosine linked to a fatty acid. Biochemical information about lipid asymmetry of the plasma membrane indicates that both sphingomyelin and glycosphingolipids are localized within the exoplasmic leaflet of the bilayer. Phosphatidylethanolamine and phosphatidylserine are suggested to localize at the cytoplasmic leaflet of the bilayer. Phospholipids that contain unsaturated acyl chains of variable length tend to exist in membranes in a liquid crystalline state in which the acyl chains are fluid and disordered. In contrast, sphingolipids with long saturated acyl chains are capable of packing tightly together to form a gel phase (Pike 2004). Cholesterol molecules orient themselves in the bilayer with



their hydroxyl groups close to the polar head groups of the phospholipid molecules (Figure 1.10c and 1.10d). In this position, their rigid steroid rings interact with those regions of the hydrocarbon chain closest to the polar head groups. By decreasing the mobility of the hydrocarbon chain of the phospholipid molecules, cholesterol stabilizes the lipid bilayer in this region. The plasma membrane of animal cell is thought to contain many microdomains. Because the hydrocarbon chains of the lipids concentrated in these microdomains are longer and straighter than the fatty acid chains of the most membrane lipids, these domains are thicker than other parts of the bilayer and can better accommodate certain membrane proteins (Figure 1.10a and 1.10b).



**Figure 1.10: The lipid rafts.** (a) the influence of cis-double bonds in hydrocarbon chains, because the fatty acid chains of unsaturated lipids are more spread apart, lipid bilayers containing them are thinner than bilayers formed exclusively from saturated lipids. (b) lipid rafts are small, specialized areas in membranes where sphingolipids and cholesterol are concentrated, because the bilayer is thicker in the rafts, certain membrane proteins accumulate. (c) cholesterol molecule interacting with two phospholipids molecules. (d) polar head group and the non polar tail group of sphingomyelin molecule (Alberts *et al.* 2002).

One subtype of membrane microdomains represent lipid-enriched microdomains, lipid rafts, which are capable of forming platforms. Lipid rafts play a central role in many cellular processes, including membrane sorting and trafficking, cell polarization, and signal transduction processes. Lipid rafts are small structures enriched in cholesterol and

sphingolipids where associated proteins are likely to be concentrated (Simons & Ikonen 1997).

Two morphological subsets of lipid rafts have been identified: caveolae and noncaveolae lipid rafts (Li & Gulbins 2007). Caveolae are small surface invaginations (Figure 1.11) seen in many cell types including human keratinocytes and adipocytes (Gniadecki *et al.* 2002).

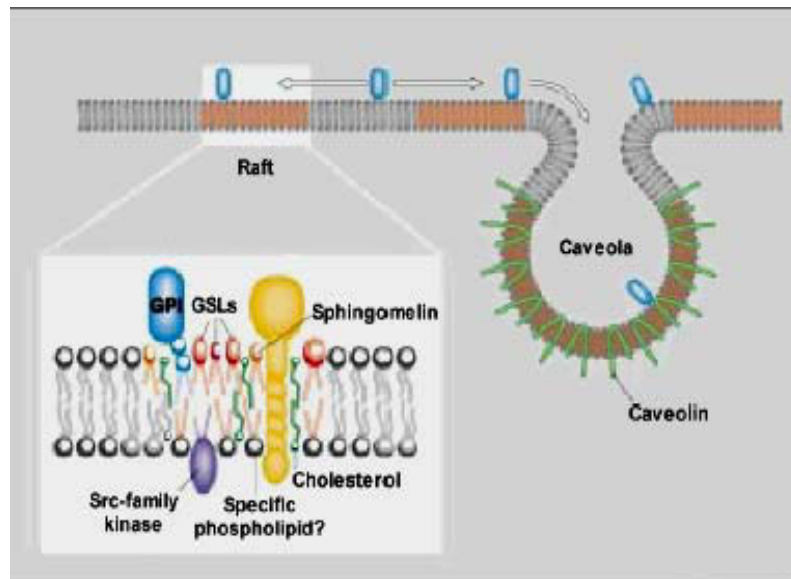


**Figure 1.11:**Arrangement of „ rafts“ and caveolae in the plasma membrane of eucaryotic cells (Hooper 1998).

Caveolar invagination is driven by polymerization of caveolins (Simons & Ehehalt 2002). Caveolins are a family of 3 different 21- to 25-KDa integral membrane proteins. Caveolin-1 and caveolin-2 are ubiquitously expressed, while the expression of caveolin-3 is restricted to muscle (Smart *et al.* 1999). Caveolins are raft-associated proteins, they interact with other membrane proteins and recruit specific cytosolic proteins to caveolae through their scaffolding domain (Couet *et al.* 1997b; Sargiacomo *et al.* 1995) (Figure 1.12). Caveolin-1 contains a central 33-amino acid hydrophobic stretch (amino acids 102-135) localized directly behind the scaffolding domain representing a membrane segment (see section 4.7).

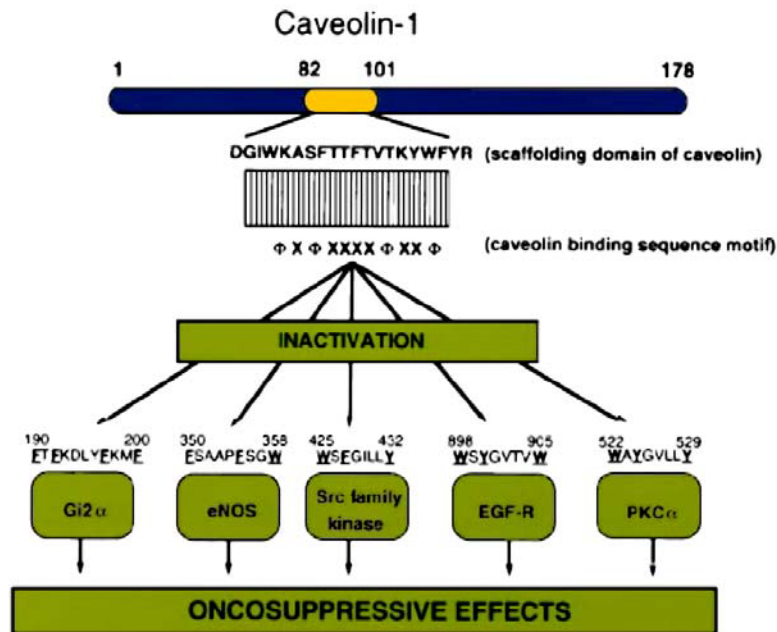


**Figure 1.12:** The caveolin scaffolding domain and caveolin-binding sequence motifs (Okamoto *et al.* 1998).

Both N- and C-terminal domains face the cytoplasm. In addition, both the N- and C-terminal domains undergo cytoplasmic modifications: the N-terminus is tyrosine phosphorylated by Src kinase on Tyr 14 and several cysteines within the C-terminal domain are S-acylated by palmitoylation (Smart *et al.* 1999).

Caveolae usually remain attached to the cell surface, but they can be endocytosed e.g. after infection with Simian virus-40 (Norkin & Kuksin 2005)

The recent identification of the primary protein constituent of caveolae, caveolin-1, has provided a reasonable biochemical marker for establishing the putative presence of actual caveolae. It is now clear that membrane domains with physical characteristics of a liquid-ordered phase can also be isolated from numerous cell types which lack caveolae and have a small size (10-200 nm). These domains are enriched with glycosphingolipids, cholesterol, sphingolipids and lipid-modified signaling molecules. Non-caveolar lipid rafts express the structural protein flotillins, also called cavatellins. Flotillins are considered as protein markers for the non-caveolar domains that are observed in certain cells that fail to express caveolins (Smart *et al.* 1999). Moreover, caveolae and non-caveolar domains may exist together in the same cell and have distinct roles in processing surface-bound ligands (Schnitzer *et al.* 1995) or sphingolipid signal transduction (Dobrowsky 2000; Iwabuchi *et al.* 1998). Non-caveolar domains are present in all cell types (Smart *et al.* 1999). There is a strong suggestion that non-caveolar domains serve as precursors for proper insertion of caveolins into membrane (Brown & London 1998). Thus, in cells that express caveolin,

these domains may represent precaveolae that simply lack caveolins. Insertion of caveolins into these domains occurs only at late phase of caveolae formation. Insertion of caveolins may provide a necessary brake in signal transduction (Okamoto *et al.* 1998).

Membrane proteins are assigned to three categories: (i) proteins that are mainly found in rafts, (ii) proteins that are present in the liquid-disordered phase (i.e. in non rafts) and (iii) intermediate proteins which move in and out of rafts (Simons & Ehehalt 2002). Constitutive raft proteins include glycosylphosphatidylinositol-anchored (GPI-anchored) proteins, doubly acylated proteins such as tyrosine kinases of the Src family, G $\alpha$  subunits of heterotrimeric G proteins, and endothelial nitric oxide synthase (eNOS); cholesterol linked and palmitate-anchored proteins like Hedgehog and transmembrane proteins e.g. influenza virus hemagglutinin and  $\beta$ -secretase. A peripheral membrane protein such as a non receptor tyrosine kinase e.g. Src kinase family can be reversibly palmitoylated and can lose its raft association depending on the status of lipid modification. Src family kinases are 52-62 KDa proteins composed of distinct functional regions (Figure 1.13): (a) the Src homology (SH4) domain, (b) the unique region, (c) the SH3 domain, (d) the SH2 domain, (e) the catalytic domain (SH1), and (f) a short negative regulatory tail. The N-terminal SH4 domain contains a 15-amino acid sequence with a glycine at position 2 for covalent linkage to myristic acid allowing membrane insertion. The SH3 and SH2 domain are two peptide binding modules involved in regulation the kinase. Intramolecular interactions of SH3- and SH2 domain stabilize the inactive conformation of Src kinases. Both domains lie on the side of the kinase domain opposite the catalytic cleft (Figure 1.13). The initially described phosphorylation sites include an activating phosphotyrosine 416 resulting from autophosphorylation and an inhibiting phosphotyrosine 527 resulting from phosphorylation by C-terminal Src kinase (Csk) and Csk homologous kinase.

In the inactive state, the SH2 domain interacts with phosphotyrosine 527 localized in the linker region between the SH2 and the kinase region and SH3 is bound to an internal peptide in a way that distorts the active site of the enzyme and helps to render it inactive. Turning the kinase on involves at least two specific inputs: removal of the inhibitory phosphate C-terminal phosphate at Y527 and the binding of SH3 domain by a specific activating protein. Phosphorylation of tyrosine 527 keeps the Src kinase in a closed, inactive form. The autophosphorylation site at tyrosine 416 within the catalytic domain is often involved in Src kinase activation in response to a single stimulus. This phosphorylation is predicted to permit sequences in the N-terminal lobe to orient properly and allow the kinase to adopt an active conformation.

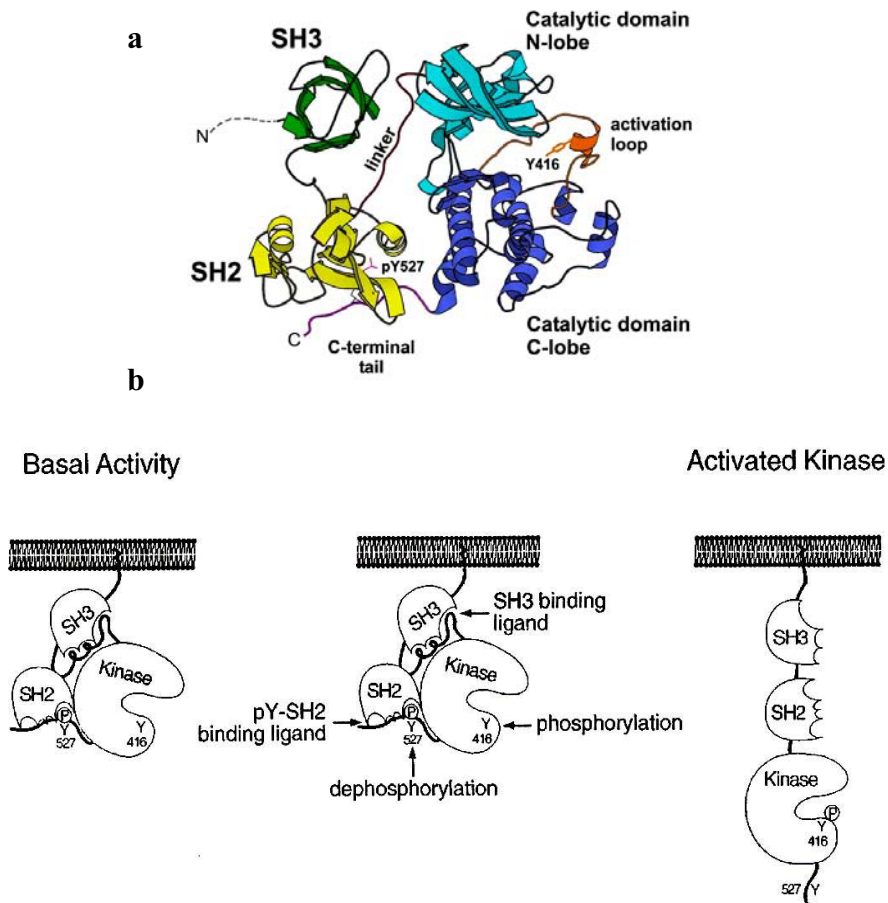


**Figure 1.13: The structure and regulation of human Src kinase.** (a) structure of Src kinase ([www.hxms.neu.edu/research/srcfam.html](http://www.hxms.neu.edu/research/srcfam.html)). (b) mechanisms involved in activation of Src kinases. The left panel shows the inactivated Src kinase that is phosphorylated on the C-terminal tyrosine (Y527) based on the crystal structure of Src kinase (Sicheri & Kuriyan 1997). The middle panel shows possible mechanisms involved in the activation of Src kinase. Y416 represents the autophosphorylation site in the activation loop of Src kinase. The right panel represents a model for the activated state of Src kinase in which the intermolecular interactions of the SH3 and SH2 domains are disrupted (Thomas & Brugge 1997).

Src family kinases are enriched in rafts due to N-terminal myristoylation and formation of complexes with caveolin. Palmitoylation of caveolin-1 at Cys 156 is essential for Caveolin/Src kinase interaction. Caveolin-1 prefers the inactive conformation of Src kinase. Caveolin-1, due to its direct interaction via the caveolin scaffolding domain (also see chapter 4, section 4.7), suppresses the activity of Src kinase (Li *et al.* 1996). Phosphorylation of caveolin-1 leads to Src kinase translocation into caveolae. This may induce a feedback loop that leads to inactivation of the Src kinases enriched in caveolae (Cao *et al.* 2002). Tyrosine phosphorylated caveolin-1 (Tyr 14) facilitates recruitment of SH2 domain containing proteins. Caveolin-1 mediates the association of other proteins with Src kinases (Patel *et al.* 2008).

### 1.5.1. Plasma membrane-associated neuraminidase (Neu3)

Neuraminidases (*N*-acylneuraminosyl glycohydrolase), also known as sialidases, are a family of exoglycosidases that catalyze the hydrolytic cleavage of non-reducing sialic acid (*N*-acetylneuraminic acid) residues ketosidically linked to mono- or oligosaccharide chains of glycoconjugates (Figure 1.14). Neuraminidases catalyze the removal of sialic acid from glycoproteins and glycolipids. They are widely distributed in nature, from viruses, and microorganisms such as bacteria and fungi to mammalian species. In mammals, these enzymes have been proven to be involved in several cellular phenomena, including cell proliferation, differentiation, membrane function, and antigen masking (Monti *et al.* 2002), whereas, in microorganisms the same enzymes appear to play roles limited to nutrition and pathogenesis. The most commonly known neuraminidase is the viral neuraminidase, a drug target for prevention of influenza infection. Viral neuraminidase activity is essential for viral release. The unsaturated sialic acid derivative 2-deoxy-2,3-didehydro-*D*-*N*-acetylneuraminic acid (DANA), a sialosyl cation transition-state analogue (Figure 1.14), was the first neuraminidase inhibitor described by Mindel and Tuppy (Mindel and Tuppy 1969). DANA has been recognized as a potent inhibitor of various neuraminidases of pathophysiological importance e.g. in viral and bacterial infections (e.g. caries and periodontitis, or gas oedema). Application of this compound for medical use (*in vivo*) was not possible, although it was effective in cell culture due to its rapid excretion after oral and intravenous administration (Nöhle *et al.* 1982). Many DANA-based compounds have been synthesized and tested so far for their potential to inhibit influenza virus neuraminidase (Smith *et al.* 2001). The synthesis of these antiviral drugs was based on rational computer-assisted design using the crystal structure of influenza virus neuraminidase. These compounds include 4-guanidino-2-deoxy-2,3-didehydro-*N*-acetylneuraminic acid (Zanamivir) (see also chapter 4). Zanamivir is a more potent inhibitor of influenza neuraminidase than DANA and does not inhibit human neuraminidases (Woods *et al.* 1993).

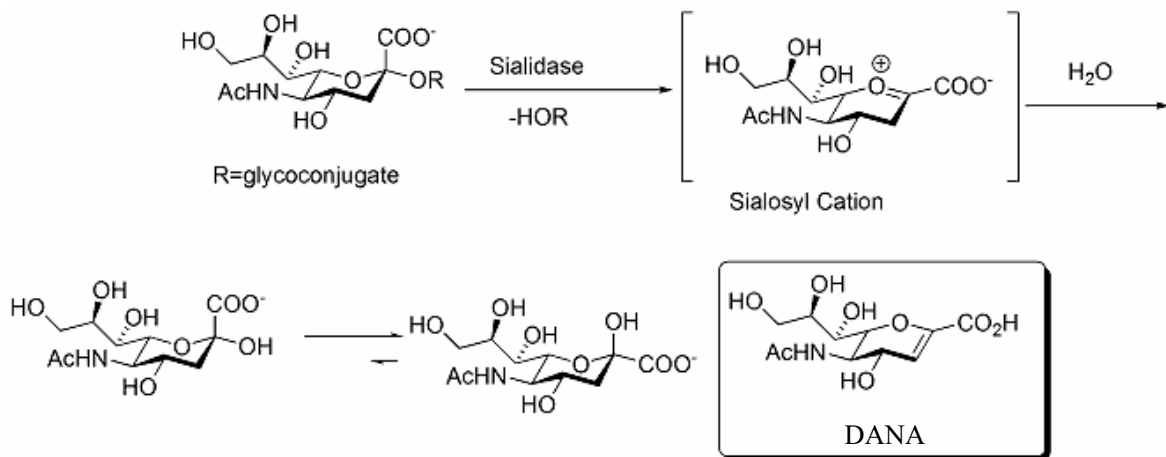


**Figure 1.14: Removal of sialic acid residue from glycoconjugate by the action of sialidase.** Depicted in box is the structure of the classical sialidase inhibitor 2-deoxy-2,3-didehydro-D-N-acetylneuraminic acid (DANA), which is a transition-state analogue inhibitor of sialidase activity (<http://en.wikipedia.org/wiki/File>).

Four types of mammalian neuraminidases have been cloned and identified to date and designated as Neu1, Neu2, Neu3, and Neu4 (Miyagi *et al.* 2008b). They differ in their subcellular localization and enzymatic properties, as well as in the chromosomal location, and are expressed in a tissue-specific manner. Neu1 is abundant in pancreas, Neu2 is generally present at very poor level, the protein was detectable in skeletal muscle, Neu3 and Neu4 are ubiquitous in all human tissues, in both adult and fetal tissues (Monti *et al.* 2002). Neu1 is localized predominantly in the lysosomes as well as on the plasma membrane, hydrolyzes preferentially oligosaccharides and glycopeptides but poorly gangliosides, and present as a high molecular weight multienzyme complex with the protective protein/cathepsin A and  $\beta$ -galactosidase. Many mutations in the NEU1 gene have been identified in sialidosis patients (Monti *et al.* 2002). Neu2 and Neu4 can act on gangliosides as well as oligosaccharides and glycoproteins at nearly neutral pH and acidic pH, respectively. Neu4 has been suggested to exist in lysosomes and mitochondria (Miyagi *et al.* 2008b).

Among neuraminidases, Neu3 is a key enzyme for ganglioside degradation because of its strict substrate preference to gangliosides, which co-localize with this enzyme at the plasma membrane. Neu3 shows 19%, 34%, 38% amino acid sequence identity to Neu1, Neu2, and to Neu4, respectively. Table 1.2 summarizes the different characteristics of the different members of human neuraminidase family.

**Table 1.2: Comparison of four types of human neuraminidases** (Miyagi *et al.* 2008a)

	Neu1	Neu2	Neu3	Neu4
<b>Major location</b>	Lysosomes	Cytosol	Plasma membrane	Lysosomes Mitochondria
<b>Major substrate</b>	Oligosaccharides 4-methylumbilliferyl-neuraminic acid	Oligosaccharides 4-methylumbilliferyl-neuraminic acid Glycoproteins Gangliosides	Gangliosides	Oligosaccharids 4-methylumbilliferyl neuraminic acid Glycoproteins Gangliosides
<b>Optimal pH</b>	4.4-4.6	6.0-6.5	3.8*-4.8	4.4-4.5
<b>Total amino acids</b>	415	380	428	496
<b>Chromosome location</b>	6p 21.3	2q 37	11q 13.5	2q 37.3

\*(Monti *et al.* 2000)

Proteomics studies have shown that Neu3 does not present typical transmembrane domains, suggesting that the association of Neu3 to the membrane should involve different mechanisms of anchorage to the lipid bilayer. All of the human neuraminidase proteins have potential *O*-glycosylation sites and a great number of amino acid residues that can be covalently modified by phosphorylation (Monti *et al.* 2002). Evidence is provided that Neu1 sorting to the plasma membrane is associated with tyrosine phosphorylation. Unlike lysosomes, the membranes do not contain a set of glycosidases for degradation, implying that Neu3 may have other functions at the plasma membrane rather than the catabolism of gangliosides. Modulation of functional molecules involved in many biological processes is one of these functions. The activity levels of Neu3 were found to fluctuate with cell differentiation, cell growth, and malignant transformation. Interestingly, the activity of Neu3 is exerted also on gangliosides exposed on the extracellular leaflet of the plasma membrane of adjacent cells by cell-cell interaction (Papini *et al.* 2004). Hydrolysis by Neu3 was essentially specific for various gangliosides e.g. GM3 (see Table 1.3), in the presence of Triton X-100 with considerable activity under acidic conditions. The enzyme does not act on the sialoglycoprotein fetuin.



**Table 1.3: Neuraminidase activity toward various substrates in the homogenate of COS-7 cells transfected with plasma membrane-associated sialidase (Neu3) cDNA**

Hydrolysis relative to GD3 (%)	
Substrates	human Neu3
GD3	100
GD1a	79
GD1b	52
GT1b	NA
GM3	84
GM2	2
GM1	NA
Fetuin	1
Sialyllactose ( $\alpha$ 2-3)	5
4-methylumbelliferyl-neuraminic acid	11

The reaction mixture contained up to 50 nmol of substrate as bound sialic acid, 0.2 mg of bovine serum albumin, 10  $\mu$ mol of sodium acetate buffer, pH 4.6 and 0.2 mg of Triton X-100 in a final volume of 200  $\mu$ l. after incubation of 37°C for up to 30 min, released sialic acid was measured with the thiobarbituric acid method; where NA indicates not assessed (Monti *et al.* 2002).

### 1.5.2. Localization of neuraminidase 3 in caveolae

Transient expression of Neu3 in COS7 cells permitted the detection of a neuraminidase activity with high activity towards ganglioside substrate at a pH optimum of 3.8. The expressed protein has a calculated molecular mass of 48 KDa and a theoretical pI of 6.8. The human putative Neu3 protein is 428 amino acids long. The protein is divided into two segments located on the opposite layers of the membrane by a hydrophobic stretch of 17 amino acids. The primary structure analysis revealed a high cysteine content (4.9% of the total), and the secondary structure prediction showed several  $\beta$ -sheet regions, a characteristic feature to all neuraminidases enzyme studied so far (Monti *et al.* 2000). All mammalian neuraminidases cloned so far show a high degree of homology and share amino acid blocks of highly conserved residues, F(R)YIP motif and Asp boxes in topologically equivalent positions through out the primary structure. 9 of 12 amino acid residues that form the catalytic site of *Salmonella typhimurium* enzyme are conserved in mammalian neuraminidases. Comparison of the three dimensional structure of *Salmonella typhimurium* neuraminidase with a human neuraminidase (NEU2) by X-ray crystallography revealed a striking similarity in spatial arrangement of the conserved amino acid residues. In addition, it has been found that the differences between the

microbial neuraminidase and mammalian neuraminidases are concentrated in the hydrophobic residues (Trp-121, Trp-128, and Leu-175) that form the hydrophobic pocket accommodating the N-acetyl group of sialic acid. This could explain the difference in the substrate preference between these enzymes. Because a strong correlation of this catalytic behavior with active site architecture has been demonstrated, this strongly suggests that the microbial and the mammalian neuraminidase have similar active site topology even though the proteins do not share high amino acid sequence similarities (Figure 1.15) (Monti *et al.* 2002).

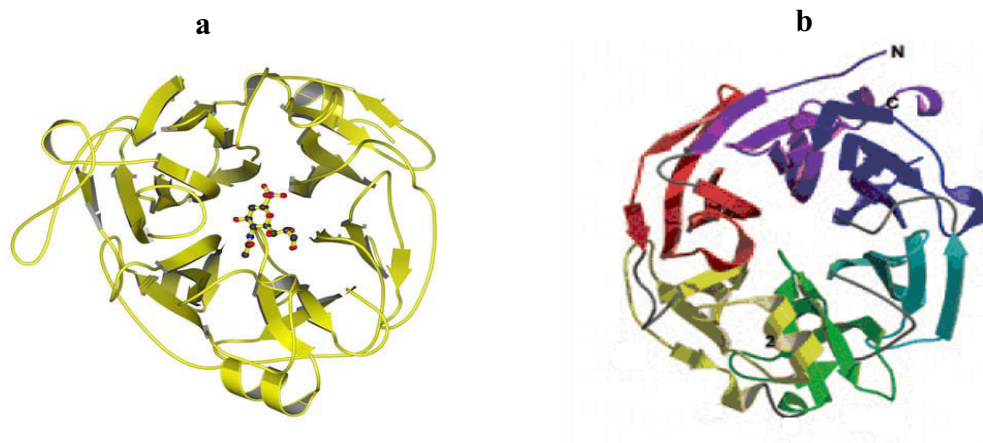


**Figure 1.15: Crystal structure of a bacterial neuraminidase shows the same folding pattern as the human neuraminidase.** (a) ribbon diagram of neuraminidase from *Salmonella typhimurium* in complex with DANA (Crennell *et al.* 1993). (b) ribbon diagram of Neu2 in stereo, viewed into the active site. Individual six blades of the propeller are colored differently (Chavas *et al.* 2005).

Neu3 is a peripheral membrane-protein associated with the external leaflet of the plasma membrane (Zanchetti *et al.* 2007). Neu3 has been found located in rafts of neuroblastoma cells (Kalka *et al.* 2001) and in caveolae of HeLa cells, closely associated with caveolin-1 (Wang *et al.* 2002b). Deduced caveolin-binding motifs ( $\phi$ X $\phi$ XXXX $\phi$  and  $\phi$ XXXX $\phi$ XX $\phi$ , where  $\phi$  is an aromatic residue W, F or Y) are present in most caveolae-associated proteins, including Src kinase, mitogen-activated protein kinase, and the EGF receptor (Figure 1.12). The residues 179-186 (YTTYIPSW) within the hydrophobic stretch of the putative transmembrane domain sequence of the human Neu3 were identified as a possible analogous region. A single amino acid exchange in the caveolin-binding motif led to inhibition of recruitment of Neu3 to caveolae, accompanied by reduction of the enzyme activity, whereas Neu3 was activated by increased caveolin-1 expression (Wang *et al.* 2002b). A tight association of Neu3 with caveolin-1 was supported further by co-immunoprecipitation of Neu3 by anti-caveolin-1 antibody (Wang *et al.* 2002b).

Human Neu3 is not always detected on the cell surface but may exist in the intracellular membranes. Presence of Neu3 at different cellular pools, one at the cell surface and the other in the endosomal compartment that exist in a dynamic equilibrium with each other has been suggested by Zanchetti and co-workers (2007). The mechanism of Neu3 anchorage to the lipid bilayer was found to be phospholipid-independent because no consensus sequences necessary for the post-translational modifications of GPI-anchored protein family or fatty acylated or prenylated proteins have been found within the amino acid sequence of Neu3. Given that Neu3 is a hydrophilic protein which segregates in the aqueous phase, it is possible that Neu3 may interact with an integral membrane protein partner. This partner protein may regulate the presence of Neu3 on the cell surface (Zanchetti *et al.* 2007).

### **1.6. State of the art**

One focus of our research group is the analysis of photobiological and molecular mechanisms underlying gene induction by physiological doses of ultraviolet radiation in epidermal and dermal cells of the skin. Over the last few years our research group has focused on the analysis of UVA signaling in human skin (Grether-Beck *et al.* 1996) and has shown that UVA radiation-induced gene expression in primary human keratinocytes is mediated via a non-enzymatic hydrolysis of plasma membrane localized sphingomyelin resulting in the generation of ceramides (Grether-Beck *et al.* 2000). These ceramides in turn act on the mitochondria via the voltage dependent megachannel giving rise to the release of cytochrome C into the cytosol where it undergoes rapid reduction resulting in oxidation of transcription factor AP-2. By this the DNA binding capacity of AP-2 to its recognition sites within AP-2 driven promoters (Grether-Beck *et al.* 2003) is increased.

Besides biphasic events such as the mRNA upregulation of proinflammatory genes, e.g. intercellular adhesion molecule-1, usually occurring 8h and 24h post UVA irradiation we have also observed an upregulation of serine palmitoyltransferase, the key enzyme of ceramide de novo synthesis (Grether-Beck *et al.* 2005b). The increased enzyme activity results in a second ceramide formation which also activates transcription factor AP-2 and leads to a second induction of ICAM-1 mRNA 24h post UVA treatment (Grether-Beck *et al.* 2005b) (Figure 1.16).

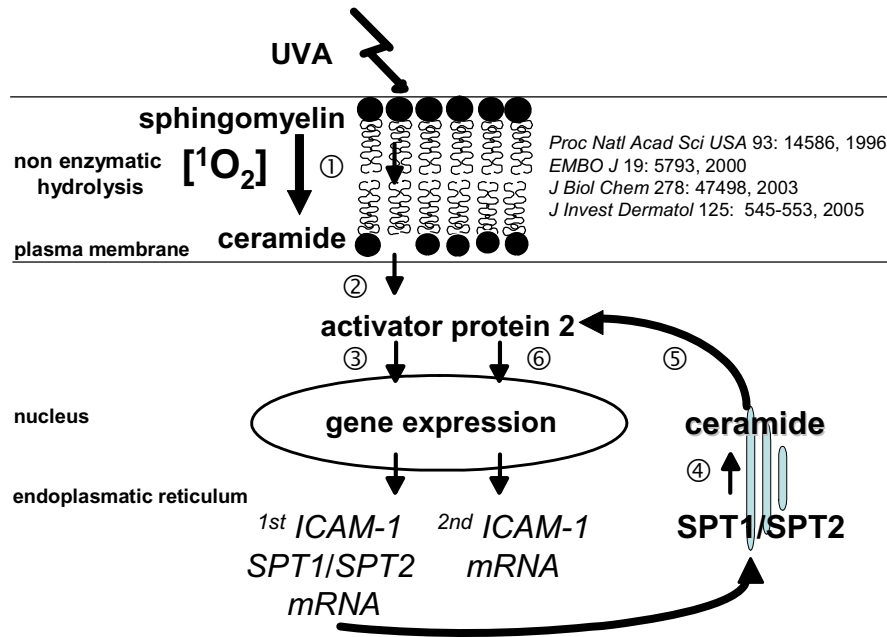


**Figure 1.16: UVA-induced signal transduction leading to gene expression in keratinocytes.**

Very recent findings indicate that besides ceramides also the cholesterol level within the cytoplasmic membrane critically determines these signaling events (Grether-Beck *et al.* 2008). Signaling occurs if the molar ratio of ceramide versus cholesterol is  $> 1$ . Accordingly, depletion of cholesterol results in an increased UVA response whereas preincubation with cholesterol causes inhibition of UVA-induced signaling. Moreover, a detailed balance of the lipid composition in rafts on a molar basis indicates that the non-enzymatic hydrolysis of sphingomyelin contributed to approximately 60% of the ceramides formed upon UVA treatment and therefore additional mechanism(s) could be involved in UVA-induced ceramide formation in rafts. In addition, UVA radiation not only alters the lipid composition within rafts but also results in activation of the non-receptor tyrosine kinase family Src. Inhibition of Src kinase phosphorylation by means of PP2 or SU6656 prevented UVA radiation-induced (i) caveolin-1 phosphorylation at tyrosine 14 and (ii) translocation of caveolin-1 from rafts into non-raft fractions of the cytoplasmic membrane. Most importantly, caveolin-1 phosphorylation and translocation were of functional relevance for UVA radiation-induced gene expression (Figure 1.17). Their inhibition by retrovirus-mediated caveolin-1 knockdown suppressed completely UVA radiation-induced gene expression in cultured human keratinocytes as compared to the wild type cells.

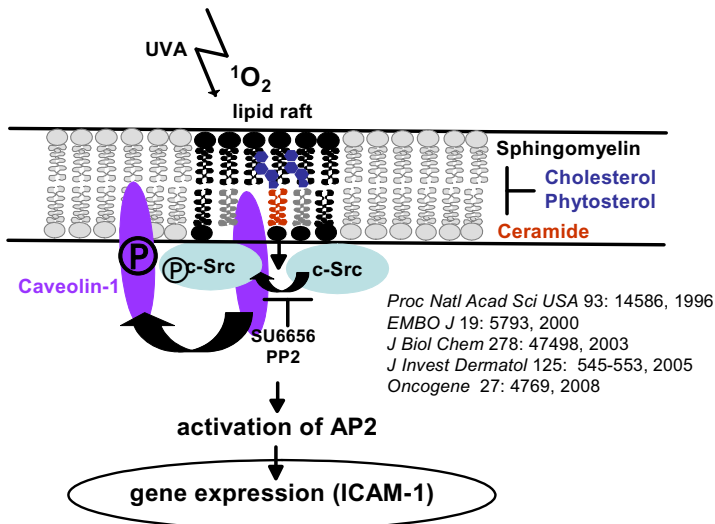


**Figure 1.17: UVA-induced signaling in keratinocytes.**

### 1.7. Aim and scopes of the study

As lipid analysis in rafts of UVA treated caveolin-1 knockdown cells presented an increased content of GM3 - the major ganglioside in keratinocytes- the changes of this glycosphingolipid were assessed with regards to UVA-signaling. In particular, the effect of UVA radiation on activation of the raft associated ganglioside specific neuraminidase 3 has been addressed, because desialylation of GM3 to form lactosylceramide is catalyzed by this enzyme. Moreover, we assessed whether UVA-induced activation of neuraminidase 3 is of functional relevance for UVA-induced signal transduction and subsequent upregulation of gene expression.

Since caveolin-1 knockdown in human keratinocytes prevents UVA-induced GM3 decrease, we have further assessed the role of caveolin-1 in UVA-induced gene expression and signal transduction. In this regard, it was of particular interest to address the effect of caveolin-1 depletion on UVA-induced (i) neuraminidase 3 activation, AP-2 activation and (iii) gene expression in human keratinocytes.

## **2. Materials and Methods**

### **2.1. Chemicals**

#### **2.1.1. Generally used chemicals**

**Table 2.1: List of generally used chemicals in this work**

<b>Chemical Product</b>	<b>Manufacturer / Supplier</b>
Acrylamide/Bisacrylamide solution (37,5:1)-40% (w/v)	Roth
BCA protein assay	Pierce
Bradford protein assay	Roth
Bromophenol blue	Serva
BSA (Albumin bovine fraction V)	PAA
Coomassie Brilliant Blue G 250	Sigma-Aldrich
Dichlormethane AMD	Merck
DMSO (Dimethyl sulfoxide)	Sigma
DTT (Dithiothreitol)	Roth
EDTA (Ethylenediaminetetraacetic acid)	Merck
Development and Fixation for x-ray films	Agfa
Glycine	Roth
Methanol	Roth
Milk powder blotting grade	Roth
n-Hexane	Merck
OptiPrep	Axis-Shield
Ponceau S	Fluka
Protein marker IV (Prestained)	Invitrogen
SDS (Sodium dodecyl sulfate)	Serva
SYBR Green	Invitrogen
TEMED (N,N,N',N'-Tetramethylethylenediamine)	Sigma-Aldrich
Triton-X-100	Fluka
Tween 20	Fluka

### 2.1.2. Chemicals used in cell culture

**Table 2.2: List of chemicals used in cell culture**

<b>Chemical Product</b>	<b>Manufacturer/ Supplier</b>
Antibiotic-Antimycotic	Invitrogen
BPE (Bovine Pituitary Extract)	Invitrogen
Cholesterol	Sigma-Aldrich
Dispase Grade I (Neutral Protease)	Boehringer, Mannheim
Ethanol	Fluka
Fetal Calf Serum (FCS)	Invitrogen
Gentamycin	Invitrogen
L-Glutamine (200 mM)	Invitrogen
Glycerol	Sigma-Aldrich
$\beta$ -Methylcyclodextrin ( $\beta$ MCD)	Sigma-Aldrich
NEAAs (Non-Essential-Amino-Acids)	Biochrom
PBS (Phosphate Buffered Saline)	Invitrogen
Puromycin	BDTransduction Laboratories
Trypsin-EDTA-solution (1:250)	Invitrogen
Vitamin E succinate	Sigma-Aldrich

### 2.1.3. Pharmacological inhibitors used in cell culture experiments

**Table 2.3: List of pharmacological inhibitors used in this work**

<b>Inhibitor</b>	<b>Manufacturer/ Supplier</b>
2-Deoxy-2,3-didehydro-N-acetyl neuramnic acid DANA (Ganglioside neuraminidase inhibitor)	Calbiochem
4-Amino-5-(4-chlorophenyl)-7-(t-butyl)pyrazolo[3,4- <i>d</i> ]pyrimidine PP2 (Src family tyrosine kinase inhibitor)	Calbiochem
2,3-Dihydro-N,N-dimethyl-2-oxo-3-[(4,5,6,7,-tetrahydro-1H-indol-2-yl)methyle]-1-H-indole-5-sulfonamide SU6656 (Tyrosine kinase inhibitor)	Calbiochem
PhosphoStop, phosphatase inhibitor cocktail	Roche
Complete ®, protease inhibitor cocktail	Roche

### 2.1.4. Equipments and Materials

**Table 2.4: List of equipments and materials used in this work**

<b>Equipment &amp; Material</b>	<b>Manufacturer / Supplier</b>
AMD 2 Automated Multiple Development device	CAMAG
Benchtop centrifuge Eppendorf 5417R	Eppendorf
Benchtop Megafuge 1.0R	Thermo Fisher Scientific
Chromatogram Immersion Device III	CAMAG
Costar® Cell lifter	VWR
Glass Homogenizer Dounce	Kleinfeld Labortechnik
Glass Chamber for HPTLC plates	Desaga
Hamilton Syringe	CAMAG
Heracell CO <sub>2</sub> incubators	Thermo Fisher Scientific
Hofer Dual Gel Caster	NovoDirect GmbH
HPTLC-Plates (20x10cm) 60F 254s	Merck
Inverses research Microscope IMT-2	Olympus Optical CO. (EUROPA) GmbH
laminar flow LaminAIR HBB 2448	Thermo Fisher Scientific
Linomat IV sample applicator for HPTLC	CAMAG
Optima™ TLX Ultracentrifuge with TLA 120.2 Rotor	Optima
Opticon MJ1 Real Time PCR System	Biozym Diagnostik GmbH
Oven	Thermo Fisher Scientific
Photometer	Eppendorf
Sample concentrator Techne Dri-Block DB-3	Techne Inc.
Nitrocellulose Transfer Membranes Schleicher & Schuell	Bioscience
Semi-dry electroblotter	Biometra
Sellas 2000, System Dr. Sellmeier, UVA1 irradiation device	Sellas GmbH
Sonifier® B-12, Cell Disruptor	Branson Inc.
Standard Power Pack 25 power supply	Biometra
TLC Scanner 3	CAMAG
Ultrasonic Unit Elma Transsonic T310	Singen
Ultracentrifuge L8-M with 50.2 Ti Rotor	Beckman Coulter, Inc.
Ultracentrifuge Evolution RC with SS-34 Rotor	Thermo Fisher Scientific
Vacuum pump for AMD2 Edwards RV3	CAMAG
Whatman 3 MM blotting paper	Whatman Inc.
X-ray films	Kodak
XCell SureLock™ Electrophoresis system	Invitrogen



## 2.2. Cell culture

### 2.2.1. Cells and cell lines

Primary human keratinocytes as well as an immortalized keratinocyte derived cell line, HaCaT, were used in this work to study the effects of UVA radiation on human skin cells. Primary keratinocytes were isolated from neonatal foreskin.

#### 2.2.1.1. Isolation of human keratinocytes from foreskin

Immediately after surgical excision of foreskins, these skin biopsies were kept in transport medium (Keratinocytes medium (see table 2.5), 1 % antibiotic-antimycotic, and 10 µg/ml gentamycin). For preparation, these skin pieces were rinsed in fresh, sterile PBS buffer without Ca<sup>2+</sup> and Mg<sup>2+</sup>, but containing gentamycin. The subcutaneous adipose tissue is removed using curved scissor, the remaining skin was dissected into approximately 5 mm x 5 mm pieces using a scalpel. These pieces were kept in PBS buffer containing dispase (25 caseinolytic unit/ml) and the aminoglycoside antibiotic gentamycin (5 µg/ml) overnight at 4°C. Dispase was used to separate the epithelial compartment from the underlying dermal connective tissue by destructing the junctions named hemidesmosomes between the epidermal keratinocytes and the extracellular matrix. The epidermal layer was easily peeled off the dermal layer with forceps. The epidermal layers were collected in 50 ml centrifugal tube containing 6 ml trypsin (0.25% trypsin, 1 mM EDTA) and incubated for 30 min at 37 °C with gentle shaking every 10 min. Trypsin was used to disintegrate the epidermis and release the keratinocytes as single cells. The enzymatic activity of trypsin was stopped by adding about 40 ml PBS buffer. After this incubation procedure, single cell keratinocytes were settled at 200 x g for 10 min at R.T. Keratinocytes were then resuspended by repeated pipetting in serum free medium supplemented with specific growth factors (see table 2.5). This selective medium was used to prevent growth of stromal cells such as dermal fibroblasts and vascular endothelial cells. As many factors contained in serum have a strong mitogenic effect on fibroblasts and tend to inhibit epithelial proliferation by inducing terminal differentiation, keratinocytes were grown in low (0.03-0.06 mM) Ca<sup>2+</sup> concentration, which inhibits keratinocyte differentiation and stratification.

### 2.2.1.2. Preparation of keratinocytes medium

Keratinocyte medium is made by mixing one part of keratinocyte-SFM (GIBCO–Invitrogen) medium with one part of MCDB 153 (Biochrom). 1 liter of keratinocyte medium is composed of the following ingredients:

**Table 2.5: Composition of keratinocyte cell culture medium**

<b>Ingredient</b>	<b>Final concentration</b>
Bovine pituitary extract “BPE” (GIBCO–Invitrogen)	37.5 mg/l
Human recombinant epidermal growth factor “EGF” (Biochrom)	5 µg/l
Insulin (Biochrom)	2.5 mg/l
Hydrocortisone (Biochrom)	25 µg/l
Ethanolamine (Biochrom)	3.05 mg/l
Phosphoethanolamine (Biochrom)	7.05 mg/l
L-Glutamine 200 mM (GIBCO–Invitrogen)	1% (v/v)
Antibiotic-Antimycotic consisting of penicillin G 10000 U/ml, streptomycin 10000 µg/ml, amphotericin B 25 µg/ml (GIBCO–Invitrogen)	1 % (v/v)

### 2.2.1.3. Culturing of the human cell line HaCaT

This cell line originates from the adult normal human keratinocytes, that are spontaneously transformed but non-tumorigenic cells (Boukamp *et al.* 1988). They have been obtained by long term culturing of primary keratinocytes in low calcium medium (0.2 mM) and elevated temperature (38.5°C). The name “HaCaT” is an abbreviation derived from their descriptive name, which is **H**uman **a**dult skin keratinocytes, low **C**alcium (0.2 mM), high **T**emperature (38.5 °C).

Retroviral *Vector* pRVH-1-puro was used for the insertion of caveolin-1 antisense mRNA which was used for generation of caveolin-1 knockdown HaCaT cells. The plasmids were kindly provided by Joachim Füllekrug (Max Plank Institute of Molecular Cell Biology and Genetics, Dresden, Germany).

The retroviral transfection of HaCaT cells was performed by Ingo Felsner (Department of Cell Biology, Leibniz-Institut für Umweltmedizinische Forschung (IUF) an der Heinrich-Heine Universität Duesseldorf, Germany) according to the method described by Schuck (Schuck *et al.* 2004).

#### 2.2.1.4. Preparation of culture medium of HaCaT cells

HaCaT cells are cultured in Dulbecco's Modified Eagle's Medium (DMEM), low glucose (1 g/L). DMEM medium (PAA) was supplied by the following ingredients:

**Table 2.6: Composition of HaCaT cell culture medium**

<b>Ingredient</b>	<b>Final concentration</b>
Fetal calf serum (GIBCO–Invitrogen)	5 % (v/v)
L-Glutamine 200 mM (GIBCO–Invitrogen)	1 % (v/v)
Antibiotic-Antimycotic, penicillin G 10000 U/ml, streptomycin 10000 µg/ml, amphotericin B 25 µg/ml (GIBCO–Invitrogen)	1 % (v/v)

Caveolin-1 knockdown HaCaT cells and the control plasmide pRVH-puro transfected cells were cultured in the DMEM medium supplied with 4 µg /ml puromycin (Alixes) in addition to the ingredients mentioned in Table 2.6.

#### 2.2.3. Passaging cells

Primary keratinocytes were subcultured when 50-70% confluency was reached. They can be cultured up to passage 4 without losing their growth potential. Primary keratinocytes were propagated in a split ratio of 1:4. In contrast, for HaCaT cells confluency of 80-90% was considered to be ready for subculturing, a split ratio of 1:16 was usually sufficient. Cells were rinsed with PBS buffer to remove FCS which inhibits the activity of trypsin, then 2 ml trypsin (0.25 % trypsin, 1 mM EDTA) were added, and cells were incubated for 10 min at 37° C. To remove the excess of trypsin, the disaggregated cells were resuspended in 12 ml PBS buffer. Cells were then settled at 200 x g for 10 min at R.T and resuspended in fresh medium and dispensed in new culture flasks. The culture medium was changed twice a week.

#### 2.2.4. Cell culture conditions

All cell types used were cultivated at 37° C and 5% CO<sub>2</sub> in an incubator with constant humidity to prevent drying of the cells by a water saturated atmosphere. Cells were subcultured in 175 cm<sup>2</sup> cell culture flasks and propagated in 145 mm culture dishes (Greiner-bio-one).

### 2.2.5. Cryopreservation of cells

For long-term storage, cells have to be cryopreserved. In order to avoid damage due to intracellular or extracellular ice formation and dehydration, cryoprotectants such as glycerol or dimethyl sulfoxide are added. The cryoprotectants are designed to permeate the cell membrane where their large molar volumes (due to high molecular weight) slow water loss from cells during freezing as well as lowering the freezing temperature and delaying ice crystal formation. Moreover, a protocol for slow freezing is applied to avoid further damage of the cellular membranes which might result in increased cell death. After thawing it is important to remove the cryoprotectant immediately, because high concentrations of glycerol or dimethyl sulfoxide might be toxic to the cells. Primary keratinocytes or HaCaT keratinocytes were cryopreserved in a medium composed of the following ingredients:

**Table 2.7: Composition of cell cryopreservation medium**

<b>Ingredient</b>	<b>Final concentration</b>
Culture medium	80 % (v/v)
Fetal calf serum	10 % (v/v)
Glycerol	10 % (v/v)

In order to prepare cryostocks, confluent cells were rinsed with PBS buffer and detached using trypsin (0.25% trypsin–1 mM EDTA) for 10 min. Cells were resuspended in PBS buffer and settled by centrifugation at 200 x g for 10 min. Cell pellets were then resuspended in 1 ml cryopreservation medium and stored in cryopreservation vials for 24 h at -80° C in a cryogenic freezing container (Nalgene or Nunc cooler) containing isopropanol, which gives a cooling rate of approximately 1°C/min in the vials. After cooling down slowly, the vials are stored for long term in liquid nitrogen containing Dewar vessels at approximately -196 °C.

To recover the cells after storage, the vials are removed from the Dewar vessel and are placed for ~ 2 min in a 37° C water bath. To remove the cryopreservation medium, cells are resuspended in 10 ml fresh medium and pelleted by centrifugation at 200 x g for 10 min at R.T. Cell pellets are resuspended and seeded in fresh culture medium which is renewed after 24 h.

### 2.2.6. UVA irradiation

For irradiation, the culture medium was replaced by PBS buffer. As UVA1 light source a Sellamed 2000 system (Sellas GmbH, Gevelsberg, Germany) was used. The UVA1 lamp used in the present study is characterized by an UV-spectrum ranging mainly between 340-400 nm as shown in Figure 2.1. The relative percentages of radiant energy in the UVA1 (340-400 nm), UVA2 (320-340 nm), and visible (400-780 nm) ranges amounted to 96.9 %, 0.018 % and 3.1 %, respectively. No radiation in the infrared or UVB region was detectable (Vielhaber *et al.* 2006). The UVA1 output was determined with a UVAMETER type II (Waldmann, Villingen-Schwenningen, Germany) and was found to be approximately 150 mW/cm<sup>2</sup>. After irradiation, the PBS buffer in the cell culture plate was exchanged against culture medium and the cells were incubated in a CO<sub>2</sub> incubator for additional period of time as given in the experimental plane e.g. for additional 8 h and / or 24 h, respectively, in the biphasic ICAM-1 expression analysis. The culture medium was then removed, the cells were rinsed with PBS buffer and the whole plate was frozen in liquid nitrogen.

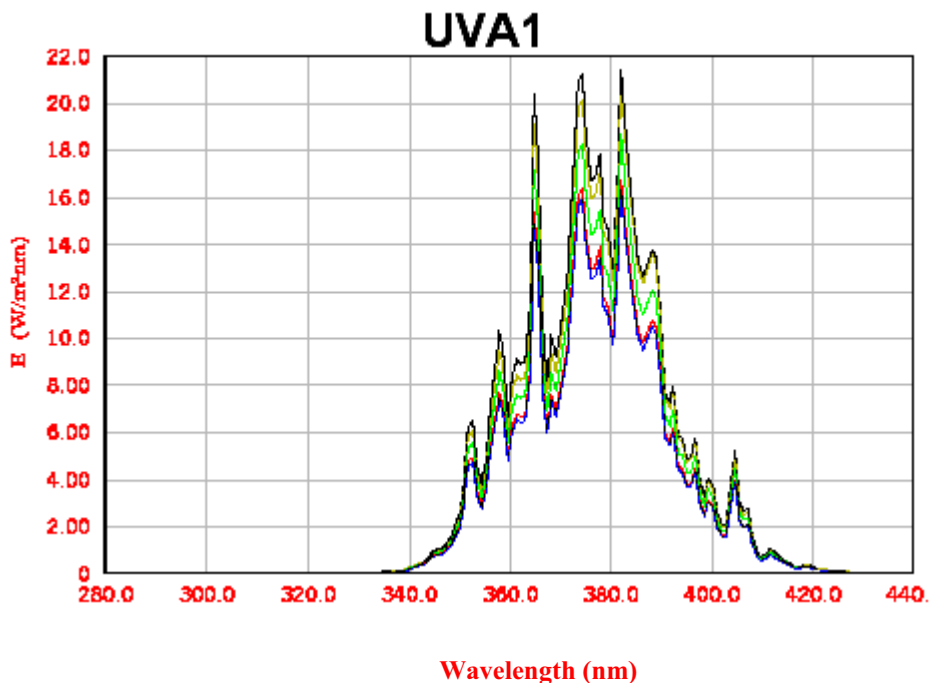


Figure 2.1: UV-spectrum of UVA1 lamp from Sellamed system 2000

## 2.3. Preparation of cellular extracts

### 2.3.1. Preparation of whole cell extracts for lipid analysis by HPTLC

To investigate the effect of UVA radiation or the effect of some exogenously added substances on the whole cell lipid content (total cell extract), two 145 mm dishes with

confluent cells were required for each sample. After removal of the medium from the cells, cells were washed with 12 ml pre-warmed PBS buffer (R.T) on the dish, and scraped off the plate on ice. Cells were placed in a 15 ml test tube (e.g. BD Falcon) using ice cold PBS buffer. Cells were then pelleted by 1.280 x g for 15 min at 4°C. About 500 µl of the supernatant was left on the top of the cell pellet. Cell pellets were resuspended in this volume of the supernatant and transferred into a 1.5 ml test tube (e.g. Eppendorf test tube). Cells were centrifuged by 400 x g for 10 min at 4°C. The supernatant was completely discarded and the pellets were suspended in 600 µl distilled water. Cells were then homogenized using ultrasound (35 kHz for 30 sec). Protein quantification was carried out using Bradford assay (see section 2.9).

### 2.3.2. Preparation of whole cell extract for western blot analysis

Confluent cells grown on 60 mm culture dishes were lysed in 200 µl 2x Laemmli sample buffer (Laemmli 1970) and scraped off the dishes by Teflon scraper. To ensure cell disruption, lysates were sonicated on ice for 10 sec at 10 % level (Sonifier® B-12). Lysates were then heated for 5 min at 95° C to achieve protein denaturation and prior to electrophoresis, samples were shortly centrifuged in order to spin down cellular debris.

**Table 2.8: Composition of 2x Laemmli sample buffer**

Substance	Concentration
Tris-HCl (pH 6.8)	125 mM
Glycerol	20% (v/v)
Sodium dodecyl sulfate SDS	4% (w/v)
Dithiothreitol (DDT)	300 mM
Bromophenol blue	0.3% (w/v)

### 2.3.3. Preparation of lipid raft extract for western blot analysis

After isolation of lipid rafts, equal protein amount from all samples was taken in equal volume (see section 2.3.4). 2x TNE buffer was used to correct the volume differences between the samples. To this volume appropriate volume of 4x Laemmli buffer was added and well mixed with the sample. Protein denaturation was carried out by heating the samples for 5 min at 95° C.

### 2.3.4. Isolation of plasma membrane microdomains (Lipid rafts)

Lipid rafts are small plasma membrane domains containing high levels of cholesterol and sphingolipids (Pike 2006). Traditional methods for the biochemical isolation of lipid rafts involve the extraction of cells with non-ionic detergents (e.g. Triton X-100) followed by separation of the low density, detergent-resistant membrane fraction on density gradients. The high lipid / protein ratio of lipid rafts makes them markedly lower in density than other membrane proteins and allows them to be isolated from these proteins by density gradient ultracentrifugation (Schuck 2003). OptiPrep gradient was used in the process of lipid raft isolation by density gradient centrifugation. OptiPrep® is a 60 % (w/v) solution of iodixanol in water with a density of 1.32 g/ml, this high density facilitates the fractionation of the cellular components through a discontinuous density gradient by preparing different concentrations of this solution.

In this work, lipid rafts from keratinocytes were isolated according to the method published by Brown and Rose (Brown & Rose 1992). Four 145 mm plates (80% confluence) were used per sample. Cells were rinsed first with pre-warmed PBS buffer (R.T) and next with ice cold PBS buffer. The cells of each dish were scraped into 2-3 ml ice cold TNE buffer (pH 7.4) containing: protease inhibitors (chymostatin, leupepin, antipain and pepstatin A, at a final concentration of: 25 µg/ml) and 1% Triton X-100. Cells were then homogenized by passage through a G25 needle 20 times and allowed to stand on ice for 30 min. The lysate was adjusted to 40 % OptiPrep using 60 % OptiPrep solution in TNE buffer and placed in the bottom of the centrifugal tube. 2.1 ml of 30 % Optiprep and 0.9 ml of 5 % Optiprep solution in TNE buffer were carefully poured on the top of the lysate, respectively. Gradients were centrifuged at 170.000 x g for 4 h at 4 °C in an L8-M70 ultracentrifuge with a 50-2 Ti Rotor from Beckman. The resulting gradients were then fractionated at 4 °C into seven fractions. Each fraction is made by carefully withdrawing of 600 µl from the top of the tube to the bottom. Protein determination was carried out by BCA method (section 2.9). Samples were stored at -80 °C.

**Table 2.9: Composition of TNE buffer**

Substance	Concentration
Tris-HCl (pH 7.4)	50 mM
NaCl	150 mM
EDTA	2 mM

### 2.3.5. Preparation of nuclear extracts for band shift assay

For analysis of transcription factor activation a protocol originally described by Dignam and coworkers (Dignam *et al.* 1983) was used for preparation of nuclear extracts.

One cell culture plate with confluent cells (145 mm diameter) was sufficient for each sample. Cells were routinely harvested 15 or 30 min post UVA treatment, because previous studies have shown significant activation of AP-2 under these conditions. Cells were scrapped off the plate with 10 ml ice cold PBS buffer and pelleted in 15 ml test tubes using 800 x g for 10 min at 4 °C. Pellets were homogenized with 5x volume of buffer A and incubated on ice for 10 min. After centrifugation using 800 x g for 10 min at 4° C, 2x volumes of buffer A containing protease inhibitors were added. The pellets were homogenized in a Dounce homogenizer by 20 strokes. The homogenates were transferred into 1.5 ml Eppendorf test tubes and centrifuged by 800 x g for 10 min at 4° C. The produced supernatants are transferred into other fresh test tubes and used for preparation of cytosolic extracts as it will be described below.

For preparation of nuclear extracts, the resulting pellets were resuspended in 500 µl of buffer A containing protease inhibitors and centrifuged using 25.000 x g for 20 min at 4° C. The resulting pellets were resuspended in 500 µl buffer C, containing protease inhibitors, in a Dounce homogenizer by 20 strokes. The homogenates were incubated for 10 min on ice, and were then centrifuged using 25.000 x g for 20 min at 4 °C. The obtained supernatants were dialysed in buffer D overnight at 4 °C in a semi-permeable membrane resulting in concentrated extracts, which represent the nuclear fraction. Protein quantification was carried out with Bradford test where 10 µl of the extract are required. The extracts were stored in aliquots and kept at -80°C until use.



**Table 2.10: Composition of buffers used for preparation of nuclear and cytosolic extracts**

Buffer	Ingredient	Concentration
Buffer A	HEPES (pH 7.9)	10 mM
	MgCl <sub>2</sub>	1.5 mM
	KCl	10 mM
	DDT	0.5 mM
Buffer B	HEPES (pH 7.9)	0.3 mM
	KCl	1400 mM
	MgCl <sub>2</sub>	0.03 mM
Buffer C	HEPES (pH 7.9)	20 mM
	NaCl	420 mM
	MgCl <sub>2</sub>	1.5 mM
	DDT	0.5 mM
	Glycerol	25 %
Buffer D	HEPES (pH 7.9)	20 mM
	KCl	100 mM
	EDTA	0.2 mM
	DTT	0.5 mM
	Glycerol	20 %

### 2.3.6. Preparation of cytosolic extracts

Cytosolic extracts were prepared in the same experiments as the nuclear extracts. The homogenates were centrifuged in Eppendorf test tubes using 800 x g for 10 min at 4 °C. The obtained supernatants were transferred to a 1.5 ml Eppendorf test tube and 111 µl buffer B containing protease inhibitors were added. The produced lysates were centrifuged for 1 h at 4° C using 100.000 x g. The obtained supernatants were dialysed in a semi-permeable membrane against buffer D overnight at 4 °C. The dialysates were centrifuged for 5 min at 4°C with 20.000 x g in Sorvall a centrifuge. 10 µl of the extract were taken for protein quantification with Bradford test, the remaining extract was stored in aliquots at -80 °C.

### 2.3.7. Isolation of cellular membrane fraction

Isolation of cellular membrane fraction for neuraminidase 3 activity assay was performed as previously published by Miyagi and co-workers (Miyagi *et al.* 1999). In detail, cells were grown on 145 mm cell culture plates (4 plates for each sample were required). When the confluency of the cells reached about 80-90%, cells were stimulated and harvested as given by the experimental design. Cells were washed first with pre-warmed (R.T) PBS buffer and next with ice cold PBS buffer. Cells from each plate were scraped off the plate

into 2 ml cold PBS buffer on ice and pelleted with 800 x g for 10 min at 4 °C. The resulting pellets were resuspended in 1 ml of the lysis buffer. Cells were then disrupted by sonification on ice for 15 sec with 10% level (15 watts) in Sonifier® B-12 and allowed to stand on ice for 15 min. Cellular debris and nuclei were removed by centrifugation with 1000 x g for 10 min at 4 °C. The resulting supernatants were centrifuged with 100.000 x g for 1 h at 4 °C in an L8-M70 ultracentrifuge with a 50-2 Ti Rotor from Beckman. The remaining pellets were considered as membrane fraction.

**Table 2.11: Composition of the lysis buffer used for cellular membrane extraction**

Ingredient	Concentration
EDTA	1 mM
DTT	1 mM
Protease inhibitors (chymostatin, leupepin, antipain and pepstatin A)	25 µg/ml each

## 2.4. Lipid analysis by HPTLC

### 2.4.1. Extraction of lipids with hydrolysis

In this work lipid extraction was carried out as originally described by Folch (Folch *et al.* 1957). Lipids such as ceramides need to be extracted from the biological sample by alkaline hydrolysis. In this method, total lipids in a sample (usually contains 500 µg protein in 500 µl volume) were first extracted by vortexing with 2.5 ml chloroform/methanol solvent (2:1 v/v). Separation of the organic layer from the inorganic layer was achieved by centrifugation with 1.280 x g for 15 min at 14 °C. The upper inorganic layer was removed and the lower organic layer was concentrated at 37 °C under nitrogen steam till complete dryness, the remaining concentrate was hydrolysed overnight in a closed test tube with 250 µl NaOH (0.5 M in methanol) and 250 µl chloroform in a water bath at 37 °C. To this hydrolysate 250 µl HCl (0.1 M in methanol), 850 µl chloroform, 430 µl H<sub>2</sub>O, and 500 µl chloroform/methanol (2:1 v/v) were added and well mixed by vortexing. To extract ceramides to the lower organic layer, centrifugation was carried out at 14°C for 15 min with 1.280 x g. The resulting lower organic layer was then washed two times with 250 µl HCl (0.1 M in methanol), 850 µl chloroform, 430 µl H<sub>2</sub>O, and 500 µl chloroform/methanol (2:1 v/v). Finally this layer was concentrated under nitrogen steam till complete dryness. The concentrate was then dissolved in 200 µl

chloroform/methanol (2:1 v/v). Ceramide content of the sample was determined by HPTLC analysis against a standard solution containing C<sub>6</sub>-ceramide.

#### **2.4.2. Extraction of lipids without hydrolysis**

Lipids such as sphingomyelin and glycosphingolipids are extracted from the biological sample without the hydrolysis process described above. In a glass test tube 2.5 ml chloroform/methanol solvent (2:1 v/v) were added to 500 µl sample containing 500 µg protein and mixed by vortexing. The organic layer was separated from the inorganic layer by centrifugation at 1.280 x g for 15 min at 14°C. The upper inorganic layer was removed carefully with a capillary glass pipette. The glass tube containing the organic layer was placed under nitrogen steam at 37°C till the volume of its content was minimized to about 1 ml, this content was then transferred to an amber glass vial and concentrated by nitrogen steam concentrator till complete dryness. The lipid extracts can be stored at this point at -20°C or directly analyzed by adding 200 µl chloroform/methanol solvent (2:1 v/v).

#### **2.4.3. HPTLC analysis of lipids by AMD2 method from CAMAG**

Automated Multiple Development (AMD) for high performance thin layer chromatography (HPTLC) analysis from GAMAG is a sophisticated method of separating mixtures containing up to forty compounds on a separation distance of 80 mm. The separation is accomplished by the distribution of the mixture between two phases, one that is stationary and one that is moving. Chromatography works on the principle that different compounds will have different solubilities and adsorption to the two phases between which they are to be partitioned.

Thin layer chromatography is a solid-liquid technique. As stationary phase we used silica gel (SiO<sub>2</sub> x H<sub>2</sub>O).

#### **2.4.4. Plate preparation**

The HPTLC plates were from Merk (Merk, 60F 254s, 20 x 10 cm), the plates were placed in isopropanol for at least 60 min in a saturated glass tank, the plates were then activated in oven for 20 min at 120°C. The sample was applied in three separated bands along with a standard using Linomat IV (CAMAG) under a nitrogen cover gas atmosphere.

### 2.4.5. Plate development with AMD2 technique

The mobile phase of HPTLC analysis was made by automatically mixing a solvent gradient using AMD2 technique. The universal gradient solvent system for lipid analysis from CAMAG is composed of three solvents, namely, methanol, dichloromethane, and n-hexane. The gradient is started with the most polar solvent 100 % methanol and changes stepwise by an increase of dichloromethane and a corresponding decrease of methanol till it ends with the most non-polar solvent 100 % n-hexane as explained in Figure 2.2. The plate is developed repeatedly in the same direction and each successive run extends over a longer solvent migration distance than the one before. Between runs, the solvent is completely removed from the developing chamber and the layer is dried under vacuum. The elution strength decreases run by run. In this way, a stepwise elution gradient is formed. The combination of focusing effect and gradient elution results in extremely narrow bands. Their typical peak width is about 1 mm. This means that, with the available separation distance of 80 mm, many components can be completely resolved (Base line separation). As the solvent rises up through the silica, differential partitioning occurs between the components of the mixture dissolved in the solvent, the solvent system, and the stationary phase. The more strongly a given component of a mixture is adsorbed onto the stationary phase, the less time it will spend in the mobile phase and the more slowly it will migrate up the plate.

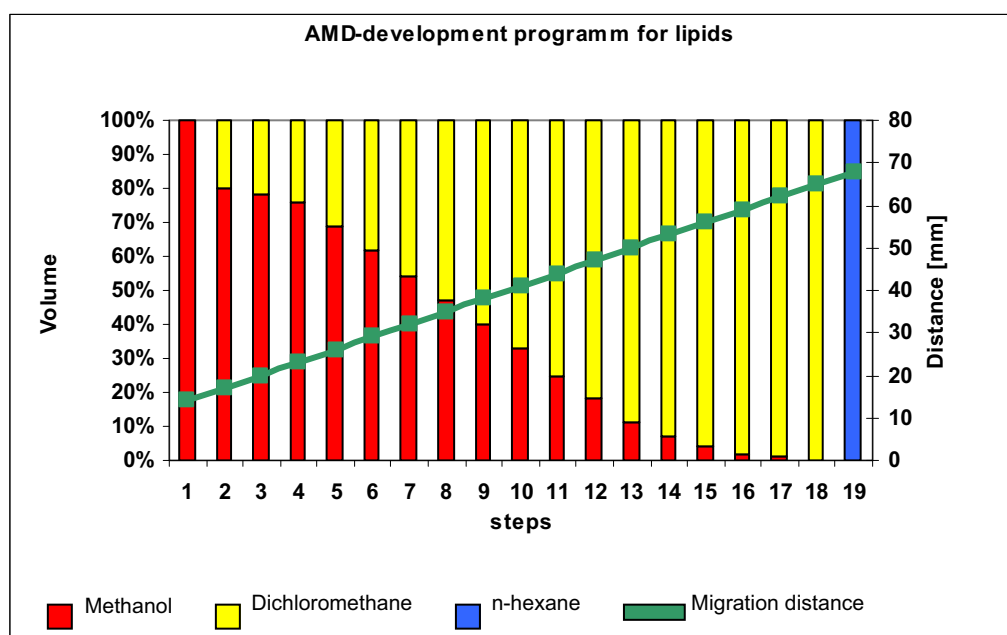


Figure 2.2: Universal gradient for lipid analysis by AMD2 method from CAMAG.

#### 2.4.6. Post-chromatic plate development and densitometry quantification of lipids

At the end of the automated plate development usually taking about 4 hours, the plate was automatically immersed for 1 sec in manganese chloride solution, using an automatic immersion device. The plate was then placed for 20 min in an oven at 120°C. Manganese chloride solution was used as coloring reagent. This reagent was prepared by dissolving 1.6 g  $\text{MnCl}_2 \cdot 4\text{H}_2\text{O}$  in 240 ml  $\text{H}_2\text{O}$ , 240 ml methanol and 16 ml conc.  $\text{H}_2\text{SO}_4$ .

The quantification of the chromatograms was performed by densitometric evaluation using a TLC scanner 3 and CAT 4.06 software from CAMAG. This method is based on measuring the optical density of the lipid band at 550 nm of the sample and of the standard solution which was applied routinely on every HPTLC plate resulting in a calibration curve.

**Table 2.12: Composition of the standard used for lipid analysis**

Substance	concentration
Sphingomyelin (Sigma)	50 ng/ $\mu\text{l}$
L- $\alpha$ -Phosphatidyl cholin (Sigma)	100 ng/ $\mu\text{l}$
D- <i>erythro</i> -Sphingosine, n-hexanoyl (C <sub>6</sub> -ceramide) (Calbiochem)	100 ng/ $\mu\text{l}$
Cholesterol-3-sulfate (Calbiochem)	50 ng/ $\mu\text{l}$
Cholesterol (Calbiochem)	50 ng/ $\mu\text{l}$
Lactosylceramide from bovine buttermilk (Matreya)	100 ng/ $\mu\text{l}$
GM1: Ganglioside from bovine brain (Alexis)	50 ng/ $\mu\text{l}$
GM3: Ganglioside from bovine brain (Alexis)	50 ng/ $\mu\text{l}$

#### 2.5. SDS polyacrylamide gel electrophoresis (Western blot analysis)

Sodium dodecyl sulfate (SDS), in combination with a reducing agent and heat, is the most common dissociating agent used to denature native proteins. Denaturation of proteins prior to electrophoresis allows for enhanced resolution and discrimination of proteins on the basis of molecular size rather than charge or shape (Bonifacino *et al.* 2003). Denatured proteins are separated in an electric field, as they move through a polyacrylamide gel network toward the anode, according to their molecular weight. Binding of SDS results in having identical charge per unit mass and therefore allows fractionation by size. The pore size of the gel depends on the amount of acrylamide and bisacrylamide in the gel. The protein of interest can be captured in the gel by selecting a proper pore size.

### 2.5.1. Separating protein sample by electrophoresis

In this work, 16 % acrylamide gel was used for separation of proteins of 10-30 kDa (e.g. caveolin-1  $\approx$  24 kDa), 11 % gel for 25-60 kDa (e.g. Src tyrosine kinase  $\approx$  60 kDa). Electrophoresis was performed in a Novex Mini-Cell apparatus (Invitrogen) and the electrophoresis procedure was carried out as previously described (Sambrook *et al.* 1989). Protein separation was performed under constant voltage 200 V until the bromophenol blue tracking dye reached the bottom of the separating gel. The composition of the electrophoresis buffer used for separating the protein sample is given in Table 2.14. A protein standard (PeqGold protein marker IV, Peqlab) was used to control protein separation and to estimate the position of the protein of interest.

**Table 2.13: Recipes for polyacrylamide separating and stacking gels**

Components	Separating gel			Stacking gel
	8 % (10 ml)	12 % (10 ml)	16 % (10 ml)	5 % (3 ml)
40 % (w/v) Acrylamide /Bisacrylamide solution (37.5 : 1)	2 ml	3 ml	4 ml	0.3 ml
1.5M Tris-HCl pH 8.8	2.5 ml	2.5 ml	2.5 ml	-
1.5M Tris-HCl pH 6.8	-	-	-	0.8 ml
10 % SDS	100 $\mu$ l	100 $\mu$ l	100 $\mu$ l	30 $\mu$ l
TEMED	5 $\mu$ l	5 $\mu$ l	5 $\mu$ l	3 $\mu$ l
10 % APS	50 $\mu$ l	50 $\mu$ l	50 $\mu$ l	16 $\mu$ l
Deionized water	4.5 ml	3.5 ml	2.5 ml	1.9 ml

### 2.5.2. Protein blotting

Protein blotting means electrophoretic transfer of a protein from the polyacrylamide gel to a membrane. In this work, transfer of proteins on a nitrocellulose membrane (pore size of 0.2  $\mu$ m) was achieved with semidry blotting technique in presence of transfer buffer (Table 1.14). Protein blotting was carried out for 1.5 h at 0.8 mA/cm<sup>2</sup>.

To verify transfer efficiency, nitrocellulose membrane was reversibly stained with Ponceau S for 5 min. The stain was then removed by washing the membrane three times, 10 min each, with TBST buffer (Table 2.14).

### 2.5.3. Membrane blocking

To block non-specific antibody binding sites, the membrane with the transferred proteins was incubated for 1 h with blocking buffer (5 % w/v non-fat dried milk prepared in TBST solution) at R.T on a shaker. To remove traces of milk, the membrane was then washed using two changes of TBST buffer.

### 2.5.4. Immunological detection of the protein

The blocked membrane was incubated overnight at 4 C° with a diluted solution of a primary antibody in blocking buffer as recommended by the supplier (Table 2.15) and directed to the protein of interest. The membrane was then washed with TBST buffer three times, 10 min each, at R.T on shaker.

### 2.5.5. Detection of membrane-bound protein by enhanced chemiluminescence (ECL)

In this work a horseradish peroxidase labelled secondary antibody (Table 2.15) was used to detect the primary antibodies. The secondary antibody was diluted in the blocking buffer and incubated with the membrane for 2 h at R.T on a shaker. Then the membrane was washed three times, 10 min each, with TBST buffer and soaked in the ECL working reagent containing luminol. In a darkroom, blue light sensitive X-ray film (Hyperfilm ECL, Amersham) was exposed to the membrane.

Oxidation of luminol by horseradish peroxidase in the presence of a chemical enhancer such as phenol results in enhanced chemiluminescence (Figure 2.3). Horseradish peroxidase/hydrogen peroxide catalyzes the oxidation of luminol under alkaline conditions. Immediately following oxidation, the luminol is in an excited state which then decays to ground state via a light emitting pathway. The generated light at the site of the reaction is detected by a X-ray film. Development of the X-ray film was carried out using the reagents from Adefo.

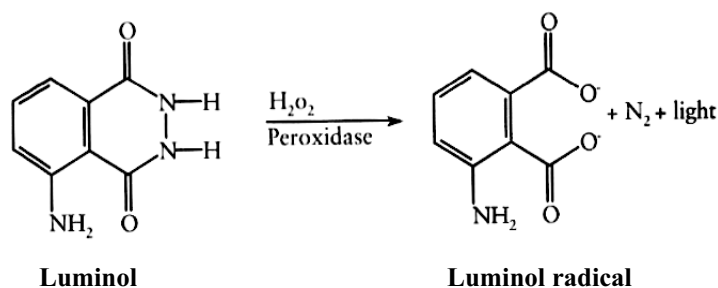


**Figure 2.3: Oxidation of luminol by horseradish peroxidase/hydrogen peroxide for enhanced chemiluminescence**

### 2.5.6. Western stripping

The complete removal of primary and secondary antibodies from the membrane is performed by stripping. The proteins can be stripped from the membrane by incubation in stripping buffer (Table 2.14) for 15 min at 55 °C. The membrane was then washed three times, 10 min each, with TBST buffer at R.T. The detection of a second protein was performed in a similar manner as with the previous one.

**Table 2.14: Buffers used for western blot analysis**

Buffer	Composition
1 X TBST buffer (pH 7.6)	150 mM NaCl 50 mM Tris 0.1 % (v/v) Tween 20
Transfer buffer	20 % (v/v) Methanol 50 mM Tris 40 mM Glycine 0.037 % SDS
Stripping buffer (pH 6.8)	100 mM 2-mercaptoethanol 60 mM Tris 2 % (w/v) SDS
Laemmli electrophoresis buffer (pH 8.3)	20 mM Tris 200 mM Glycine 0.1 % (w/v) SDS
Ponceau S stain-solution	0.2 % (w/v) Ponceau S 0.01 % (v/v) Acetic acid

**Table 2.15: Antibodies used for western blot analysis**

Primary Antibody	Provider	Dilution
Caveolin 1 Mouse IgG	BDTransduction Laboratories	1:1000 in 5 % (w/v) dry milk/ TBST
Caveolin pY14 Mouse IgG	BDTransduction Laboratories	1:1000 in 5 % (w/v) dry milk / TBST
Calnaxin Rabbit IgG	SantaCruz Biotechnology	1:200 in 5 % (w/v) dry milk/ TBST
Flotillin-1 Mouse IgG	SantaCruz Biotechnology	1:1000 in 1 % (w/v) milk powder / TBST
GAPDH Mouse IgG	SantaCruz Biotechnology	1:200 in 5 % (w/v) dry milk/ TBST
GRASP Rabbit IgG	SantaCruz Biotechnology	1:200 in 5 % (w/v) dry milk/ TBST
Nucleoporin p62 Goat IgG	SantaCruz Biotechnology	1:200 in 5 % (w/v) dry milk/ TBST

*To be continued*



Prohibitin	Rabbit IgG	SantaCruz Biotechnology	1:1000 in 5 % (w/v) dry milk/ TBST
Src pY529	Rabbit IgG	Cell Signaling	1:1000 in 5 % (w/v) dry milk / TBST
Src pY418	Rabbit IgG	Cell Signaling	1:1000 in 5 % (w/v) dry milk / TBST
Src Pan	Rabbit IgG	Cell Signaling	1:1000 in 5 % (w/v) dry milk / TBST
Transferrin	Goat IgG	SantaCruz Biotechnology	1:1000 in 5 % (w/v) dry milk/ TBST
<b>Secondary antibody</b>		<b>Provider</b>	<b>Dilution</b>
anti-Mouse IgG, Peroxidase- coupled HRP		DakoCytomation	1:1000 in 1 % (w/v) dry milk /TBST
Anti-Rabbit IgG, Peroxidase- coupled HRP		DakoCytomation	1:1000 in 1 % (w/v) dry milk /TBST

## 2.6. Identification of lipid rafts by western blot analysis

Non-caveolar lipid rafts cofractionate with caveolae in many different subcellular membrane fractionation procedures because they exhibit similar physical properties (Parton & Simons 2007). For identifying lipid rafts, marker proteins proven to be localized within lipid rafts such as caveolins and flotillins were used (Bickel *et al.* 1997; Le *et al.* 2002). Flotillins might be interesting raft markers, because flotillins are also expressed in non-caveolae containing cells such as lymphocytes and neuronal cells. In skin, caveolae organelles are particularly abundant in keratinocytes within the basal layer but also in the hair follicle (Capozza *et al.* 2003). Therefore, in this study, caveolar and non-caveolar rafts are not distinguished, and the microdomains isolated from cell cultures representing basal keratinocytes are generally named rafts.

To study the localization of these proteins, equal amounts of protein (3  $\mu$ g) from the seven fractions obtained within the isolation procedure of rafts by OptiPrep gradient ultracentrifugation (section 2.3.4), were analyzed by western blotting.

As shown in Figure 2.4a, caveolin-1, the 22 kDA structural component of caveolae was detected in the fractions 1 through 3 (the low density fractions) of the gradient as described from the top to the bottom of the centrifugal tube. Since the 2<sup>nd</sup> fraction was highly enriched in caveolin-1 as compared to the other two fractions (fraction 1 and 3), I have used the 2<sup>nd</sup> fraction as the raft fraction to be analyzed.

To determine whether these fractions were also enriched in other markers for lipid rafts, the seven isolated fractions were screened for the presence of such a protein. The data in Figure 2.4b demonstrate that flotillin-1 was similarly enriched in the 2<sup>nd</sup> fraction.

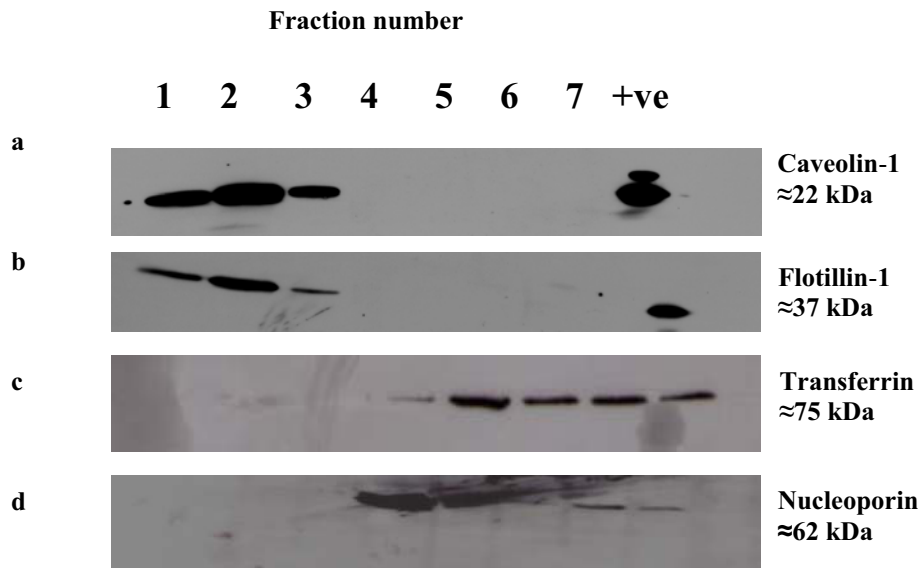


**Figure 2.4: Distribution of caveolin-1, flotillin-1, transferrin, and nucleoporin across OptiPrep gradient.** Seven fractions (numbered as 1 to 7, from the top of the gradient to the bottom) were separated in the process of raft isolation (Brown and Rose, 1992) from HaCaT cells. (a) and (b) 3  $\mu$ g protein in 100  $\mu$ l volume from each fraction was subjected to western blot analysis on 16% PAGE for (a) caveolin-1 (b) flotillin-1. (+C) indicates the positive control, which was 20  $\mu$ l of an endothelial cell lysate (Transduction Laboratories), marked signals were seen at  $\approx$  22 kDa in the fractions 1, 2, and 3 for caveolin-1 and at  $\approx$ 37 kDa for flotillin-1. (c) and (d) 8  $\mu$ g protein in 100  $\mu$ l volume from each fraction were subjected to western blot analysis on 11% PAGE. (+ve) indicates the positive control sample, which was 20  $\mu$ l of an A431 cell lysate (Transduction Laboratories), marked signals were seen in the fractions 4 through 7.

As it can be seen from Figure 2.4c, this raft fraction (2<sup>nd</sup> fraction) contains no transferrin receptor protein, which is a non-raft plasma membrane protein (Harder *et al.* 1998) indicating that a good separation of raft fractions from the non-raft plasma membrane was obtained by the procedure used in this work. Moreover, this raft fraction appears to be free of contamination by nuclear membranes (Figure 2.4d), as nucleoporin p62 was absent in this fraction. Nucleoporin p62 is a glycoprotein localized on the nuclear envelope and is involved in the nuclear import of proteins (Paschal & Gerace 1995).

The raft fractions isolated also contained no calnexin (Figure 2.5a), a calcium binding protein localized to the membrane of the endoplasmic reticulum (Tjoelker *et al.* 1994), and no GRASP65 (Golgi reassembly stacking protein of 65 kDa; (Wang *et al.* 2005)) a peripheral membrane protein associated with the Golgi apparatus (Figure 2.5b). Since the employed method (Brown & Rose 1992) provided a clean preparation of rafts free from contaminating intracellular membranes, we used this method for further studies with regards to the role of lipid rafts in UVA induced signaling.

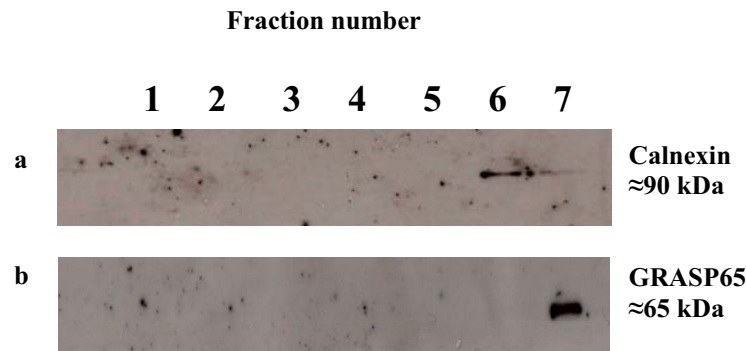


**Figure 2.5: Distribution of calnexin and GRASP65 receptor protein across OptiPrep gradient.** Seven fractions (numbered as 1 to 7, from the top of the gradient to the bottom) were separated in the process of raft isolation (Brown and Rose, 1992) from HaCaT cells. 8 µg of protein in 100 µl volume from each fraction was subjected to western blot analysis on 11% PAGE. A marked signal was seen at ≈ 90 kDa in fractions 6 and 7 for calnexin and at ≈65 kDa in fraction 7 for GRASP65.

## 2.7. Gene expression analysis by real time-PCR

Gene expression is a process by which the DNA sequence of a gene is converted in a functional structure via transcription from DNA into mRNA and via translation from mRNA into a protein. This is a multi-step process which can be regulated on the level of transcription, translation and even post-translationally. In molecular biology, real time polymerase chain reaction is a technique to amplify and simultaneously quantify a targeted DNA molecule. In combination with reverse transcription, this method can be used to quantify mRNA.

In order to robustly detect and quantify gene expression from small amounts of RNA, amplification of the gene transcript is necessary. Real time-PCR is a technique applied to quantify the transcribed cDNA, which is synthesized from mRNA by reverse transcriptase.

### 2.7.1. RNA isolation

The starting material for gene expression analysis by real time-PCR is total RNA, which was isolated from primary keratinocytes or HaCaT cells grown in 6 wells microplates (Greiner Bio One) using peqGOLD Total RNA Kit (Peqlab Biotechnologie). At a given time point, cells are harvested as given by the experimental design. Cells were washed with 2 ml PBS buffer, shock-frozen by dipping in liquid nitrogen and kept at -80° C until required. The peqGOLD Total RNA Kits use the reversible binding property of a silica-based material, the HiBind<sup>®</sup> matrix. This property combined with the high speed of mini-column spin technology allows more than 100 µg of RNA molecules bind to the matrix. Cells were first lysed under denaturing conditions that inactivate RNases. Samples were

then applied to the HiBind<sup>®</sup> spin columns to which total RNA binds, while cellular debris and other contaminants were effectively washed out. According to the manufacturer's instructions total RNA isolation was performed by lysing the cells with 350  $\mu$ l of TRK lysis buffer containing 2 %  $\beta$ -mercaptoethanol. The lysate was transferred into a shredder spin column placed in a 2 ml collection tube, and centrifuged at 12.000 x g for 1 min at R.T. 350  $\mu$ l of 70 % ethanol were mixed with the lysate. The mixture was loaded onto the membrane of a HiBind<sup>®</sup> spin column which was placed in a 2 ml collection tube. The column was then centrifuged at 10.000 x g for 1 min. The flow-through was discarded and 600  $\mu$ l Wash Buffer I were added to the column which was then centrifuged at 10.000 x g for 1 min. The flow-through and the used collection tubes were discarded. The column was set into a new 2 ml collection tube and 500  $\mu$ l Wash Buffer II were added to the column. The column was centrifuged at 10.000 x g for 1 min, this washing step was repeated two times. To ensure that no ethanol was carried over during RNA elution the HiBind<sup>®</sup> spin column containing RNA was dried by centrifugation at 10.000 x g for 1 min and then placed in a new 1.5 ml Eppendorf test tube. To elute RNA, 60  $\mu$ l of RNase-free water was added directly to the column membrane and the column was then centrifuged for 1 min at 10.000 x g.

Determination of RNA concentration was done using an Eppendorf BioPhotometer by measuring the absorption at 260/280 nm in plastic cuvettes, where 1 absorption unit at 260 nm represents 40  $\mu$ g/ml. Approximately 50  $\mu$ g/ $\mu$ l RNA was used for cDNA synthesis.

### **2.7.2. cDNA-synthesis by RT-PCR**

Complementary DNA synthesis is a process where RNA is converted to DNA using reverse transcriptase. GeneAMP<sup>®</sup>RNA PCR Core Kit (Applied Biosystems) was used to reversely transcribe isolated total RNA with M-MLV (Moloney Murine Leukemia Virus) reverse transcriptase (Invitrogen). This transcriptase uses single-stranded RNA to synthesize a cDNA strand in the presence of random primer oligonucleotides (hexamer) under specific conditions. The reaction mixture contained the following components:

---

 1 x cDNA synthesis reaction mixture
 

---

 1  $\mu$ l random-hexamer-primer (50 ng)

 1  $\mu$ l dNTP-Mix (1mM each)

50 ng total RNA

 4  $\mu$ l 1 x reaction buffer II (50 mM KCl, 10 mM Tris-HCL pH 8.3)

 2  $\mu$ l DDT (0.1 M)

 1  $\mu$ l RNase inhibitor (1 U/ $\mu$ l)

 1  $\mu$ l MuLV Reverse Transcriptase (2.5 U/ $\mu$ l)

 Ad 20 $\mu$ l RNase free Aqua bidest.
 

---

According to the number of the genes which are under investigation the end volume of the cDNA synthesis reaction can be varied from 20  $\mu$ l for one gene to 20 \* X  $\mu$ l, where X is the number of genes to be analysed.

The reverse transcriptase reaction was carried out at 42°C for 60 min, followed by denaturation at 95°C for 5 min at the end of this process, the reaction vessels were immediately cooled to 4°C. This reaction was carried out in a thermocycler (PTC-200, MJ Research).

### 2.7.3. Quantification of gene expression via real time-PCR analysis

All real-time PCR systems rely upon the detection and quantification of a fluorescent reporter, the signal of which increases in direct proportion to the amount of PCR product in a reaction. The simplest and most economical format is the double-strand DNA-specific dye SYBR® Green (Molecular Probes) which has excitation and emission maxima of 494 nm and 521 nm. SYBR Green binds double-stranded DNA, and upon excitation emits light. Thus, as a PCR product accumulates, fluorescence increases. The advantages of SYBR Green are that it is inexpensive, easy to use, and sensitive. The disadvantage is that SYBR Green will bind to any double-stranded DNA in the reaction, including primer-dimers and other non-specific reaction products, which results in an overestimation of the target concentration. For single PCR product reactions with well designed primers, SYBR Green works extremely well, with spurious non-specific background only showing up in very late cycles. Quantification of gene expression was done using a specific primer pair for the gene of interest and a specific primer pair for a so-called housekeeping gene. The latter is supposed to be constitutively expressed because it codes for molecules that are necessary for basic maintenance and essential cellular functions and is therefore suitable as

an internal control. We used 18S rRNA, because it turned out to be the most stable housekeeping gene and hence superior for normalization in comparative analysis of mRNA expression levels in human keratinocytes as compared to  $\beta$ -actin or glyceraldehyde-3-phosphate dehydrogenase (GAPDH) (Bas *et al.* 2004). Three independent experiments were performed with 4 determinations each and the mean value of these was calculated. The PCR reactions were carried out on an Opticon 1 (MJ Research, Waltham, MA, USA) using SYBR Green<sup>®</sup> PCR Master Mix (Applied Biosystems, Darmstadt, Germany). For comparison of relative expression in real-time PCR control cells and treated cells the  $2^{-\Delta\Delta C(T)}$  method according to Livak & Schmittgen (Livak & Schmittgen 2001) was used. In detail, real time-PCR analyzes the relative abundance of PCR products during the exponential phase, in which reagents are not limited. During the exponential phase, PCR products will ideally double during each cycle if the amplification efficiency is perfect. It is possible to make the PCR amplification efficiency close to 100 % in the exponential phases of PCR reactions, if the PCR conditions, primer characteristics, template purity, and amplicon lengths are optimal. Therein lies the ability to compare initial abundance of template, e.g., to compare transcript abundance between two different samples, since the PCR product quantity in the exponential phase correlates with the initial template abundance. The relative quantification can be achieved with analyzing so-called ‘Ct value’. In the real-time PCR data processing, a baseline and a threshold can be set for further analysis. The cycle number at the threshold level of log-based fluorescence is defined as Ct number (Figure 2.6), which is the observed value in most real-time PCR experiments, and therefore the primary statistical metric of interest.

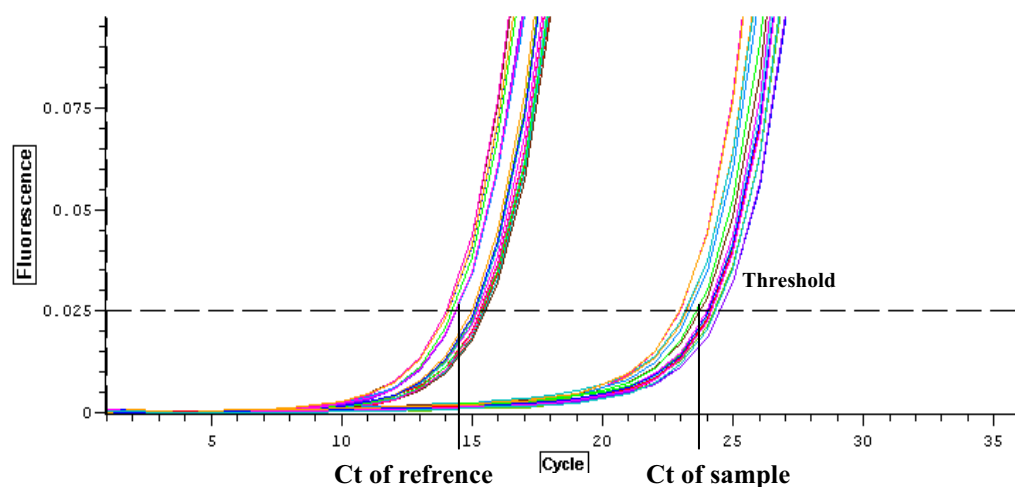


**Figure 2.6: Definition of Ct value**

The  $2^{-(\Delta\Delta C_T)}$  method, is also known as the comparative Ct method. It involves comparing the Ct values of the samples of interest with a control or calibrator such as a non-treated sample. The Ct values of both the calibrator and the samples of interest are normalized to an appropriate endogenous housekeeping gene. where  $[\Delta\Delta]Ct = [\Delta]Ct_{\text{sample}} - [\Delta]Ct_{\text{reference}}$

Here,  $[\Delta]Ct_{\text{sample}}$  is the Ct value for any sample normalized to the endogenous housekeeping gene and  $[\Delta]Ct_{\text{reference}}$  is the Ct value for the calibrator also normalized to the endogenous housekeeping gene.

The volume of each PCR reaction was 25  $\mu\text{l}$  made from 3  $\mu\text{l}$  cDNA and 22  $\mu\text{l}$  SYBR Green pre-mix. The pre-mix for 12 reactions was made as follows:

**Table 2:16: Composition of SYBR Green pre-mix**

Ingredient	Volume
SYBR Green	125 $\mu\text{l}$
Primer A	10 $\mu\text{l}$
Primer B	10 $\mu\text{l}$
HPLC-H <sub>2</sub> O	75 $\mu\text{l}$

The quantitative RT-PCR was performed with the following program.

**Table 2.17: RT-PCR program**

Temperature (°C)	Time (min)	objective
94	10	Hot start Taq polymerase activation
95	0.20	Denaturation
55	0.20	Annealing
72	0.5	Extension

#### 2.7.4. Determination of primer sequences for real time-PCR

For each gene, a specific PCR primer pair was designed using Primer Express 2.0 software (Applied Biosystems, Darmstadt, Germany) based on the cDNA sequence published as referenced in Table 2.18. The primers were synthesized by Eurofins MWG Operon, Ebersberg, Germany and supplied in a highly purified salt-free form.

**Table 2.18: Sequences of the primer pairs for real time PCR**

Gene	Primer Pair	Reference
<b>18S rRNA</b>	5'-GCCGCTAGAGGTGAAATTCTTG-3' 5'-CATTCTTGGCAAATGCTTTTCG-3'	(McCallum & Maden 1985)
<b>ICAM-1</b>	5'-CCTGGCACCCAGCACAAT-3' 5'-GCCGATCCACACGGAGTACT-3'	(Staunton <i>et al.</i> 1988)
<b>Neu3</b>	5'-TGCTGGATGTTTCATGGAGTGA-3' 5'-CAAATGTGGCCCAGTGCTT-3'	(Monti <i>et al.</i> 2000)

#### 2.8. Gel electrophoresis mobility shift assay

Interaction of proteins with DNA is central to the control of many cellular processes including DNA replication, recombination, repair, and transcription. One technique that is important for studying gene regulation and determining protein / DNA interactions is the electrophoretic mobility shift assay (EMSA). Based on the observation that protein / DNA complexes migrate more slowly than free DNA molecules when subjected to non-denaturing polyacrylamide or agarose gel electrophoresis (Fried & Crothers 1981). This technique determines if a protein or mixture of proteins is capable of binding to a given DNA sequence. For visualization purposes, the nucleic acid fragment is usually labeled with a radioactive label (Garner & Revzin 1981).

It has previously been shown that a dose of 30 J/cm<sup>2</sup> UVA radiation leads to activation of the transcription factor AP-2 in human keratinocytes and subsequent upregulation of ICAM-1 gene expression (Grether-Beck *et al.* 1996). The sequence used for AP-2 binding was derived from the ICAM-1 promoter (Stade *et al.* 1990). This sequence was (5'-GACCCTCTCGGCCCGGGCACCCCT-3') which was synthesised by the company Operon and delivered as salt free purified preparation.



### 2.8.1. Radiolabelling of AP-2 oligonucleotide at 5' end

Oligonucleotides can be radiolabelled at the 5' end by T4 polynucleotide kinase (PNK), which catalyzes the transfer of the  $\gamma$ -phosphate from [ $\gamma$ - $^{32}$ P] ATP to a free 5' hydroxyl group. Chemically synthesized oligonucleotides have a free 5'-hydroxyl group.

**Table 2.19: Composition of the radiolabelling reaction**

Ingredient	Volume
Water	7 $\mu$ l
10x PNK buffer	2 $\mu$ l
Oligonucleotide (20 pmol)	5 $\mu$ l
[ $\gamma$ - $^{32}$ P]-ATP (20pmol)	5 $\mu$ l
T4 PNK-kinase (10-15 units)	1 $\mu$ l

10x PNK buffer is composed of 700 mM Tris-HCl (pH 7,6); 200 mM MgCl<sub>2</sub> and 50 mM DTT.

The radiolabelling reaction was carried out in a 1.5 ml safelock Eppendorf test tube at 37° C. After 30 min incubation, the labelling reaction was stopped by adding 14  $\mu$ l STE buffer.

**Table 2.20: Composition of STE buffer**

Ingredient	Final concentration
NaCl	100 mM
EDTA	1 mM
Tris-HCl (pH 8)	10 mM

### 2.8.2. Purification of the radiolabelled oligonucleotide

Purification of the radiolabelled oligonucleotide was performed by NucleoTrap®-kit from Macherey-Nagel, according to the manufacturer instructions, 600  $\mu$ l NT2 buffer were well mixed with 150  $\mu$ l labelled oligonucleotide. 20  $\mu$ l NucleoTrap® suspension containing silica-matrix were incubated with the labelled oligonucleotide for 10 min at R.T. This suspension was then centrifuged with 10.000 x g for 30 sec at R.T. The produced pellet was then resuspended with 600  $\mu$ l NT3 buffer and the suspension was centrifuged with 10.000 x g for 30 sec at R.T. This step was performed twice. The produced silica-matrix pellet was then dried for 15 min at 37°C. To elute the bound DNA from the silica matrix, 50  $\mu$ l TE buffer was added and incubated with the pellet for 15 min at R.T. This suspension was then centrifuged with 10.000 x g for 30 sec at R.T. The produced supernatant was transferred into a new 1.5 ml test tube (e.g. Eppendorf test tube). This step

was repeated and the produced supernatant was collected with the previous one and centrifuged for 30 sec with 10.000 x g at R.T. The produced supernatant (which contains the purified radiolabelled oligonucleotide) was kept at -20°C.

### 2.8.3. The binding reaction

Non-specific competitor DNA such as poly (dI-dC) is included in the binding reaction to minimize the binding of non-specific proteins to the radiolabelled oligonucleotide. These repetitive polymers provide an excess of non-specific sites to adsorb proteins in crude lysates that will bind to any general DNA sequence (Larouche *et al.* 1996). The order of addition of reagents to the binding reaction is important in that, to maximize its effectiveness, the competitor DNA must be added to the reaction along with the extract prior to the radiolabelled oligonucleotide. To stabilize the protein / DNA complex, BSA and Ficoll were included in the binding reaction.

**Table 2.21: Composition of the binding reaction in EMSA**

Ingredient	Amount
5x Ficoll-binding buffer	4 µl
1 mg/ml Poly(dI-dC)	2 µl
1 mg/ml BSA	2 µl
Nuclear protein	1-2 µg Protein
labelled oligonucleotide( 20.000 cpm/µl)	4 µl
Ad 20µl Aqua dest.	

**Table 2.22: Composition of 5x Ficoll-binding buffer**

Substance	Concentration
HEPES (pH 7.5)	20 mM
KCl	50 mM
MgCl <sub>2</sub>	2.5 mM
DDT	1 mM
Ficoll	20 % (v/v)

### 2.8.4. Gel retardation electrophoresis

Non-denaturing TBE-polyacrylamide gels are used to resolve protein / DNA complexes from free DNA. The polyacrylamide percentage required depends on the size of the target DNA and the nature of the protein(s) binding to it. 4 % polyacrylamide gel was used to

study the AP-2 activation upon UVA radiation. The ingredients for gel preparation were given in Table 2.23.

Gels are pre-run at a constant voltage (100 V for 30 min). The primary reasons for pre-running gels are, to remove all traces of ammonium persulfate (used to polymerize polyacrylamide gels), to distribute / equilibrate any special stabilizing factors or ions that were added to the electrophoresis buffer, and to ensure a constant gel temperature (Pierce protein research products 2009).

Before loading samples onto the gel, 5  $\mu$ l of bromophenol dye (25 % Ficoll, 0.05 % xylene cyanol, 0.05 % bromophenol blue) were mixed with the sample. 25  $\mu$ l of each sample were loaded onto the gel together with a free radiolabelled oligonucleotide.

**Table 2.23: Composition of Non-denaturing TBE-polyacrylamide**

Substance	Volume
40% (w/v) Acrylamide/Bisacrylamide solution (29:1)	10 ml
Aqua dest.	70 ml
5x TBE	20 ml
10 % APS	700 $\mu$ l
TEMED	35 $\mu$ l

The protein / DNA complexes were separated under 200 V for about 1 hour in the electrophoresis buffer 1x TBE buffer (89 mM Tris; 89 mM H<sub>3</sub>BO<sub>3</sub>; 20 mM EDTA). After that the gels were dried under vacuum for at least 2 hours at 70°C. The detection of the signal was performed by exposing the dry gel to an X-ray film (Fudji, 18 x 24 cm) at least for 12 hours.

### **2.9. Enzymatic activity assay of the plasma membrane-associated neuraminidase (Neu3)**

The neuraminidase reaction is an essential step of the degradation of gangliosides. Neuraminidases of mammalian origin have been implicated not only in lysosomal catabolism but also in modulation of functional molecules involved in many biological processes. The plasma membrane-associated neuraminidase (Neu3) has been found to be clearly distinct from cytosolic (Neu2) and lysosomal neuraminidase (Neu1) with regards to enzymatic properties. Neuraminidase 3 has a strict substrate specificity for the hydrolysis

of gangliosides under acidic pH, and does not degrade glycoproteins or oligosaccharides to any great extent (Miyagi *et al.* 2008; Monti *et al.* 2002).

The cellular membrane fraction and the raft preparations were used routinely for Neu3 activity assay with the ganglioside GM3 as substrate. The assay was performed immediately after the preparation of the neuraminidase 3 containing cellular extracts due to the high instability of the enzyme.

Owing to the low protein contents of rafts, raft preparations were concentrated using ultra-4 centrifugal filter units (Millipore), which are disposable ultrafiltration devices. These devices are available in different molecular weight sizes. For concentrating samples containing neuraminidase a 10 kDa cellulose membrane filter devices with 2 ml volume (Ultracel-10 membrane) was used according to the manufacturer's instructions.

The quantification of neuraminidase 3 is based on the measurement of sialic acid released from the substrate GM3. One unit of neuraminidase 3 was defined as the amount of enzyme catalyzing the release of one nmol of sialic acid per hour at 37°C.

The enzyme containing cellular preparation was incubated with bovine milk derived GM3 for one hour. The reaction volume was 200 µl, which also included 0.1 % (v/v) Triton X-100, 1 % BSA, and 20 mM sodium acetate buffer (pH 3.8). These ingredients were well mixed and the glass tubes containing them were closed and allowed to stand for one hour at 37 °C. At the end of the incubation period, the reaction was stopped by immersing the tubes in ice for 3 min. Preliminary measurement of neuraminidase 3 activity was also performed at pH 5, no differences between the measured activities under the two pH conditions have been observed.

All enzyme assays were performed in triplet. Sample counts were corrected for appropriate blank counts.

A positive control containing a purified preparation of neuraminidase from *Clostridium perfringens* (Roche) was also included in the assay. The neuraminidase of *Clostridium perfringens* has a broad substrate specificity including GM3. This enzyme preparation was allowed to run in the same manner as the extracts from the keratinocytes.

Boiled cellular extract (membrane fraction or raft preparation) was allowed to run a long with the samples in the same assay. Boiling of the cellular extracts for 30 min at 95°C prior the assay led to complete abolishment of the observed sialic acid release by neuraminidase 3 activation (negative control). This observation has been previously reported by (Sakarya *et al.* 2004) where the clostridial neuraminidase activity was diminished by prior boiling.

The quantity of the released sialic acid (*N*-acetylneuraminic acid) was determined colorimetrically by the thiobarbituric / periodic acid method, also termed Warren method. This method is the most widely used for quantitative analysis of the released sialic acid in measuring neuraminidase 3 activity. This is due to its sensitivity and specificity (Greffard *et al.* 1997; Ha *et al.* 2004; Miyagi *et al.* 1999; Monti *et al.* 2000; Wang *et al.* 2004; Young-Sun & Gil-Ja 1995).

The method of thiobarbituric / periodic acid was first introduced by Warren (1959). A special feature of this method is that only free sialic acids are estimated (Paerels & Schut 1965; Schauer & Corfield 1982). The reaction mechanism is based on oxidation of free sialic acid by periodic acid under strong acidic conditions. This step leads to the formation of a prechromogen, a six carbon aldehyde (I), which then yields the chromogen  $\beta$ -formyl pyrovic acid (III) by aldol cleavage between the carbon atoms 4 and 5 (Figure 2.7). This chromogen reacts with thiobarbituric acid to produce the red chromophore. An excess of sodium arsenite is used to destroy the periodate present. The extraction of the pink pigment formed in the aqueous solution into an organic solvent serves to stabilize and intensify the chromophore for measurement (Schauer & Corfield 1982).

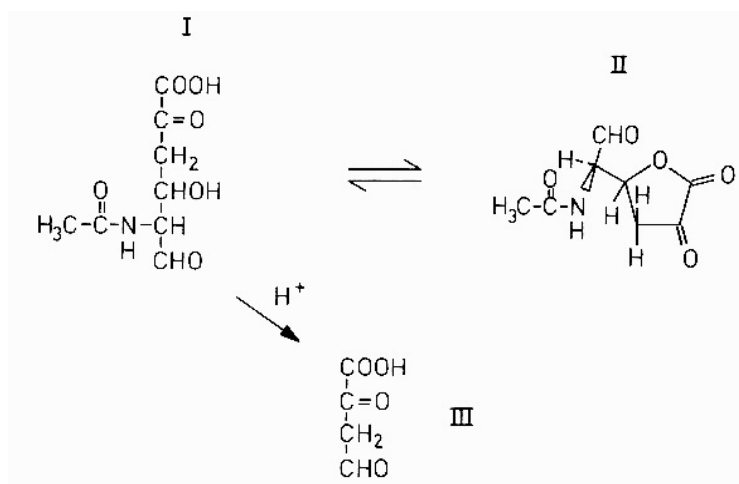


**Figure 2.7: Compounds formed during the oxidation step of periodic acid / thiobarbituric acid assay.** The six carbon aldehyde (I) and the hypothetical lactone (II) give rise to the chromogen  $\beta$ -formyl pyrovic acid (III) (Schauer & Corfield 1982).

In detail, 100  $\mu$ l of 0.2 M sodium (meta) periodate in 9 M phosphoric acid were added to the 200  $\mu$ l sample in a glass test tube. The tubes were allowed to stay at R.T for 20 min, then 1 ml of 10 % (w/v) sodium arsenite, in 0.5 M sodium sulphate-0.1 N H<sub>2</sub>SO<sub>4</sub> solution, was added. The tubes were shaken until the brown colour disappeared and 2.5 ml of 0.6 % (w/v) 2-thiobarbituric acid in 0.5 M sodium sulfate were added. After good vortexing, the tubes were then closed and placed in a vigorously boiling water bath for

30 min. After that, the tubes were placed on ice for 5 min and 1 ml of their content was transferred to other test tubes, each containing 1 ml of cyclohexanone. The tubes were vortexed and centrifuged with 150 x g for 3 min at R.T. The optical density of the produced red layer of the cyclohexanone was measured at 549 nm. In order to eliminate the interference that may arise from the presence of 2-deoxyribose, and since the light absorbance of this substance at 549 nm is considerable, the optical density of the sample is measured also at 532 nm. Then the concentration of sialic acid present in each sample is calculated by inserting the obtained optical density values in the following equation.

$$\mu\text{Moles Sialic acid} = 0.0209 \times \text{O.D}_{549} - 0.0076 \times \text{O.D}_{532}$$

**Table 2.24: Compounds and their sources used in neuraminidase assay**

Substance	Manufacturer / Supplier
Sodium acetate	Sigma-Aldrich
Sodium arsenite	Sigma-Aldrich
Sodium (meta) periodate	Sigma-Aldrich
Sodium sulfate	Sigma-Aldrich
Thiobarbituric acid	Sigma-Aldrich
Neuraminidase from <i>Clostridium perfringens</i>	Roche
Bovine serum albumin fraction IV (BSA)	Sigma-Aldrich
Triton 100-X	Sigma-Aldrich
GM3: ganglioside from bovine brain	Alexis

To determine whether the lysosomal neuraminidase (Neu1), which might contaminate the membrane fraction, was also affected by exposure to UVA irradiation, the isolated cellular membrane fraction was analyzed for neuraminidase activity towards the glycoprotein fetuin at pH 5 using the Amplex® Red neuraminidase assay kit from Invitrogen. We could not detect any marked difference between the control sample and the UVA-treated sample. This could indicate that the observed increase in activity in the membrane fraction upon UVA treatment was mainly due to Neu3, since Neu3 had no activity against fetuin (Ha *et al.* 2004; Monti *et al.* 2000).

## 2.9. Protein determination

### 2.9.1. Bradford test for quantification of protein

This assay is based on the binding specificity of the acidic dye Coomassie® Brilliant Blue-G250 (Figure 2.8) to primarily basic and aromatic amino acid residues, especially arginine (Bradford 1976). A differential colour change of a dye occurs in response to various concentrations of protein. The absorbance maximum for an acidic solution of Coomassie® Brilliant Blue G-250 dye shifts from 465 nm to 595 nm when binding to protein occurs. The absorbance of light by the dye-protein complex at 595 nm is proportional to the amount of protein bound over a limited range (0.2-20 µg). Comparison to a standard curve using BSA provides a relative measurement of protein concentration. A calibration curve was prepared by plotting the absorbance at 595 nm against a set of standard samples of known concentrations of BSA (1, 2, 5, 10, 20, 30 µg).

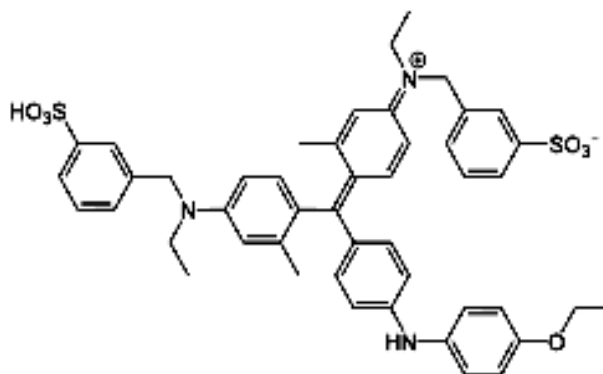


Figure 2.8: Chemical structure of Coomassie® Brilliant Blue G-250

Interferences may be caused by chemical-protein and / or chemical-dye interactions such as basic buffer conditions and detergents (SDS>0.1 %, Triton X-100>0.1 %) (Zor & Selinger 1996).

In this work, 10 µl of the sample were added to 1000 µl Bradford reagent in 1.5 ml Eppendorf test tube. After good mixing, the reaction was allowed to stand for 30 min at R.T in a dark place, followed by measuring the optical density at 595 nm. The absorbance was corrected for a blank value prepared with 1000 µl Bradford reagent and 10 µl H<sub>2</sub>O.

### 2.9.2. BCA protein assay

The BCA protein assay is a detergent-compatible protein assay for colorimetric quantification of total protein (Smith *et al.* 1985). This assay combines the well-known reduction of Cu<sup>2+</sup> to Cu<sup>1+</sup> by protein in an alkaline medium with the highly sensitive and selective colorimetric detection of the cuprous cation (Cu<sup>1+</sup>) by bicinchoninic acid (BCA).

The first step is the chelation of copper with protein in an alkaline environment to form a blue-coloured complex. In this reaction, known as the biuret reaction, peptides containing three or more amino acid residues form a coloured chelate complex with cupric ions in an alkaline environment containing sodium potassium tartrate. This became known as the biuret reaction because a similar complex forms with the organic compound biuret ( $\text{NH}_2\text{-CO-NH-CO-NH}_2$ ) and the cupric ion. Biuret, a product of excess urea and heat, reacts with copper to form a light blue tetradentate complex. In the second step of the colour development reaction, BCA reacts with the cuprous cation ( $\text{Cu}^{1+}$ ) formed in step 1. The purple-coloured reaction product is formed by the chelation of two molecules of BCA with one cuprous ion (Figure 2.9). This complex is water-soluble and exhibits a strong absorbance at 560 nm. The intensity of the colour is proportionally increased as the protein concentration increases. The assay is quite sensitive even for low amounts of protein. Interference with the assay can occur if compounds that reduce copper are present. Also cysteine or cystine, tyrosine, and tryptophan will do that.

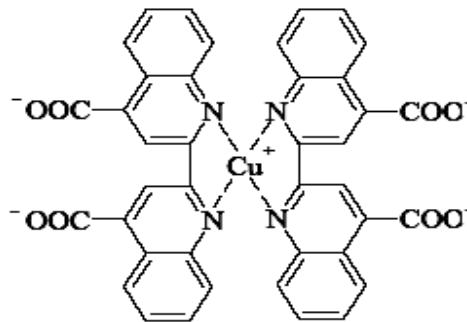


**Figure 2.9: Chemical structure of the chelation complex of two molecules of BCA with one cuprous ion**

Prior to protein quantification working reagents have to be prepared by mixing 50 parts of  $\text{BCA}^{\text{TM}}$  reagent A with 1 part of reagent  $\text{BCA}^{\text{TM}}$ B. 100  $\mu\text{l}$  of sample were added to 2 ml of the working reagent in a test tube. The solution was mixed well and the covered test tubes were allowed to stand for 30 min at 37 °C. After that the absorbance of 1 ml of the solvent was measured at 562 nm. The absorbance was corrected for a blank value prepared with 1 ml  $\text{H}_2\text{O}$ .

A calibration curve was prepared by plotting the absorbance at 562 nm against a set of standard samples of known concentration of BSA ranging from 25  $\mu\text{g/ml}$  to 2000  $\mu\text{g/ml}$ .



### **3. Results**

A large body of evidence suggests that membrane microdomains, also called lipid rafts, act as signaling platforms within the plasma membrane of the cell helping to assemble signaling complexes that control many cellular events. In order to understand the mechanisms by which UVA radiation exerts its detrimental effects on human skin cells, our research group has years ago started to examine the signaling events occurring during irradiation of human keratinocytes with a dose of 30 J/cm<sup>2</sup> UVA. This physiological dose was chosen because it significantly induces UVA stress responses in these cells. As an endpoint, upregulation of intercellular adhesion molecule (ICAM-1) mRNA expression, a marker for inflammation, was used to monitor the stress response (for details see Introduction). Previous studies of our group (Grether-Beck *et al.* 2000) had shown, that UVA radiation-induced gene expression was initiated at the plasma membrane via the non-enzymatic release of the second messenger ceramide. Recently a detailed balance of the lipids within the rafts indicated that besides the described non-enzymatic release of ceramides other mechanisms have to contribute to the amount of ceramide formed. In detail, 30 min after UVA treatment we had observed a decrease of sphingomyelin from about 450 to 200 pmol (from this decrease maximally 250 pmol ceramide could be obtained), based on the lipid equivalent of 150 µg protein, which had been followed by an increase of ceramide from 550 to 950 pmol (=netto 400 pmol), indicating that more than 60% (250 pmol/400 pmol = 62,5%) of the ceramide formed might originate from the non-enzymatic hydrolysis of raft localized sphingomyelin (Grether-Beck *et al.* 2008). This balance also indicates that besides the previously described non-enzymatic generation of ceramides from hydrolysis of sphingomyelin (Grether-Beck *et al.* 2000) an additional mechanism or additional mechanisms of ceramide formation might be involved.

Therefore, the current study aimed to further investigate how ceramides might be formed in rafts and how rafts contribute to the downstream signaling events. More precisely, I have investigated the role of the raft-associated sialidase, also called neuraminidase 3 (Neu3), in the UVA response as well as the consequences of caveolin-1 knockdown on this response in human keratinocytes. To achieve this, I have isolated these microdomains from human primary keratinocytes or from the HaCaT cell line using the method of Brown & Rose (1992) as described in this work under the chapter of Materials and Methods. In addition, high performance thin layer chromatography (HPTLC) analysis was used to quantitatively compare the lipid contents of the rafts isolated from UVA-irradiated and sham-irradiated control keratinocytes.

### 3.1. UVA radiation leads to a decrease of ganglioside GM3 content in rafts and total cell extracts of human keratinocytes

The predominant ganglioside of keratinocyte membranes is GM3, which has been found to influence cellular functions, including adhesion (Paller *et al.* 1993). As hundreds of glycosphingolipid species can be found on the surfaces of mammalian cells, changes in GM3 which is a direct sialylated derivative of lactosylceramide, were representatively studied.

To investigate the effects of UVA radiation on GM3 content of lipid rafts and total cell extracts of human keratinocytes, HaCaT cells were irradiated with a UVA dose of 30 J/cm<sup>2</sup> and harvested 30 min post irradiation. Total cell extracts or lipid rafts were immediately prepared and their GM3 content was assessed by HPTLC analysis.

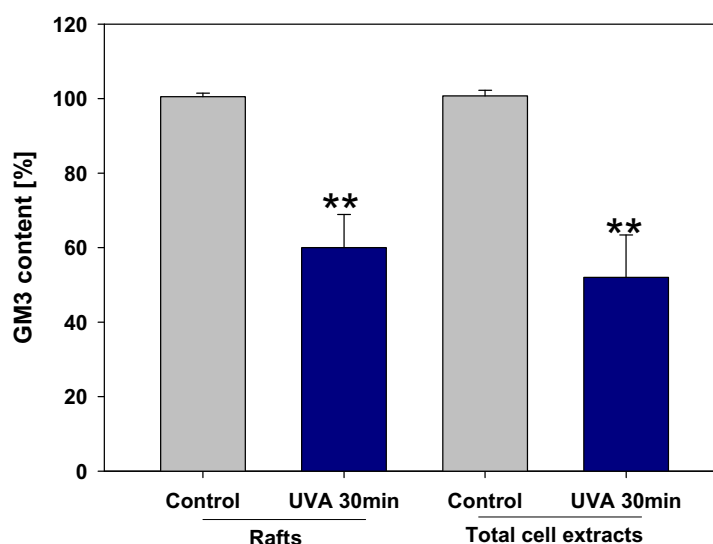


**Figure 3.1: UVA radiation results in a decreased GM3 content in lipid rafts and in total cell extracts.** GM3 content of HaCaT cells, which had been either irradiated with 30 J/cm<sup>2</sup> UVA or left untreated, was determined in lipid rafts and in total extracts. GM3 content was analyzed based on 150 µg protein in rafts and on 500 µg protein in total cell extracts. Controls were set equal to 100%. Data represent mean ± SD of three independent experiments. (\*\* indicates a statistically significant difference compared to untreated control, as determined by paired student's t test, p < 0.01)

As it can be seen in Figure 3.1, exposure of HaCaT cells to UVA radiation results in a significant decrease of GM3 content in lipid rafts and in total cell extracts. GM3 content in lipid rafts was significantly diminished to approximately 60% of that estimated in rafts of unstimulated control cells (set to 100% content). Likewise, GM3 content in total extracts was significantly lowered by UVA exposure to approximately 50% as compared to GM3 content in total extracts prepared from unstimulated control cells (set to 100%).

### **3.1.1. UVA radiation-induced GM3 decrease is mediated by activation of neuraminidase 3**

The amount of gangliosides on the cell surface can be modulated by changing the balance between its biosynthesis and degradation (d'Azzo *et al.* 2006). The biosynthesis of gangliosides takes place in the ER and in the Golgi complex. It is mediated by the action of membrane-bound glycosyltransferases and sialyltransferases, which catalyze the transfer of sugar nucleotide donors to sphingolipid acceptors (see the Introduction chapter). The degradation of gangliosides occurs along the endocytic-lysosomal pathway and is controlled by hydrolytic enzymes that function at acidic pH (Huwiler *et al.* 2000). For the efficient catabolism of these membrane-bound substrates, the water-soluble lysosomal hydrolases require the cooperative action of effector proteins named sphingolipid activator proteins serving as natural detergents. After endosome-lysosome fusion, gangliosides expose their glycan chains to the luminal face of the lysosome, where a lysosomal sialidase converts multisialogangliosides into monosialogangliosides. Finally other hydrolases degrade step by step the sugar residues leading to the formation of the endproducts sphingosine and fatty acids. In previous experiments, we used the lysosomotropic agent chloroquine to change the acidic pH of the lysosome resulting in no change of ceramide formation that has been seen after UVA irradiation, indicating that neither acidic sphingomyelinase (which is localized within this organel) nor lysosomal degradation of gangliosides contributed to ceramide formation (Grether-Beck *et al.* 2005b). Besides the lysosomal degradation of gangliosides, plasma membrane sialidase (neuraminidase 3: Neu3) is the key enzyme for ganglioside hydrolysis at the plasma membrane (Sasaki *et al.* 2003).

Accordingly, one possible mechanism by which gangliosides in rafts can be diminished is the activation of raft-associated ganglioside specific neuraminidase (Neu3). Therefore, we next asked whether the decrease of GM3 content in rafts of irradiated cells is because of this mechanism. For this purpose, the Neu3 activity was measured by determination of the released sialic acid from the substrate ganglioside GM3 (Ha *et al.* 2004; Miyagi *et al.* 2008b; Monti *et al.* 2002). We have first optimized the assay using total cellular membranes prepared as described by Miyagi (Miyagi *et al.* 1999). The released sialic acid was quantified with the sensitive thiobarbituric acid assay (Warren 1959). There, sialic acid is oxidized with sodium periodate in concentrated phosphoric acid resulting in a peroxidation product which is coupled with thiobarbituric acid giving a chromophore to be extractable in cyclohexanone. In total cellular membranes of primary human keratinocytes as well as in HaCaT cells, UVA irradiation resulted in a marked increase in Neu3 activity. A comparison between the amount

of Neu3 measured in both cell types as given in Table 3.1 indicates that HaCaT cells and primary human keratinocytes contain similar amounts of Neu3 activity. Although the content in HaCaTs was slightly higher by trend, the difference was statistically not significant as measured by student's t test.

**Table 3.1: Effect of UVA irradiation on Neu3 activity in total cell extracts prepared from human keratinocytes.**

<b>Time post UVA irradiation</b>	<b>Primary human keratinocytes</b>	<b>HaCaT cells</b>
	Units/mg total protein (Mean $\pm$ SD, n=3)	
Unirradiated	2.2 $\pm$ 0.3	3.1 $\pm$ 0.2
0.5 h	9.8 $\pm$ 1.0	11.9 $\pm$ 0.4
8 h	5.5 $\pm$ 1.4	5.2 $\pm$ 0.7
24 h	4.8 $\pm$ 0.9	7.3 $\pm$ 1.0

Keratinocytes were either left untreated or irradiated with UVA (30 J/cm<sup>2</sup>). Cells were harvested after 0.5 h, 8 h, or 24 h post irradiation (30 J/cm<sup>2</sup>). Enzyme activity was detected by thiobarbituric acid assay (Warren 1959). One unit Neu3 activity considered to be responsible for release of 1 nmol sialic acid from GM3 per hour per 1 mg total protein at 37 C° and pH 3.8.

As shown in Figure 3.2a, the relative activity of Neu3 in total cellular membranes after 30 min post irradiation significantly exceeded that of the control cells approximately 3.5-fold. In contrast, the enzyme activity measured in extracts harvested 8 h or 24 h post UVA treatment was significantly decreased as compared to the early time point 30 min post UVA irradiation. Nevertheless, the measured enzyme activity in extracts harvested at 8 h or 24 h in irradiated cells is significantly increased as compared to the unirradiated control cells.

Similarly, as can be seen in Figure 3.2b, UVA irradiation results in an approximately 3-fold increase of Neu3 activity in rafts from HaCaT cells, as measured after 30 min post irradiation. The specific enzyme activity was found to be 5.6  $\pm$  0.7 U/mg total protein (mean  $\pm$  SD, n=3) in rafts from the unstimulated control cells and increased to 16.7  $\pm$  2.4 U/mg total protein (mean  $\pm$  SD, n=3) 30 min post irradiation. In contrast, 8 h or 24 h after irradiation the specific enzyme activity was significantly decreased as compared to the early time point 30 min post UVA irradiation to 5.7  $\pm$  0.9 units/mg total protein and 6.6  $\pm$  1.0 units/mg total protein (mean  $\pm$  SD, n=3), respectively. Neu3 activity in rafts

harvested 8 h after irradiation was not significantly increased as compared to the unirradiated controls.

As cultured cells endocytose about half their plasma membrane per h (Steinman *et al.* 1983), our observation of Neu3 activity at 8 h or 24 h after irradiation may indicate that the membrane is recycled many times during this time.

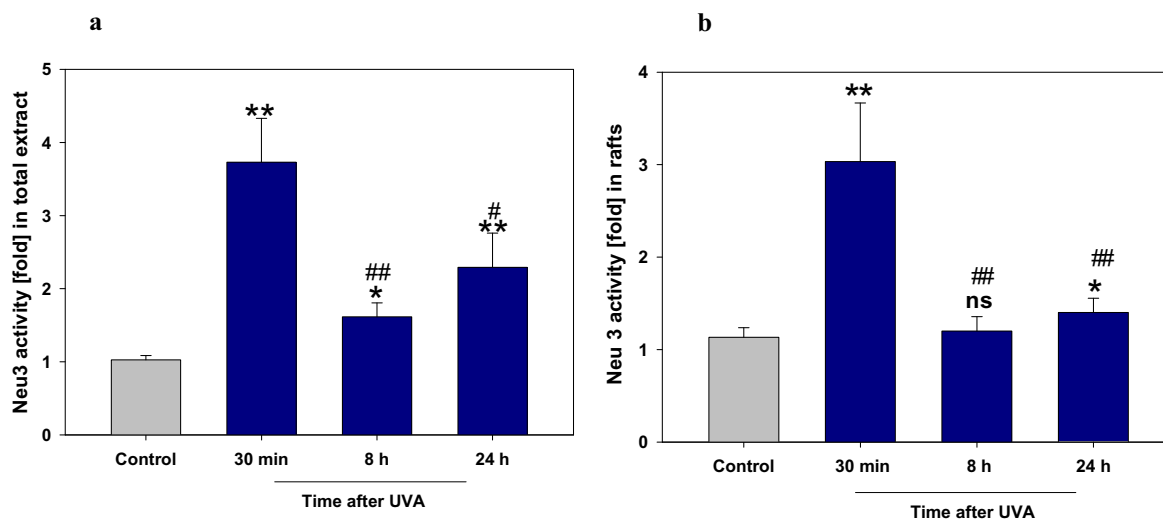


**Figure 3.2: Effect of UVA irradiation on Neu3 activity in total cellular membrane extract and rafts of HaCaT cells.** Neu3 activity was determined with the thiobarbituric acid assay immediately after isolation of (a) total cellular membranes or (b) rafts from HaCaT keratinocytes, which had been either left untreated or irradiated with UVA (30 J/cm<sup>2</sup>) and harvested after 30 min, 8 h, or 24 h post irradiation. Neu3 activity in untreated control cells was set equal to one. Data represent the mean  $\pm$  SD of 3 independent experiments. Paired student's t-test was used for statistical analysis: \* $p$ <0.05, \*\* $p$ <0.01 versus untreated time-matched control, #  $p$ <0.05, ##  $p$ <0.01 versus UVA treatment harvested 30 min post irradiation.

### 3.1.2. Alteration of UVA radiation-induced neuraminidase 3 activity by modulation of cholesterol content and by vitamin E pretreatment

We have recently shown that modulation of cholesterol content in human keratinocytes prior to UVA stimulation has a significant impact on the UVA response (Grether-Beck *et al.* 2008). Depletion of cholesterol increased and preloading with the sterol blocked the UVA effect no matter whether ceramide formation, activation of AP-2 or upregulation of ICAM-1 mRNA were addressed. Therefore, I analyzed, whether modulation of the cholesterol content also has an impact on UVA radiation-induced Neu3 activity. For this purpose, cells were preincubated with 30  $\mu$ M cholesterol for 24 h prior to UVA exposure. This dose was previously shown to inhibit UVA signaling. As shown in Figure 3.3, preloading with cholesterol has significantly lowered Neu3 activity by approximately 50% as compared to UVA exposed cells. In contrast, depletion of cellular cholesterol by pretreatment with 5 mM  $\beta$ -methylcyclodextrin ( $\beta$ MCD) for 2 h prior to irradiation enhanced UVA radiation-induced Neu3 activity.

The UVA-response, such as ceramide formation, AP-2 activation and upregulation of ICAM-1 mRNA is mediated by generation of singlet molecular oxygen (Grether-Beck *et al.* 1996; Grether-Beck *et al.* 2000) and can be blocked by addition of the singlet oxygen quencher vitamin E (Kaiser *et al.* 1990). To evaluate whether singlet oxygen is also involved in UVA radiation-induced activation of Neu3, the enzyme activity was studied after preincubation with 25  $\mu$ M vitamin E ( $\alpha$ -tocopheryl succinate) for 24 h prior to UVA irradiation. As shown in Figure 3.3, pretreatment with vitamin E led to a complete inhibition of UVA radiation-induced Neu3 activity in total cell extracts.

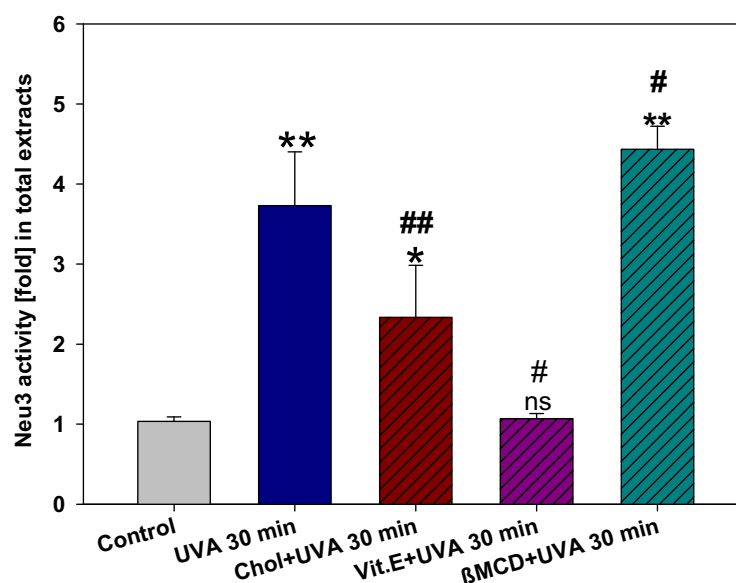


**Figure 3.3: Alteration of UVA radiation-induced Neu3 activity by modulating cholesterol level and by vitamin E pretreatment.** Neu3 activity was assessed in total cell membranes of HaCaT cells which had been harvested 30 min post UVA irradiation. In detail, the cells had been either left untreated (control), or have been UVA-irradiated (30 J/cm<sup>2</sup>) in the presence or absence of either cholesterol,  $\beta$ -methylcyclodextrin ( $\beta$ MCD), or vitamin E. Pretreatments were performed as follows: cholesterol (30  $\mu$ M, 24 h), vitamin E ( $\alpha$ -tocopheryl succinate; 25  $\mu$ M, 24 h),  $\beta$ MCD (5 mM, 2 h). Neu3 activity was assessed immediately after isolation of total cell membranes. Shown is the fold of change in Neu3 activity under each treatment as indicated compared to the activity of untreated control cells (control set equal to 1). Data represent the mean  $\pm$  SD of 3 independent experiments. (\* indicates a statistically significant difference compared to time-matched untreated control, while, # indicates a statistically significant difference as compared to time matched UVA irradiated cells. Paired student's t test was used to calculate the significance of the seen differences, where \* $p$ <0.05, \*\* $p$ <0.01, # $p$ <0.05, and ## $p$ <0.01; ns indicates not significant where  $p$ >0.05 as compared to the untreated control).

### 3.1.3. Inhibition of UVA radiation-induced neuraminidase 3 activity with 2-deoxy-2,3-didehydro-*N*-acetylneuraminic acid (DANA)

To further characterize Neu3-mediated UVA effects in human keratinocytes, cells were pretreated with the neuraminidase inhibitor 2-deoxy-2,3-didehydro-*N*-acetylneuraminic acid (DANA) in a concentration of 10  $\mu$ M. DANA was previously shown to be a potent inhibitor of Neu3 activity (Da Silva *et al.* 2005). In addition, uptake of the inhibitor DANA by cells should be low (Hirschberg *et al.* 1976) and its effect should be directed predominantly towards the plasma membrane neuraminidase rather the intracellular neuraminidase due to its negative charge.

As is shown in Figure 3.4, pretreatment of HaCaT cells with DANA for 1 h prior to irradiation leads to a strong inhibition of UVA radiation-induced Neu3 activity in rafts. Treatment with the inhibitor alone does not affect the basal enzyme activity observed in untreated cells.

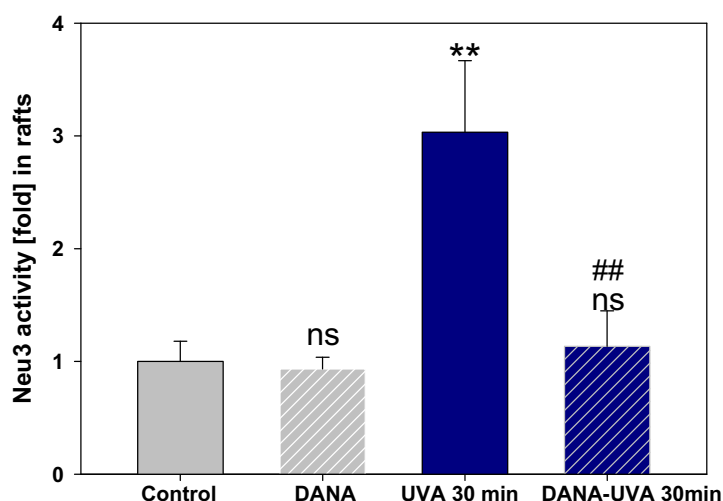


**Figure 3.4: Pretreatment with DANA inhibits UVA radiation-induced Neu3 activity in rafts of human keratinocytes.** Neu3 activity was assessed in human keratinocytes, which were either left untreated (Control), only treated with 10  $\mu$ M DANA for 1 h prior to irradiation, only UVA irradiated (30 J/cm<sup>2</sup>), or were treated with the neuraminidase inhibitor prior to UVA irradiation and harvested 30 min post UVA irradiation. Neu3 activity was assessed immediately after isolation of rafts. Shown is the fold of change in Neu3 activity as compared to the activity in untreated control cells which was set equal to 1. Data represent the mean  $\pm$  SD of 3 independent experiments. Paired student's t-test was used for statistical analysis: \*\* $p$ <0.01 versus untreated time-matched control, ##  $p$ <0.01 versus UVA treated and 30 min post incubated sample; ns indicates not significant where  $p$ >0.05 as compared to the untreated control. DANA, 2,3-didehydro-2-deoxy-*N*-acetylneuraminic acid.

To determine whether the changes in the level of endogenous Neu3 activity upon UVA irradiation correlated with changes in the expression of Neu3 gene, the relative amount of mRNA encoding Neu3 was detected in unstimulated primary human keratinocytes (Control) and in irradiated primary human keratinocytes by real-time PCR using previously reported

sequence information (Wada *et al.* 1999; Monti *et al.* 2000). As shown in Figure 3.5, exposure of primary human keratinocytes to 30 J/cm<sup>2</sup> UVA radiation significantly induced Neu3 expression after 8 h as well as after 24 h post irradiation. Neu3 mRNA was upregulated 2-fold after 8 h and 1.5-fold after 24 h post UVA treatment. This can be correlated with the observed increase in Neu3 enzyme activity in total extracts (see Figure 3.2a). Interestingly, incubation of cells with 10  $\mu$ M DANA for 1 h prior and for other 8 h or 24 h post irradiation results in a significant reduction in UVA radiation-induced Neu3 mRNA upregulation. These observations might also indicate an autocrine ceramide loop as observed for the second ceramide formation due to increased serine palmitoyl transferase formed 8 h post UVA treatment (Grether-Beck *et al.* 2005b). Moreover, lactosylceramide, the direct product of Neu3 activity upon degradation of GM3, also might serve as a second messenger to activate downstream signaling events e.g. activation of Src kinase (Li *et al.* 2001).

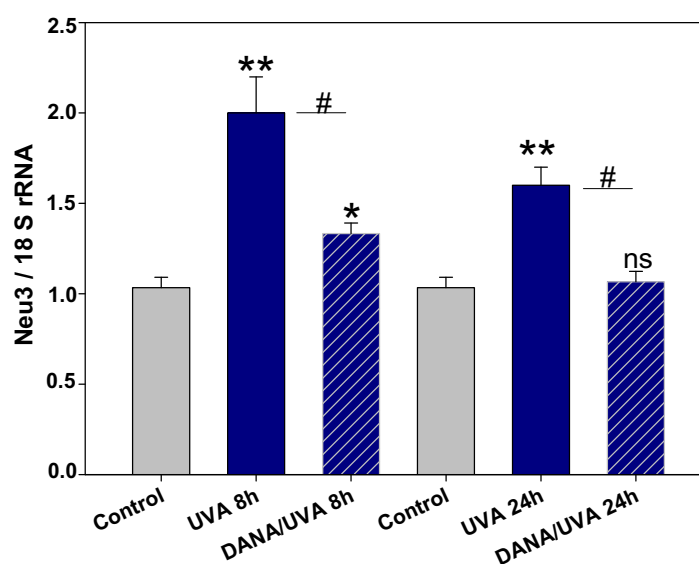


**Figure 3.5: DANA inhibits UVA radiation-induced upregulation of Neu3 mRNA in human keratinocytes.** Neu3 mRNA expression normalized to 18S rRNA was assessed by semi-quantitative real-time PCR in human primary keratinocytes, which were either left untreated (Control), only treated with 10  $\mu$ M DANA for 1 h prior to the irradiation time point, only UVA irradiated (30 J/cm<sup>2</sup>), or were treated with the neuraminidase inhibitor prior to UVA irradiation and harvested either 8 h or 24 h post UVA treatment. Shown is the fold of change in Neu3/18 S rRNA as compared to untreated control cells which were set equal to 1. Data represent the mean  $\pm$  SD of 3 independent experiments. Paired student's t-test was used for statistical analysis: \*\*p<0.01 versus untreated time-matched control, ## p<0.01 versus UVA treated and 30 min post incubated sample; ns indicates not significant where p>0.05 as compared to the untreated control. DANA, 2,3-didehydro-2-deoxy-N-acetylneuraminic acid.



### 3.1.4. Neuraminidase 3 partially contributes to UVA radiation-induced gene expression

In order to assess the effects of inhibiting Neu3 on UVA radiation-induced gene expression in human keratinocytes, we have used the expression of intercellular adhesion molecule-1 (ICAM-1) as a model gene (Grether-Beck *et al.* 1996; Grether-Beck *et al.* 2000). ICAM-1 expression was quantified with real-time PCR based on 18 S rRNA. As it appears in Figure 3.6, in comparison to sham-irradiated control cells, ICAM-1 mRNA expression in primary human keratinocytes was significantly upregulated by about 5-fold after 8 h of UVA irradiation and by about 3-fold after 24 h of irradiation. Interestingly, preincubation of the cells with 10  $\mu$ M DANA for 1 h prior irradiation and additional 8 h or 24 h after irradiation significantly decreased the UVA radiation-induced ICAM-1 mRNA upregulation, because the amount of ICAM-1 expression upon UVA treatment was reduced to about 40% after 8 h and to about 60% after 24 h in presence of DANA.

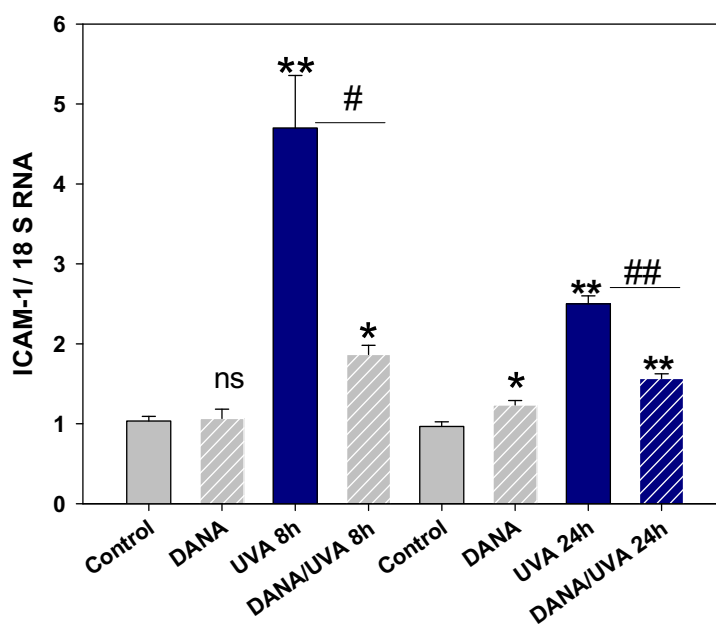


**Figure 3.6: DANA inhibits UVA radiation-induced upregulation of ICAM-1 mRNA expression.**

Expression of ICAM-1 mRNA based on 18 S in human primary keratinocytes was assessed 8 h and 24 h post irradiation with 30 J/cm<sup>2</sup>. Cells were either left untreated (Control), treated with 10  $\mu$ M DANA for 1 h prior to irradiation time point and until harvest (DANA), irradiated with UVA (UVA), or pretreated with 10  $\mu$ M DANA for 1 h prior to irradiation (DANA/UVA). Shown is the fold of change in ICAM-1 mRNA expression in treated cells compared to untreated cells (set equal to 1). Data represent the mean  $\pm$  SD of 3 independent experiments. (\* indicates a statistically significant difference compared to untreated control, while, # indicates a statistically significant difference as compared to time-matched UVA irradiated cells. Paired student's t test was used to calculate the significance of the seen difference, where \* $p$ <0.05, \*\* $p$ < 0.01, #  $p$ <0.05, and ## for  $p$ <0.01).

### 3.1.5. UVA radiation-induced GM3 degradation correlates with formation of lactosylceramide and ceramide

Very recent findings by Grether-Beck (Grether-Beck *et al.* 2008) have shown that ceramide and raft signaling are tightly linked with each other in UVA stress response in human keratinocytes. As ceramides can also be generated at the plasma membrane by degradation of gangliosides such as GM3 via raft associated Neu3 to form lactosylceramide and subsequent further hydrolysis to glucosylceramide and ceramide (Valaperta *et al.* 2006), we next asked whether inhibition of Neu3 activity in UVA-irradiated keratinocytes by pretreatment with DANA can affect the UVA radiation-induced formation of ceramides. In Figure 3.7, the effect of inhibiting Neu3 on UVA radiation-induced GM3 degradation is shown. The observed UVA radiation-induced degradation of GM3 in total cell extract was estimated to be 50%, this decrease was completely abolished upon pretreatment with DANA (Figure 3.7a). Similarly, as it can be seen in Figure 3.7b, UVA irradiation resulted in 40% decrease of GM3 in rafts. DANA pretreatment also abolishes UVA radiation-induced GM3 degradation in rafts completely.

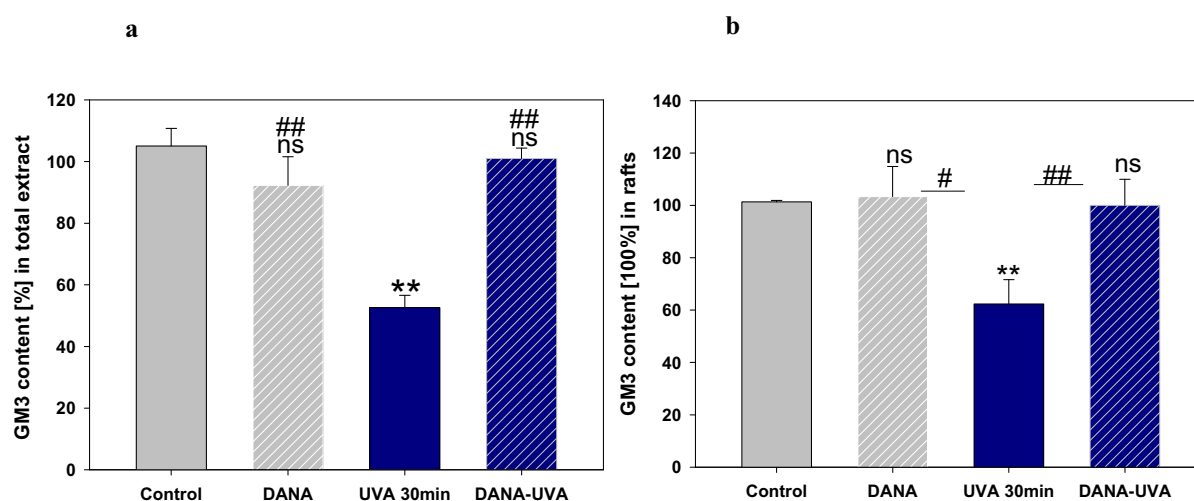


**Figure 3.7: UVA radiation-induced GM3 degradation was inhibited by DANA pretreatment.** (a) GM3 content in total cell extracts or (b) GM3 content in rafts was assessed in human keratinocytes, which had been either left untreated (Control), were pretreated with 10  $\mu$ M DANA for 1 h prior to irradiation with UVA, were irradiated with UVA (30 J/cm<sup>2</sup>) or were pretreated with DANA, irradiated and harvested 30 min after irradiation. Lipid extracts were analyzed in lipid rafts based on 150  $\mu$ g protein, and on 500  $\mu$ g protein in total extracts. Lipid content is given as % change in comparison to controls that were set equal to 100%. Data represent the mean  $\pm$  SD of 3 independent experiments. Paired student's t-test was used for statistical analysis: \* $p$ <0.05, \*\* $p$ <0.01, ns indicates not significant where  $p$ >0.05 as compared to the untreated control; # $p$ <0.05, ## $p$ <0.01 versus UVA treated sample, DANA, 2,3-didehydro-2-deoxy-*N*-acetylneuraminic acid.

To further verify whether the UVA radiation-induced degradation of GM3 also results in a corresponding increase of the expected product lactosylceramide, the formation of the latter

was assessed (Kakugawa *et al.* 2002; Ueno *et al.* 2006; Valaperta *et al.* 2006). In total extracts as well as in rafts, a significant formation of lactosylceramide has been detected upon UVA treatment (Figure 3.8a and Figure 3.8b). While UVA treatment resulted in an increase of LacCer to 160% as compared to the untreated control sample, we only observed an increase to 130% under the pretreatment with the Neu3 inhibitor DANA. In other words, DANA inhibited the LacCer formation by 50% (Figure 3.8a) in total extracts. In rafts, the UVA radiation-induced increase of lactosylceramide in presence of DANA was only 120% as compared to the untreated controls, while the UVA effects alone reached 150%, indicating that pretreatment of DANA diminished this increase by 60% (Figure 3.8b).

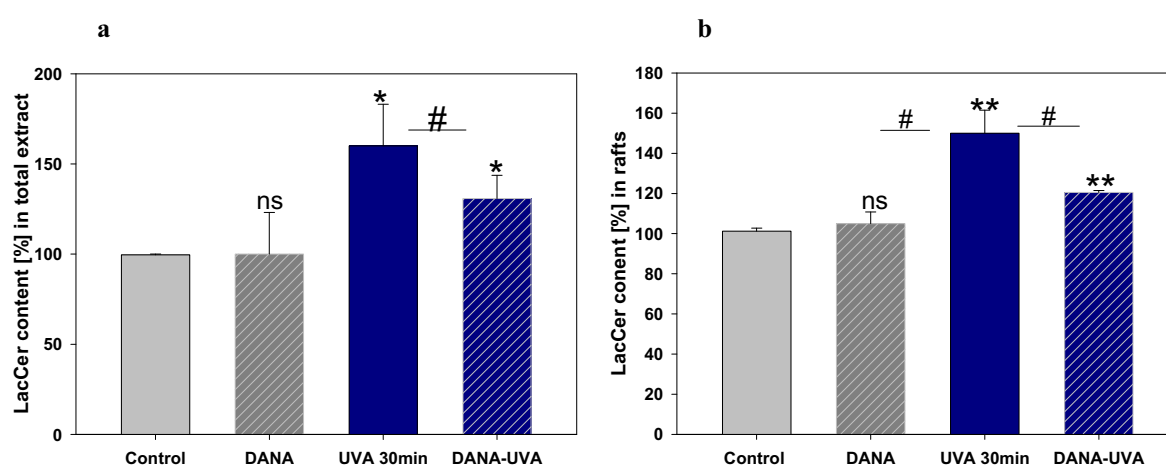


**Figure 3.8: UVA radiation-induced formation of lactosylceramide.** (a) Lactosylceramide (LacCer) content in total extracts, or (b) LacCer content in rafts, was assessed in human keratinocytes, which had been either left untreated (control), were only pretreated with 10  $\mu$ M DANA for 1 h prior without irradiation, were irradiated with UVA (30 J/cm<sup>2</sup>) or were pretreated with DANA, irradiated and harvested 30 min after irradiation. Lipid extracts were analyzed in lipid rafts based on 150  $\mu$ g protein, and on 500  $\mu$ g protein in total extracts. Lipid content is given as % change in comparison to controls that were set equal to 100%. Data represent the mean  $\pm$  SD of 3 independent experiments. Paired student's t-test was used for statistical analysis: \* $p$ <0.05, \*\* $p$ <0.01, ns indicates not significant where  $p$ >0.05 as compared to the untreated control; # $p$ <0.05, ## $p$ <0.01 versus UVA treated sample, DANA, 2,3-didehydro-2-deoxy-*N*-acetylneuraminic acid

As shown in Figure 3.9, pretreatment with DANA for 1 h prior to irradiation and for additional 30 min after irradiation partially diminished UVA radiation-induced ceramide generation observed in total cell extracts as well as in rafts. In these experiments, pretreatment with the neuraminidase inhibitor DANA prior to irradiation had no effect on basal ceramide content. Confirming the findings by Grether-Beck (Grether-Beck *et al.* 2005b), a dose of 30 J/cm<sup>2</sup> UVA radiation led to a significant increase in ceramide content in total cell extracts from human keratinocytes to approximately 450% as compared to untreated control cells. However, DANA pretreatment diminishes UVA radiation-induced ceramide formation measured in total extract by approximately 55% (Figure 3.9a). Similarly, UVA radiation induces an increase in the ceramide content within rafts to approximately 230% as

compared to the untreated control. Pretreatment with DANA results in a decrease in UVA radiation-induced ceramide formation in rafts to approximately 140%, indicating that DANA pretreatment diminishes UVA radiation-induced ceramide formation within rafts by approximately 45% (Figure 3.9b).

In previous experiments, we used the lysosomotropic agent chloroquine to change the acidic pH of the lysosome resulting in no change of ceramide formation, indicating that no lysosomal degradation of gangliosides contributed to ceramide formation (Grether-Beck *et al.* 2005b).

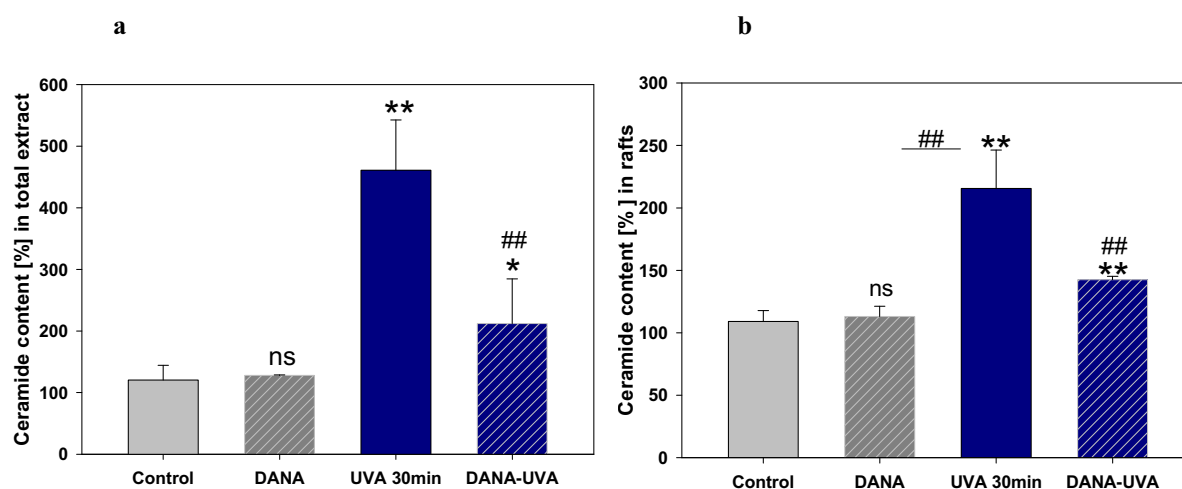


**Figure 3.9: UVA radiation-induced ceramide formation is partially inhibited with DANA pretreatment.** (a) Ceramide content in total cell extracts or (b) Ceramide content in rafts was assessed in human keratinocytes, which had been either left untreated (control), were pretreated with 10  $\mu$ M DANA for 1 h prior to irradiation with UVA, were irradiated with UVA (30 J/cm<sup>2</sup>) or were pretreated with DANA, irradiated and harvested 30 min after irradiation. Lipid extracts were analyzed in lipid rafts based on 150  $\mu$ g protein, and on 500  $\mu$ g protein in total extracts. Lipid content is given as % change in comparison to controls that were set equal to 100%. Data represent the mean  $\pm$  SD of 3 independent experiments. Paired student's t-test was used for statistical analysis: \* $p$ <0.05, \*\* $p$ <0.01, ns indicates not significant where  $p$ >0.05 as compared to the untreated control; # $p$ <0.05, ## $p$ <0.01 versus UVA treated sample, DANA, 2,3-didehydro-2-deoxy-*N*-acetylneuraminic acid.

In contrast, as shown in Figure 3.10a, inhibition of Neu3 activity has no significant effect on UVA radiation-induced decrease in GM1 content. GM1 being a more complex ganglioside with 2 non terminal sialic acid residues, GM1 is not a direct substrate for Neu3 enzyme because Neu3 removes the terminal sialic acid residues from its conjugate (Ha *et al.* 2004; Miyagi *et al.* 1999; Oehler *et al.* 2000; Kopitz *et al.* 1997b). The enzymatic degradation of GM1 is catalyzed by  $\beta$ -galactosidase, a water-soluble acid exo-hydrolase (Wilkening *et al.* 2000). The decrease in GM1 content in total cell extract can be a function of all cellular GM1-degrading enzymes, mainly the lysosomal enzymes. Accordingly, the degree of GM1 decrease measured in total cell extract upon UVA treatment (Figure 3.10a) was higher

(approximately 60%) than that measured in rafts (approximately 30%). One possible explanation for the enhanced degradation of GM1 in rafts upon UVA treatment is an activation of  $\beta$ -galactosidase which could be localized besides its known intracellular localization also within rafts. In human skin fibroblasts, Valaperta and co-workers (Valaperta *et al.* 2006) have shown a concomitant increase in  $\beta$ -galactosidase activity with an increased plasma membrane associated neuraminidase activity. Nevertheless, this explanation is to be taken as speculative and its evaluation requires additional experiments in keratinocytes.

In this regard, the main localization of the acid  $\beta$ -galactosidase is known to be within the lysosomal compartment (Hoogeveen *et al.* 1984). The lack of an effect of DANA on the degradation of GM1 was not unexpected in view of the obvious fact that GM1 is not a direct substrate of Neu3. On the other hand, the GM1-pool is filled up by desialylation of the higher gangliosides GD1a, GD1b and GT1b having at least one terminal sialic acid residue. Also this 'filling reaction' is prevented by DANA, because these gangliosides are also attacked by Neu3. In line with these findings, Kopitz and co-workers determined a faster decrease in the radioactive label in ganglioside GM1 than in the absence of the Neu3 inhibitor DANA.

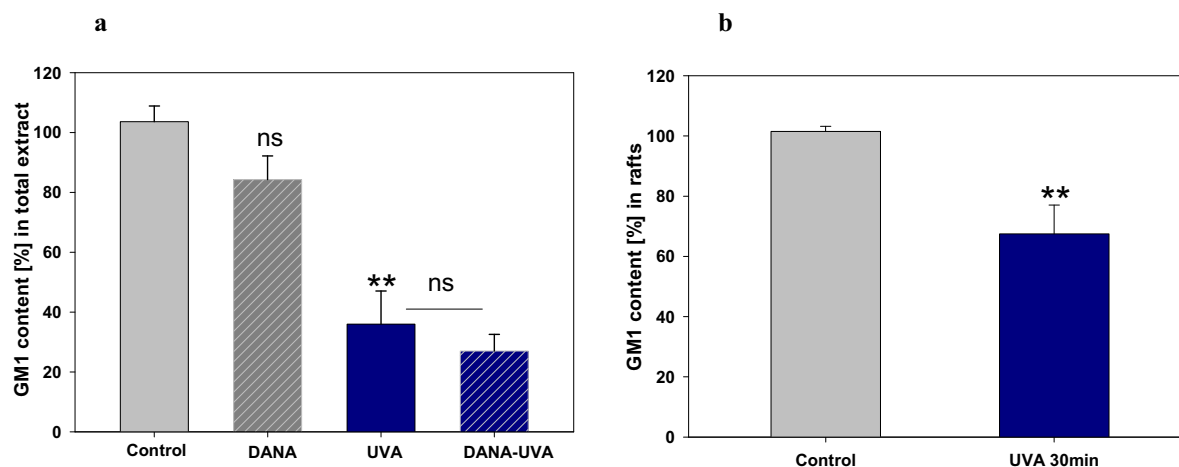


**Figure 3.10: UVA radiation-induced GM1 degradation was not inhibited with DANA pretreatment.** (a) GM1 content in total extracts, or (b) GM1 content in rafts, was assessed in human keratinocytes, which had been either left untreated (control), were only pretreated with 10  $\mu$ M DANA for 1 h prior to irradiation, were irradiated with UVA (30 J/cm<sup>2</sup>) or were pretreated with DANA, irradiated and harvested 30 min after irradiation. Lipid extracts were analyzed in lipid rafts based on 150  $\mu$ g protein, and on 500  $\mu$ g protein in total extracts. Lipid content is given as % change in comparison to controls that were set equal to 100%. Data represent the mean  $\pm$  SD of 3 independent experiments. Paired student's t-test was used for statistical analysis: \*p<0.05, \*\*p<0.01, ns indicates not significant where p>0.05 as compared to the untreated control; #p<0.05, ##p<0.01 versus UVA treated sample, DANA, 2,3-didehydro-2-deoxy-N-acetylneuraminic acid.

Recent findings in our group indicated that more than 60% (250 pmol/400 pmol = 62,5%) of the ceramide formed might originate from the non-enzymatic hydrolysis of raft localized sphingomyelin in primary keratinocytes (Grether-Beck *et al.* 2008). With regards to the

decrease of sphingomyelin upon UVA treatment similar results were obtained when instead of primary keratinocytes (Figure 3.11a) HaCaT cells (Figure 3.11b) were studied.

We next wondered whether DANA pretreatment affected UVA radiation-induced decrease of sphingomyelin content in rafts. As shown in Figure 3.11b, the observed UVA radiation-induced decrease of sphingomyelin was not significantly changed by preincubation with the neuraminidase inhibitor DANA.

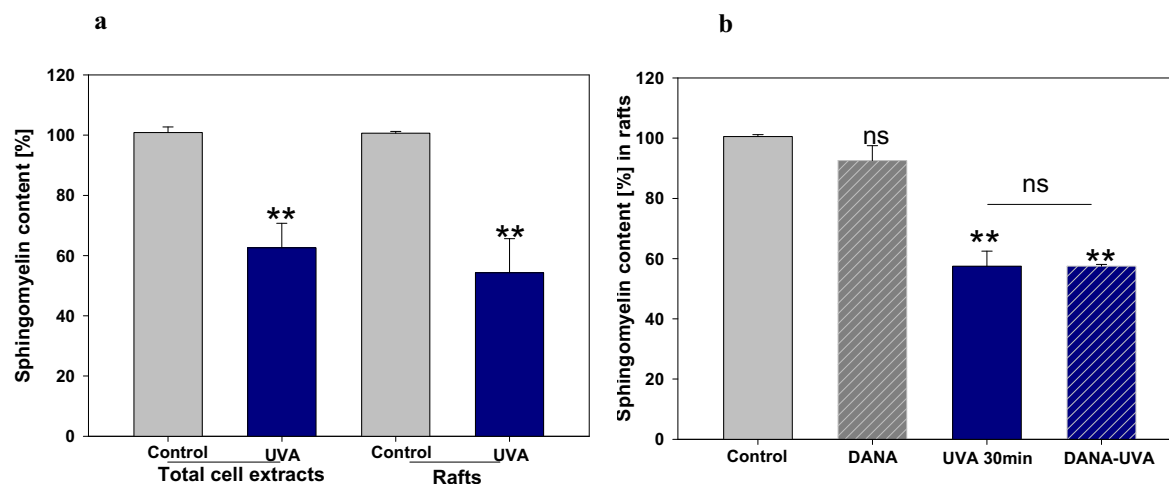


**Figure 3.11: UVA irradiation results in a significant decrease of sphingomyelin in total extracts and in rafts.** Sphingomyelin content in total cell extracts or rafts isolated from (a) primary keratinocytes and (b) HaCaTs which had been either irradiated with UVA (30 J/cm<sup>2</sup>) or left untreated (control) and harvested 30 min after irradiation. Sphingomyelin content in rafts was assessed in HaCaT cells which were either left untreated (control), only treated with 10  $\mu$ M DANA for 1 h prior to the irradiation time point, only UVA irradiated (30 J/cm<sup>2</sup>), or were treated with the neuraminidase inhibitor prior to UVA irradiation and harvested 30 min post irradiation. Lipid extracts from rafts based on 150  $\mu$ g protein, and from total extracts on 500  $\mu$ g protein. Controls were set equal to 100%. Sphingomyelin is given as % decrease in comparison to controls. Data represent the mean  $\pm$  SD of 3 independent experiments. Paired student's t-test was used for statistical analysis: \* $p$ <0.05, \*\* $p$ <0.01, versus untreated time-matched control, ns (not significant) indicates  $p$ > 0.05 versus UVA treated time-matched sample, DANA, 2,3-didehydro-2-deoxy-*N*-acetylneuraminic acid.

### 3.2. Impact of caveolin-1 knockdown on UVA radiation-induced gene expression

As Neu3 closely associates with caveolin-1, the caveolae stabilizing and cholesterol binding protein (Wang *et al.* 2002b), we addressed the question whether depletion of caveolin-1 by retrovirus-mediated RNA interference has an impact on UVA radiation-induced ICAM-1 gene expression.

The expression pattern of ICAM-1 mRNA in caveolin-1 knockdown HaCaT cells upon UVA irradiation was assessed by real-time PCR. As indicated in Figure 3.12a and Figure 3.12b, in comparison to wild type HaCaT cells, depletion of caveolin-1 gene in HaCaT cells diminished their sensitivity towards UVA radiation-induced ICAM-1 mRNA upregulation. While wild type HaCaT cells presented the typical biphasic pattern of a significant UVA

radiation-induced upregulation of ICAM-1 mRNA 8 h and 24 h post irradiation, the caveolin-1 knockdown cells showed no response towards the UVA stress.

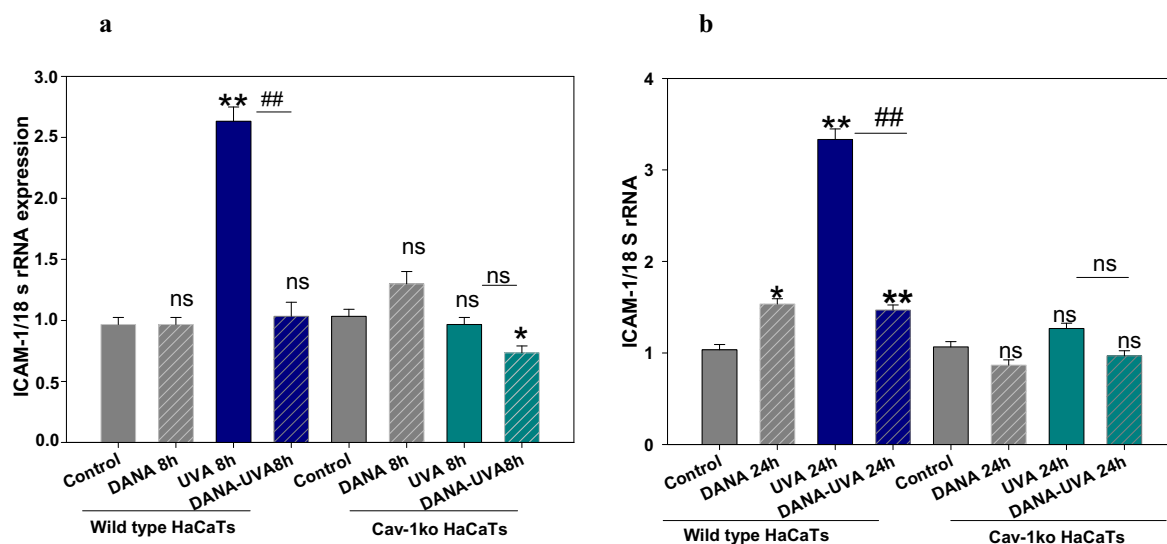


**Figure 3.12: Impact of caveolin-1 knockdown on UVA radiation-induced gene expression.** (a) and (b) Expression of ICAM-1 mRNA based on 18 S rRNA. Gene expression was assessed in wild type HaCaT cells (left) and in caveolin-1 knockdown HaCaTs (right) that had been either left untreated, treated with 10  $\mu$ M DANA for the indicated time points, irradiated with 30 J/cm<sup>2</sup> UVA, or were treated with DANA and UVA. After harvest 8 h or 24 h post irradiation, RNA was isolated and real-time PCR performed as described in Materials and Methods. For comparison of relative gene expression in control cells and treated cells the 2<sup>-</sup>(delta delta C (T)) method was used. Shown is the fold of change in mRNA expression in treated cells as compared to the untreated controls (controls set equal to 1). Data represent the mean  $\pm$  SD of 3 independent experiments. Paired student's t test was used to calculate the significance of the seen difference, where ns  $p > 0.05$  (not significant), \* $p < 0.05$ , \*\* $p < 0.01$ , DANA, 2-deoxy-2,3-didehydro-*N*-acetylneuraminic acid.

As Neu3 enzyme activity correlated with the UVA-response e.g. UVA radiation-induced ICAM-1 upregulation in primary human keratinocytes and in wild type HaCaT cells (see Figure 3.6), we addressed the question whether Neu3 activity is suppressed in caveolin-1 knockdown HaCaT cells. For this purpose, we compared the Neu3 enzyme activities in rafts from untreated versus UVA treated wild type and caveolin-1 knockdown HaCaTs in Table 3.2 using the thiobarbituric acid assay (Warren 1959). The results given in Figure 3.13, indicate that in contrast to the wild type cells caveolin-1 knockdown cells do not present a significantly increased enzyme activity due to UVA treatment. Interestingly the basal enzyme activity observed in caveolin-1 knockdown HaCaT cells was  $7.6 \pm 0.5$  units/mg protein, while the wild type had a basal activity found to be  $5.6 \pm 0.7$  units/mg protein, respectively. The basal enzyme activity in rafts of caveolin-1 knockdown cells is significantly increased as compared to the basal activity in HaCaT cells (paired student's t test:  $p = 0.01$ ,  $n = 3$ ).

**Table 3.2: UVA radiation-induced Neu3 activities in rafts from HaCaT wild type and caveolin-1 knockdown cells.**

HaCaT Cell type	Wild type	Caveolin-1 knockdown
	Units/mg total protein (Mean $\pm$ SD, n=3)	
Control	5.6 $\pm$ 0.7	7.6 $\pm$ 0.5
UVA irradiated (30 min)	16.9 $\pm$ 2.4	10.0 $\pm$ 1.4

Neu3 activity using thiobarbituric acid assay based on 1 mg protein in rafts from wild type HaCaT cells or from caveolin-1 knockdown HaCaTs that had been left untreated (control) or irradiated with a dose of 30 J/cm<sup>2</sup> UVA and harvested after 30 min post irradiation. The enzyme activity was expressed in units per mg of protein; one unit was responsible for the release of 1 nmol sialic acid after 1 hour incubation of the enzyme source with GM3 at 37 C°.

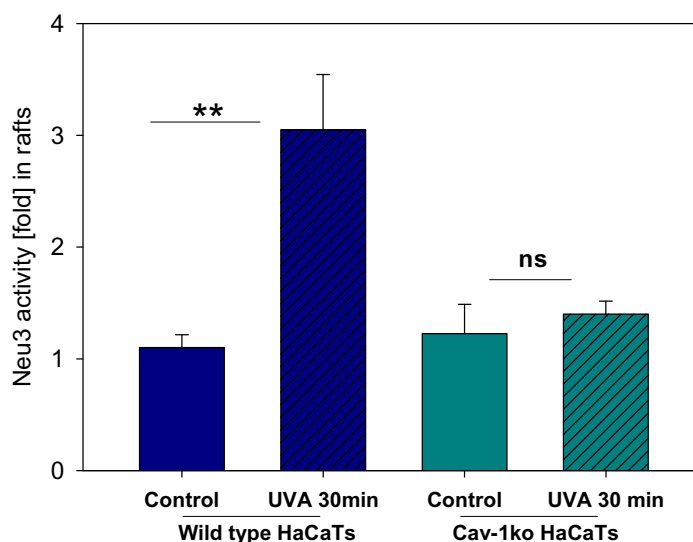


**Figure 3.13: Impact of caveolin-1 knockdown on UVA radiation-induced Neu3 activity in human keratinocytes.** Neu3 activity in rafts from irradiated wild type HaCaTs (left) or irradiated caveolin-1 knockdown HaCaT cells (right) was assayed immediately after isolation of rafts using ganglioside GM3 as a substrate at pH 3.8. Each bar in the diagram represents the mean of the factor of change in Neu3 activity as compared to the unirradiated corresponding control cells which were set equal to 1. Data represent the mean  $\pm$  SD of 3 independent experiments. Paired student's t-test was used for statistical analysis: ns (not significant), \*p<0.05, \*\*p<0.01 versus untreated time-matched control.



Consequently, as UVA radiation-induced GM3 degradation in human keratinocytes has previously been shown to be mediated via UVA radiation-induced activation of Neu3, we have examined GM3 levels in rafts from caveolin-1 knockdown cells.

A significant difference between UVA radiation-mediated changes in GM3 level in rafts from caveolin-1 knockdown and in rafts from wild type HaCaTs has been observed. Figure 3.14a indicates a slight, but significant increase in GM3 levels in caveolin-1 knockdown cells upon UVA exposure (about 110% of control), whereas, in wild type HaCaT cells UVA irradiation led to a significant decrease of about 40% resulting in remaining 60% of the control level. Interestingly, similar results were observed for GM1 which is not a direct substrate for Neu3.

As ceramide formation within rafts is proven to be an indispensable prerequisite for the UVA response (in terms of ICAM-1 upregulation) to occur (Grether-Beck *et al.* 2008), we next assessed the capability of UVA radiation to generate ceramide within rafts of caveolin-1 knockdown cells. As can be seen in Figure 3.14b, there was no increase in ceramide content in rafts from these caveolin-1 knockdown cells upon UVA treatment, whereas, in wild type HaCaT cells, ceramide content was significantly increased to approximately 230%.

Complete inhibition of UVA radiation-induced Neu3 activity in wild type cells did not correlate with complete inhibition of UVA radiation-induced ceramide release (Figure 3.9a), indicating that other mechanisms might be involved in the knockdown cells resulting in a complete inhibition of UVA radiation-induced ceramide formation.

In the wild type HaCaT cells, UVA irradiation resulted in a decrease of sphingomyelin of about 50% and a decrease of cholesterol of about 70% as compared to the control, respectively (Figure 3.14c). In contrast, in the caveolin-1 knockdown cells, the decrease of sphingomyelin reached about 30% and the decrease of cholesterol was found to be 40%, indicating a smaller effect of UVA radiation on these lipids in the rafts of caveolin-1 knockdown cells.

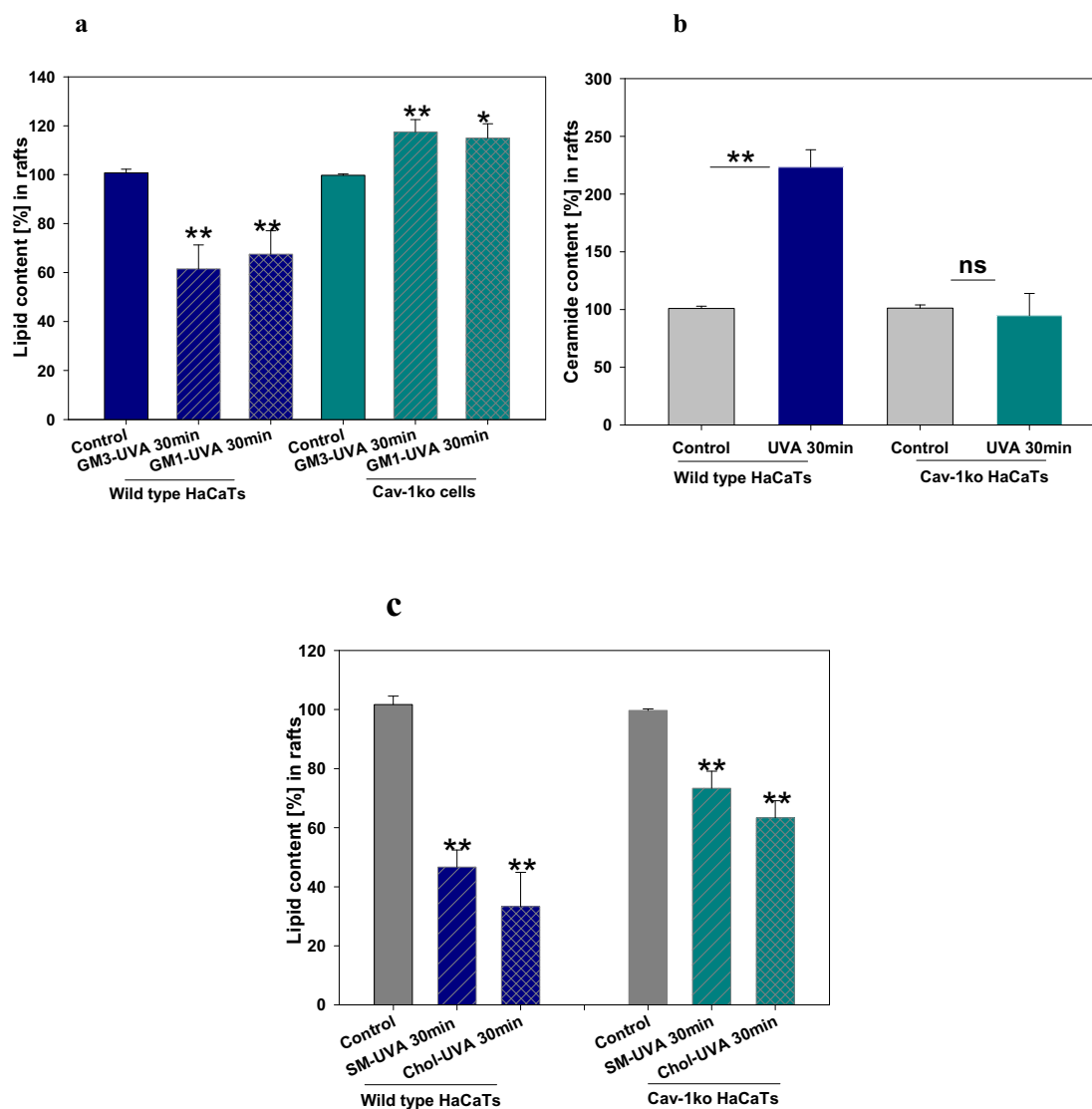


**Figure 3.14: Effect of caveolin-1 knockdown on UVA radiation-induced changes in lipid composition of human keratinocytes.** (a) GM3 and GM1 content, (b) ceramide content, (c) sphingomyelin (SM) and cholesterol (Chol) content. The contents of these lipids were assessed in rafts from wild type (left) and from caveolin-1 knockdown HaCaTs (right), that were either left untreated or were irradiated with UVA (30 J/cm<sup>2</sup>) and harvested 30 min after irradiation. Lipid extracts were analyzed based on 150 µg protein. Controls were set equal to 100%. Data represent the mean ± SD of 3 independent experiments. Paired student's t test was used to calculate the significance of the seen differences, ns (not significant) p>0.05, \*p<0.05, \*\*p< 0.01, versus the corresponding untreated control.

### 3.3. Role of caveolin-1 in ceramide-induced gene expression in human keratinocytes

In previous studies, cell permeable ceramides were able to mimic the UVA response in keratinocytes (Grether-Beck *et al.* 2005b; Grether-Beck *et al.* 2008; Grether-Beck *et al.* 2000). Therefore, cell permeable ceramides e.g. C6-ceramide were added to wild type cells as well as caveolin-1 knockdown HaCaT cells to prove whether the downstream signaling events beyond formation of ceramide would be the same in both cell types. As can be seen in Figure 3.15a, both cell types, wild type HaCaT cells as well as caveolin-1 knockdown HaCaT cells could take up cell permeable C6-ceramide as detected 10 minutes post addition of the compound in a concentration of 10  $\mu$ M. This concentration has been chosen, because previous studies had shown that viability of the HaCaT cells over a range of 24 h is not affected under these conditions (Grether-Beck *et al.* 2003; Grether-Beck *et al.* 2005b; Grether-Beck *et al.* 2008). Interestingly, ceramides themselves were able to activate Neu3 in rafts of wild type HaCaT cells by a factor of 2.2. In contrast, the caveolin-1 knockdown cells showed a still significant 1.4-fold but smaller increase of Neu3 activity in rafts (Figure 3.15b). With regards to the upregulation of ICAM-1 mRNA expression we could state that wild type cells presented a significant upregulation of ICAM-1 at early (8 h) as well as late time (16 h) points, while the caveolin-1 knockdown cells were not able to respond to the stimulus ceramide by upregulation of ICAM-1 above baseline levels (Figure 3.15c).

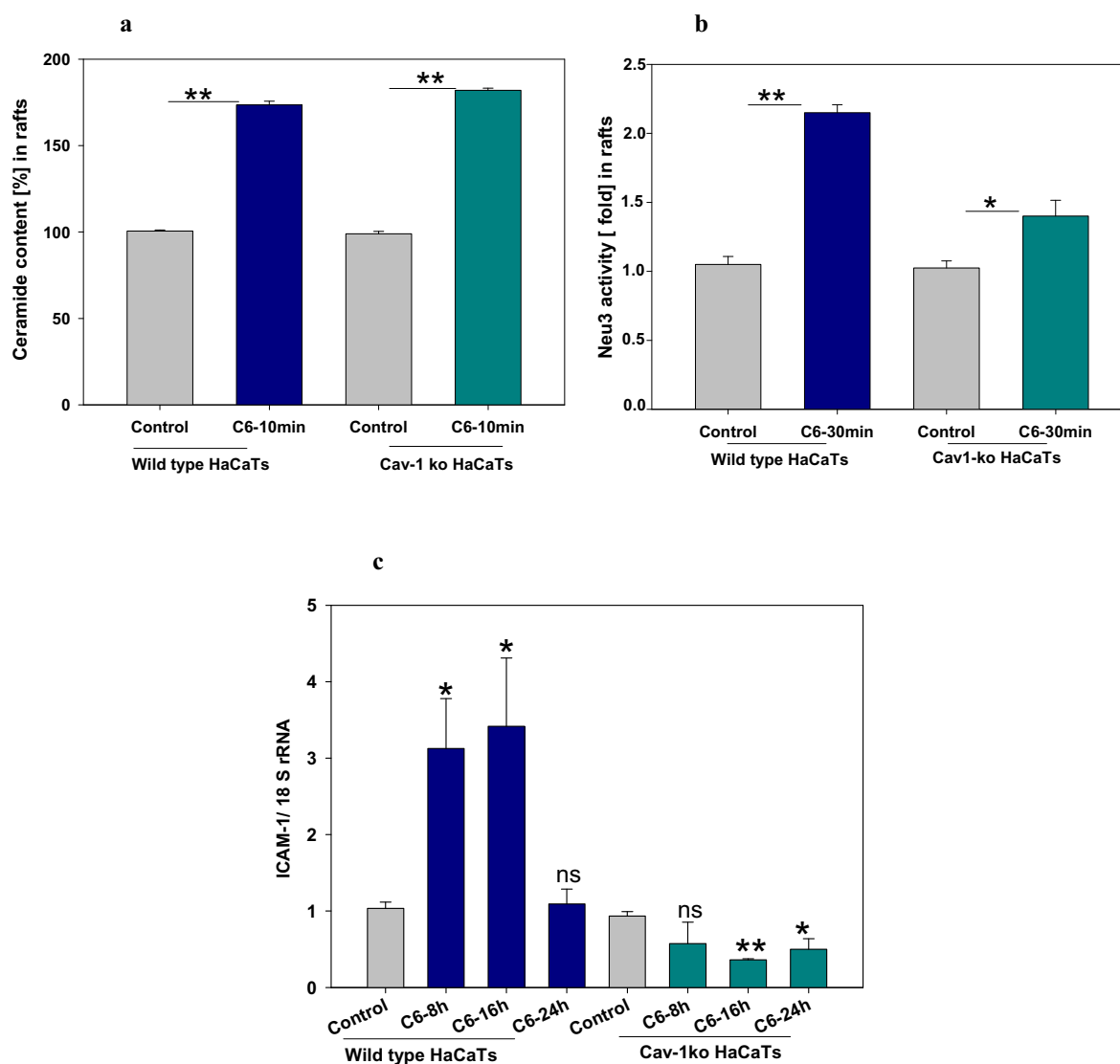


**Figure 3.15: Role of caveolin-1 knockdown in ceramide-induced ICAM-1 mRNA expression.** (a) Ceramide content in rafts of wild type HaCaT cells (left) and caveolin-1 knockdown cells (right) after addition of 10  $\mu$ M C6-ceramide for 10 min into cell culture medium in comparison to untreated corresponding cells. (b) Neu3 activity in rafts of HaCaT cells treated with C6-ceramide for 30 min. Shown is the fold of Neu3 activity in treated cells as compared to untreated controls. (c) Expression of ICAM-1 mRNA based on 18 S rRNA in HaCaT cells, that had been treated with 10  $\mu$ M C6-ceramide for 8 h (C6-8h), 16 h (C6-16h) or 24 h (C6-24h). Shown is the fold increase of ICAM-1 mRNA expression in treated cells as compared to untreated ones of the same cell type (controls set equal to 1). Data represent the mean  $\pm$  SD of 3 independent experiments. \* indicates a statistically significant difference compared to untreated corresponding controls. Paired student's t test was used to calculate the significance of the seen difference, where \* $p$ <0.05, \*\* $p$ < 0.01).

Similarly, the ganglioside GM3 could be taken up by HaCaT cells from the cell culture medium (Figure 3.16a). Addition of GM3 resulted in a transient intracellular increase of this ganglioside after 10 min to about 300% as compared to the untreated control. At later time points e.g. 30 min post addition of 10  $\mu$ M GM3 the intracellular GM3 content was found to be still increased above baseline level up to 150% compared to the untreated control. Addition of GM3 was also correlated with a 2-fold increase in Neu3 activity after 10 min (Figure 3.16b). The increased neuraminidase activity was accompanied by a significant increase in ceramide formation in total extracts to about 400% as compared to the untreated control (Figure 3.16c). These results could indicate that the amount of the endogenous GM3 was regulated by Neu3 activity in order to keep a constant level of GM3 on the plasma membrane.

Desialylation of exogenously added gangliosides GD1a and GD1b to GM1 by membrane-bound neuraminidase after 10 min of incubation had already been demonstrated in primary cultures of cerebellar neurons (Riboni & Tettamanti 1991).

With regards to GM3-induced gene expression, we observed that GM3 as well as C6-ceramide were able to significantly induce ICAM-1 mRNA expression in HaCaT wild type cells (Figure 3.16d) by a factor of 3 at 16 h post stimulation. In contrast, in the caveolin-1 knockdown HaCaT cells GM3 could not upregulate ICAM-1 mRNA expression above baseline levels (Figure 3.16d).

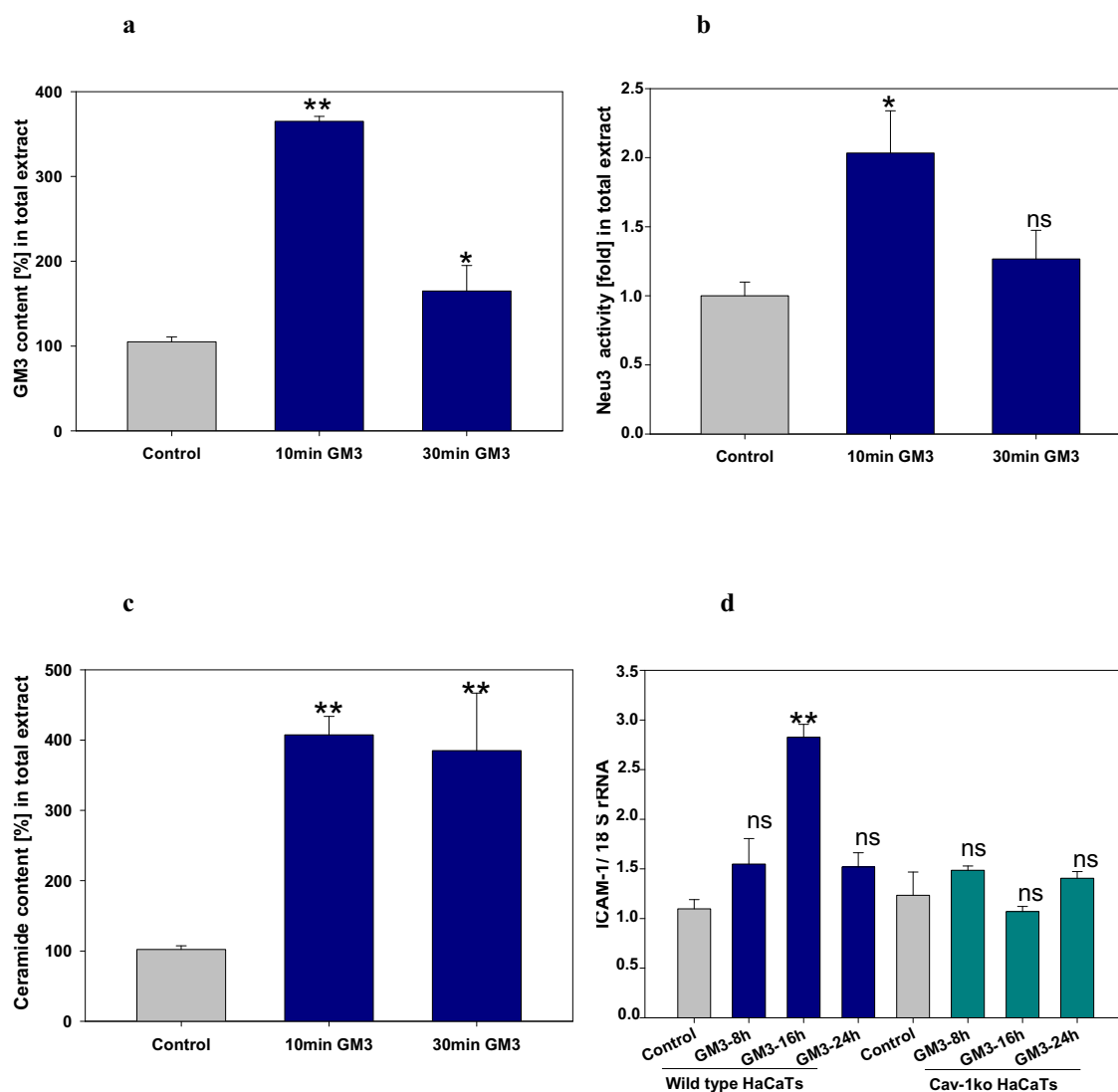


**Figure 3.16: Role of caveolin-1 in GM3-induced ICAM-1 mRNA expression.** Wild type HaCaT cells as well as caveolin-1 knockdown HaCaT cells were treated with 10  $\mu$ M GM3 for the indicated time points by addition to the cell culture medium. (a) GM3 content (in % of control) in total extract of wild type HaCaT cells after addition of 10  $\mu$ M GM3 for 10 min or 30 min into cell culture medium in comparison to untreated cells. (b) Neu3 activity in total cellular membrane extract of wild type HaCaT cells was measured using thiobarbituric acid assay. Shown is the fold increase of Neu3 activity in treated cells as compared to untreated controls. (c) Ceramide content (in % of control) in total extracts of wild type HaCaT cells was determined. (d) Expression of ICAM-1 mRNA based on 18 S rRNA was detected in wild type HaCaT cells (right) and caveolin-1 knockdown HaCaT cells as indicated. Shown is the fold increase of ICAM-1 mRNA /18S rRNA expression in treated cells as compared to untreated controls (Controls set equal to 1). Data represent the mean  $\pm$  SD of 3 independent experiments. Paired student's t test was used to calculate the significance of the seen difference, where \* $p$ <0.05, \*\* $p$ <0.01 represent comparison to the corresponding untreated control.

To understand the mechanism (s) by which UVA radiation induces Neu3 activation of human keratinocytes, we compared the magnitude of Neu3 activation in response to C6-ceramide, GM3, or UVA radiation. As shown in Table 3.3, the amount of UVA radiation-induced Neu3 activation in total cellular membrane extracts 30 min post irradiation was about 2-fold higher than in cells stimulated with C6-ceramide and about 3-fold increased as compared to GM3-treated cells.

Interestingly, there seems to be kinetic differences between the UVA-induced and the C6-ceramide-induced Neu3 activation, because at 24 h the UVA-induced Neu3 activity had decreased to 61% of the value observed at 30 minutes. In contrast, in C6-ceramide treated cells the Neu3 activity measured 24 h post application had doubled.

**Table 3.3: Comparison of Neu3 activity in total cell extracts after stimulation with UVA, GM3, or C6-ceramide.**

<b>Time after stimulation</b>	<b>GM3 (10 <math>\mu</math>M)</b>	<b>C6-ceramide (10 <math>\mu</math>M)</b>	<b>UVA (30 J/cm<sup>2</sup>)</b>
	Units/mg total protein (Mean $\pm$ SD, n=3)		
Control	3.1 $\pm$ 0.2	3.1 $\pm$ 0.1	3.1 $\pm$ 0.2
10 min	6.3 $\pm$ 1.1	not detected	2.9 $\pm$ 0.1
30 min	3.9 $\pm$ 0.6	6.0 $\pm$ 0.1	11.9 $\pm$ 0.4
8 h	3.4 $\pm$ 0.2	not detected	5.2 $\pm$ 0.7
24 h	not detected	12.4 $\pm$ 1.1	7.3 $\pm$ 1.0

HaCaT cells were either left untreated or irradiated with UVA (30 J/cm<sup>2</sup>), C6-ceramide (10  $\mu$ M), or GM3 (10  $\mu$ M). Cells were harvested after 0.5 h, 8 h, or 24 h post treatment. Enzyme activity was detected by thiobarbituric acid assay (Warren 1959). 1 unit Neu3 activity was considered to be responsible for release of 1 nmol sialic acid from GM3 per hour per 1 mg total protein at 37 C° and pH 3.8.

### **3.4. The link between Src kinase, caveolin-1 and neuraminidase 3 in UVA radiation-induced signal transduction**

A subset of the reports describing Src kinase activation in many signaling pathways, including adhesion and transformation, has demonstrated an increase in the phosphorylation level of caveolin-1. Caveolin-1 was first identified as a major Src kinase substrate (Smart *et al.* 1999). It is known that caveolin-1 functions as a scaffolding protein (Okamoto *et al.* 1998) to organize and concentrate specific lipids (cholesterol and glycosphingolipids) and lipid modified signaling molecules (including Src kinase) within the caveolae. In addition, it has been shown that Src-mediated caveolin-1 phosphorylation can influence the expression of some inflammatory genes (Patel *et al.* 2008). Direct interaction of Src kinase with caveolin-1 leads to phosphorylation of caveolin-1 at Y14 (Li *et al.* 1996). In Src kinase, there are two tyrosine residues, Y416 in the kinase domain and Y529 in the C-terminal tail, whose phosphorylation status regulates its kinase activity. Autophosphorylation at Y416 leads to increased kinase activity, whereas phosphorylation at Y529 leads to repression of kinase activity (Abram & Courtneidge 2000).

Upon UVA irradiation, we could observe a marked increase of the Src kinase activity as measured by western blot analysis using a specific antibody directed to p-Src kinase (Y416). In turn, this activation was concomitant with caveolin-1 phosphorylation at Y14. As shown in Figure 3.17a by western blot analysis of total cellular extracts from human keratinocytes, UVA irradiation, but also stimulation with C6-ceramide and GM3 resulted in activation of Src kinase as detected by phosphorylation at Y416. Moreover, these effects were at least partially inhibited if the cells had been pretreated with the neuraminidase inhibitor DANA. With regards to concomitant phosphorylation of caveolin-1 (Figure 3.17b), we observed a stimulus mediated increase in phosphorylation as compared to the untreated control no matter whether the cells were irradiated or incubated with the sphingolipids C6-ceramide or GM3, respectively. Preincubation with the Neu3 inhibitor DANA resulted in a slight decrease of the stimulus mediated phosphorylation of caveolin-1 at Y14.

Previous studies in our group had shown that UVA as well as C2-ceramide induced a transient activation of Src kinase at Y416 with the first 30 minutes post treatment. The corresponding increase of caveolin-1 phosphorylation using these stimuli could be completely inhibited if the cells had been preincubated with the Src kinase inhibitor SU6656 (Grether-Beck *et al.* 2005a; Salahshour-Fard 2006). Moreover, activation of Src kinase had been proven to be an indispensable prerequisite for UVA or C2-ceramide induced activation



of the down stream signaling events (i) activation of transcription factor AP-2 and (ii) induction of ICAM-1 mRNA expression.

As ceramide release after UVA-irradiation has been shown to comprise a non-enzymatic hydrolysis from sphingomyelin (Grether-Beck *et al.* 2005a; Salahshour-Fard 2006) and an enzymatic activation of Neu3 within rafts (this thesis) we next assessed the role of Neu3 in UVA radiation-induced signaling. Neu3 has been shown to regulate transmembrane signaling through both, (i) modulation of gangliosides by degradation and (ii) by interaction with other signaling molecules including caveolin-1 (Miyagi *et al.* 2008a). In addition, Neu3 has been found to be closely associated with caveolin-1 within lipid rafts and that its activity was highly altered by the expression level of caveolin-1 within the cells (Wang *et al.* 2002b). From this point of view, we wanted first to examine the role of Neu3 in UVA radiation-induced caveolin-1 phosphorylation. For this purpose, we employed DANA the same potent inhibitor previously showing a strong inhibitory effect on both the activity and the gene expression of Neu3 (Figure 3.5 and Figure 3.6). As can be seen in Figure 3.17a and Figure 3.17b, inhibition of Neu3 activity using DANA results in a partial decrease of UVA radiation-induced Src kinase activation and a subsequent decrease of caveolin-1 phosphorylation, indicating that Neu3 activation is only partially involved in UVA radiation-induced Src kinase activation. As increased ceramide levels have not only been observed in UVA irradiated cells but also in GM3 treated cells, we wondered whether GM3 on its own can induce Src kinase activity and if yes, whether this effect can be inhibited by DANA. Moreover, we tested the effect of DANA on ceramide-induced Src kinase activation. 10  $\mu$ M C6-ceramide have previously been shown to transiently stimulate Src kinase activity in endothelial cells (Czarny & Schnitzer 2004). In western blot analysis (Figure 3.17), addition of exogenous GM3 as well as C6-ceramide resulted in a marked increase of Src kinase phosphorylation at Y416 and of caveolin-1 phosphorylation at Y14. Pretreatment with DANA only slightly lowered the C6-ceramide induced phosphorylation of caveolin-1, while GM3-mediated Src kinase activation and caveolin-1 phosphorylation seemed to be more affected by this inhibitor.

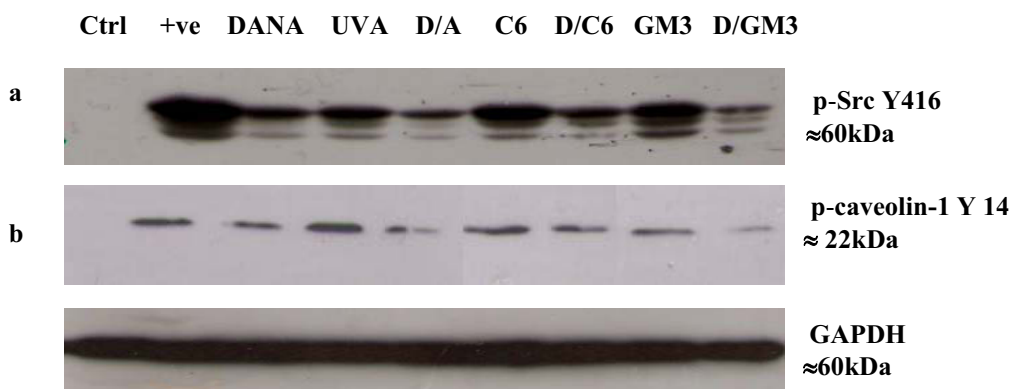


**Figure 3.17: Role of Neu3 activity in UVA radiation-induced, ceramide-induced, and GM3-induced phosphorylation of Src kinase at Y416 and caveolin-1 at Y14.** Human Keratinocytes were either left untreated (ctrl), were treated with 10  $\mu$ M DANA for 1 h (DANA), were irradiated with 30 J/cm<sup>2</sup> UVA or treated with C6-ceramide (10 $\mu$ M) or GM3 (10 $\mu$ M), or were pretreated with DANA, and subsequently irradiated (D/A) or treated with C6-ceramide or GM3 and harvested after 30 min incubation. (+ve) indicates positive control for (a) p-Src kinase (b) p-caveolin-1. The immunoblotting was carried out using specific antibodies for p-Src kinase Y416 and p-caveolin-1 Y14. GAPDH expression served as loading control. Reproducible results were obtained and representative data are presented.

To better characterize the link between caveolin-1 and Neu3 in UVA radiation-induced signaling, we tested the ability of caveolin-1 knockdown cells to maintain UVA response. Using western blot analysis, we examined Src kinase activation upon UVA exposure in caveolin-1 knockdown HaCaT cells as compared to the wild types. In the caveolin-1 knockdown cells, we could not detect increased Src kinase activity upon UVA irradiation, while the wild types showed a strong increase in phosphorylation at Y416 (Figure 3.18a). As Src kinase activity could also be negatively regulated through phosphorylation at Y529, we investigated the effect of UVA irradiation on this phosphorylation. Accordingly, total extracts from wild type and caveolin-1 knockdown HaCaT cells after irradiation for 10, 20 and 30 minutes with 30 J/cm<sup>2</sup> were made and analyzed by western blot. The results seen in Figure 3.18c, indicate that UVA radiation did not markedly affect the phosphorylation levels of Src kinase at Y529 in both cell types.

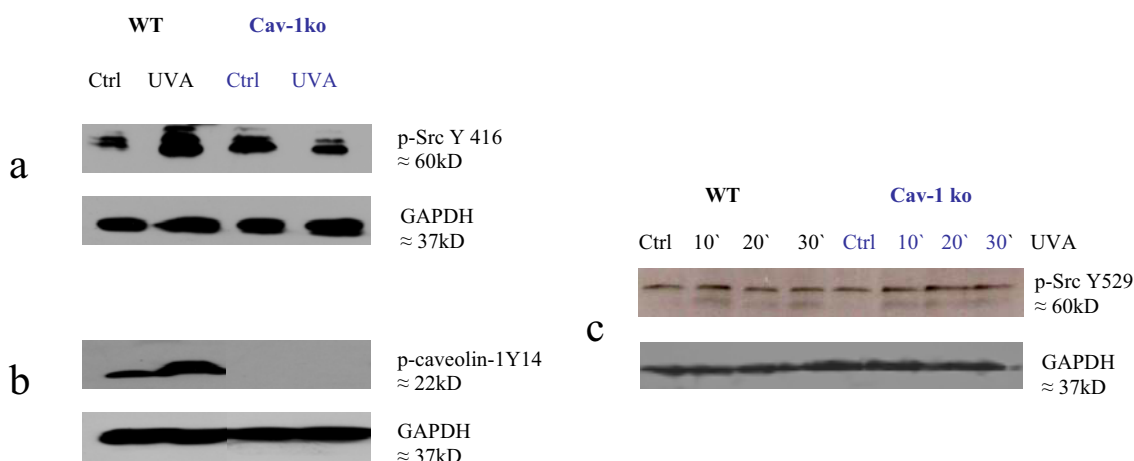


**Figure 3.18: Role of caveolin-1 in UVA radiation-induced Src kinase activation.** Wild type HaCaT (WT) and caveolin-1 knockdown HaCaT cells (Cav-1 ko) were left untreated (ctrl) or irradiated with 30 J/cm<sup>2</sup> UVA and harvested either after 30 min (panel a and b), or after the indicated time points (panel c). The immunoblotting was carried out using specific antibodies for (a) p-Src kinase Y416, (b) p-caveolin-1 Y14 and (c) p-Src kinase Y529. Reproducible results were obtained and representative data are presented.

As UVA radiation-induced activation of Src kinase was mediated via ceramide formation (Grether-Beck *et al.* 2005a) and UVA radiation-induced ceramide release in caveolin-1 knockdown cells was not observed (Figure 3.15b), we wondered whether ceramide, lactosylceramide the product of GM3 degradation, and GM3 on their own can induce Src kinase activation in caveolin-1 knockdown HaCaT cells. To this end, we used cell permeable C6-ceramide, which was shown to stimulate Src kinase activation in wild type HaCaT cells after 10 min and after 30 min incubation in a concentration of 10  $\mu$ M. As can be seen in Figure 3.18a, western blot analysis revealed that C6-ceramide could increase phosphorylation of Src kinase at Y416 in caveolin-1 knockdown HaCaT cells to a similar extent as seen for the wild type cells. Similar results have been obtained when instead of ceramide, lactosylceramide was used (Figure 3.18b). Incubation with 10  $\mu$ M of lactosylceramide could stimulate Src kinase activity in caveolin-1 knockdown cells to a similar extent as compared to the wild type cells after 10 min or after 30 min incubation. This finding is in agreement with previous studies showing that in normal skin fibroblasts lactosylceramide induced Src kinase activity which was implicated in caveolin-1 phosphorylation (Sharma *et al.* 2005). Western blot analysis of total extract prepared from GM3 stimulated cells revealed that addition of 10  $\mu$ M exogenous GM3 could not induce Src kinase activity in caveolin-1 knockdown cells after 10 min and after 30 min incubation (Figure 3.19c), whereas, the level of activated Src kinase in wild type cells was increased by this treatment. This observation probably indicates

that GM3 per se is not able to induce Src kinase activation in caveolin-1 knockdown HaCaT cells but its downstream degradation products, i.e. lactosylceramide and ceramide. In other words, degradation of Ganglioside GM3 needs the presence of caveolin-1.

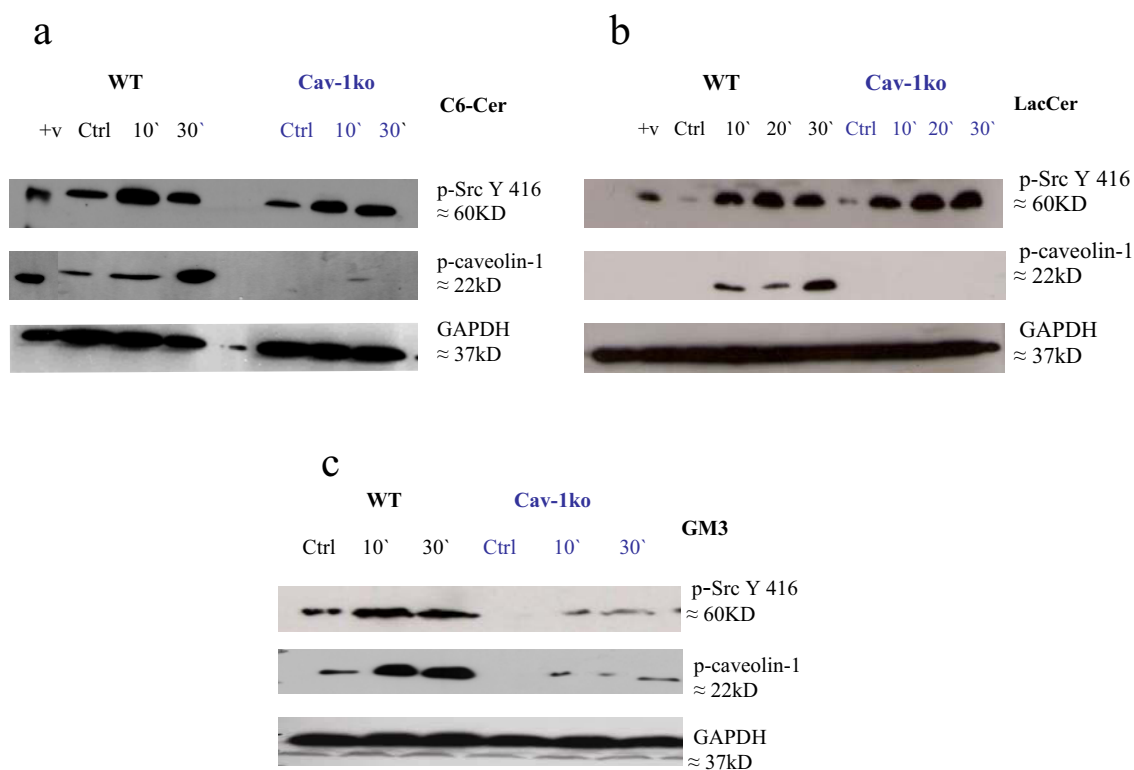


**Figure 3.19: Effect of C6-ceramide, lactosylceramide and GM3 on Src kinase activation in caveolin-1 knockdown cells.** Wild type HaCaT (WT) and caveolin-1 knockdown HaCaT cells (Cav-1ko) were left untreated (ctrl) or treated with (a) 10  $\mu$ M C6-ceramide and harvested after the indicated time points, (b) 10  $\mu$ M LacCer and harvested after the indicated time points, or (c) 10  $\mu$ M GM3 and harvested after the indicated time points. (+ve) indicates positive control for p-Src kinase Y416 and p-caveolin-1 Y14. The immunoblotting was carried out using specific antibodies for p-Src kinase Y416 and p-caveolin-1 Y14. Reproducible results were obtained and representative data are presented

Taken together, these results demonstrate a requirement for Neu3 activity to stimulate Src kinase upon UVA treatment and show that Src kinase activity is greatly affected by UVA radiation-induced lipid modulation in human keratinocytes.

Since Tyr-14 of caveolin-1 has been identified as a target of Src kinase (Lee *et al.* 2000), we wanted to examine the localization of Src kinase in human keratinocytes. Figure 3.20 shows that, despite the localization of Src kinase within lipid rafts in primary human keratinocytes, there was a considerable amount of Src kinase that was localized within fraction five. This indicates that in unstimulated cells, Src kinase could also exist out of rafts in other cellular compartments.

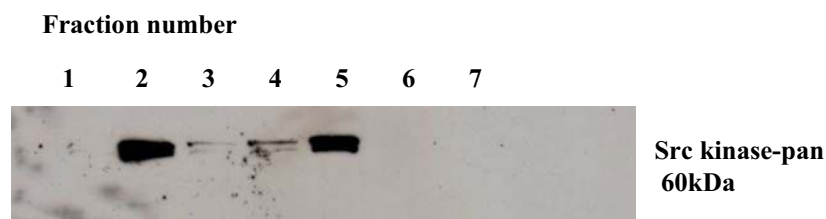


**Figure 3.20: Distribution of Src kinase across OptiPrep gradient in primary human keratinocytes.** Seven fractions (Numbered as 1 to 7, from the top of the gradient to the bottom) were separated in the process of rafts isolation (Brown and Rose, 1992) from untreated normal human primary keratinocytes. 8  $\mu$ g of protein in 100  $\mu$ l volume from each fraction was subjected to western blot analysis on 11% PAGE. The immunoblotting was carried out using a specific antibody Src kinase (pan). Marked signals were seen in the fractions 2 and 5. Reproducible results were obtained and representative data are presented.

### 3.4.1. Role of Caveolin-1, Src kinase, and neuraminidase 3 in UVA radiation-induced AP-2 activation

We next investigated the role of Src kinase activation in UVA radiation-induced activation of transcription factor AP-2. UVA radiation-induced ICAM-1 promoter activation required activation of the transcription factor AP-2 (Grether-Beck *et al.* 1996). As is shown in Figure 3.21, by using gel electrophoresis mobility-shift assays as described in the Methods and Materials chapter of this work, incubation of wild type HaCaT cells with Src kinase inhibitor PP2 (Reinehr *et al.* 2005) diminished the UVA radiation-induced activation of transcription factor AP-2 to nearly similar levels as observed for treatment with PP2 alone. Addition of PP2 resulted in slight activation of transcription factor AP-2 on its own (Figure 3.21, right panel). The precise reason for this finding is not known. Similar effects have been observed for e.g. cholesterol or vitamin E. However, in caveolin-1 knockdown cells, we could not detect any marked differences in AP-2 activation between control and UVA-irradiated cells (Figure 3.21, left panel).

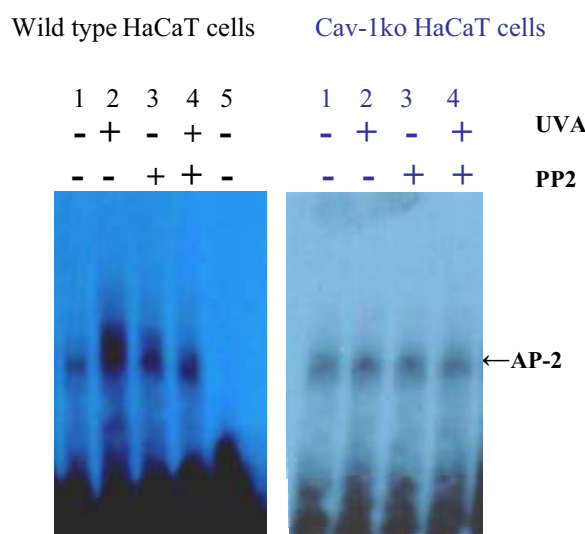


**Figure 3.21: Role of Src kinase and caveolin-1 in UVA radiation-induced AP-2 activation.** Activation of AP-2 was determined in gel electrophoresis mobility-shift assays using nuclear extracts isolated from wild type HaCaT cells (right panel) and from caveolin-1 knockdown HaCaT cells (left panel) 30 min post UVA irradiation ( $30 \text{ J/cm}^2$ ) co-incubated with a radiolabeled oligonucleotide containing the AP-2 recognition site of the ICAM-1 promoter. Radiolabeled AP-2 oligonucleotide co-incubated with nuclear extract from unirradiated cells (lane 1), from UVA-treated and harvested after 30 min cells (lane 2), from PP2 incubated cells ( $10 \mu\text{M}$ , 30 min, lane 3), from HaCaT cells, which had been pre-incubated with  $10 \mu\text{M}$  PP2 for 30 min prior to UVA irradiation (lane 4). Radiolabeled AP-2 oligonucleotide alone (lane 5). Reproducible results were obtained and representative data are presented.

To examine the functional relevance of UVA radiation-induced Neu3 activation for UVA radiation-induced AP-2 activation, the effect of the Neu3 inhibitor DANA on UVA radiation-induced-AP-2 activation was investigated. As shown in Figure 3.22 by using gel

electrophoresis mobility-shift assays as described in the chapter of Materials and Methods, DANA partially inhibited the capacity of UVA radiation to induce AP-2 activation. Similar results have been obtained for UVA radiation-induced ICAM-1 expression (Figure 3.3), indicating that Neu3 at least partially contributes to the downstream signaling events UVA radiation-induced AP-2 activation and ICAM-1 upregulation in primary human keratinocytes.

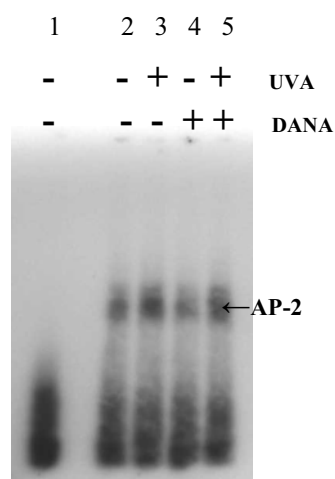


**Figure 3.22: Role of Neu3 in UVA radiation-induced AP-2 activation.** Activation of AP-2 was determined in gel electrophoresis mobility-shift assays using nuclear extracts isolated from primary human keratinocytes isolated 30 min post UVA irradiation ( $30\text{J}/\text{cm}^2$ ) co-incubated with a radiolabeled oligonucleotide containing the AP-2 recognition site of the ICAM-1 promoter. Radiolabeled AP-2 oligonucleotide alone (lane 1), radiolabeled AP-2 oligonucleotide co-incubated with nuclear extract from unirradiated cells (lane 2), from UVA-treated cells (lane 3), from cells treated with DANA alone ( $10\ \mu\text{M}$ , 1 h incubation prior to UVA irradiation time point and 30 min incubation post irradiation time point, lane 4), and from primary human keratinocytes, which had been pre-incubated with  $10\ \mu\text{M}$  DANA and UVA irradiated (lane 5). Reproducible results were obtained and representative data are presented.

### 3.4.2. Effects of cholesterol levels on UVA radiation-induced signal transduction

Caveolin-1 is a cholesterol-binding protein and may act as stabilizer of caveolae (Murata *et al.* 1995), because cholesterol is required for the integrity of caveolae since sterol-binding drugs such as nystatin or filipin disorganize morphology of caveolae (Rothberg *et al.* 1992). Regarding UVA-induced effects, it has recently been shown that UVA irradiation results in a decrease of raft localized cholesterol content. Moreover, decrease of cholesterol increased the susceptibility of human keratinocytes towards UVA radiation-induced gene expression (Grether-Beck *et al.* 2008). We, therefore, next examined the impact of modulating cellular cholesterol level of human keratinocytes on UVA radiation-induced caveolin-1 phosphorylation. To increase cellular cholesterol, we pretreated human keratinocytes with  $30\ \mu\text{M}$  cholesterol for 24 h prior to stimulation, this treatment was shown to be capable of increasing raft cholesterol to approximately 200%. In contrast, pretreating the cells with  $5\ \text{mM}$   $\beta$ -methylcyclodextrin ( $\beta\text{MCD}$ ) for 2 h was shown to decrease the cholesterol level to 50% (Grether-Beck *et al.* 2008). As shown in Figure 3.23, western blot analysis of total

extracts prepared from human keratinocytes either irradiated with 30 J/cm<sup>2</sup> UVA and harvested after 30 min post irradiation or treated with 10  $\mu$ M C6-ceramide and harvested after 30 min incubation, followed by densitometry analysis of the p-caveolin-1 Y14 signal revealed that cholesterol pretreatment attenuates caveolin-1 phosphorylation upon UVA radiation as well as upon stimulation with exogenous ceramide: In contrast, depletion of cholesterol by pretreatment with  $\beta$ MCD enhanced caveolin-1 phosphorylation upon both treatments.

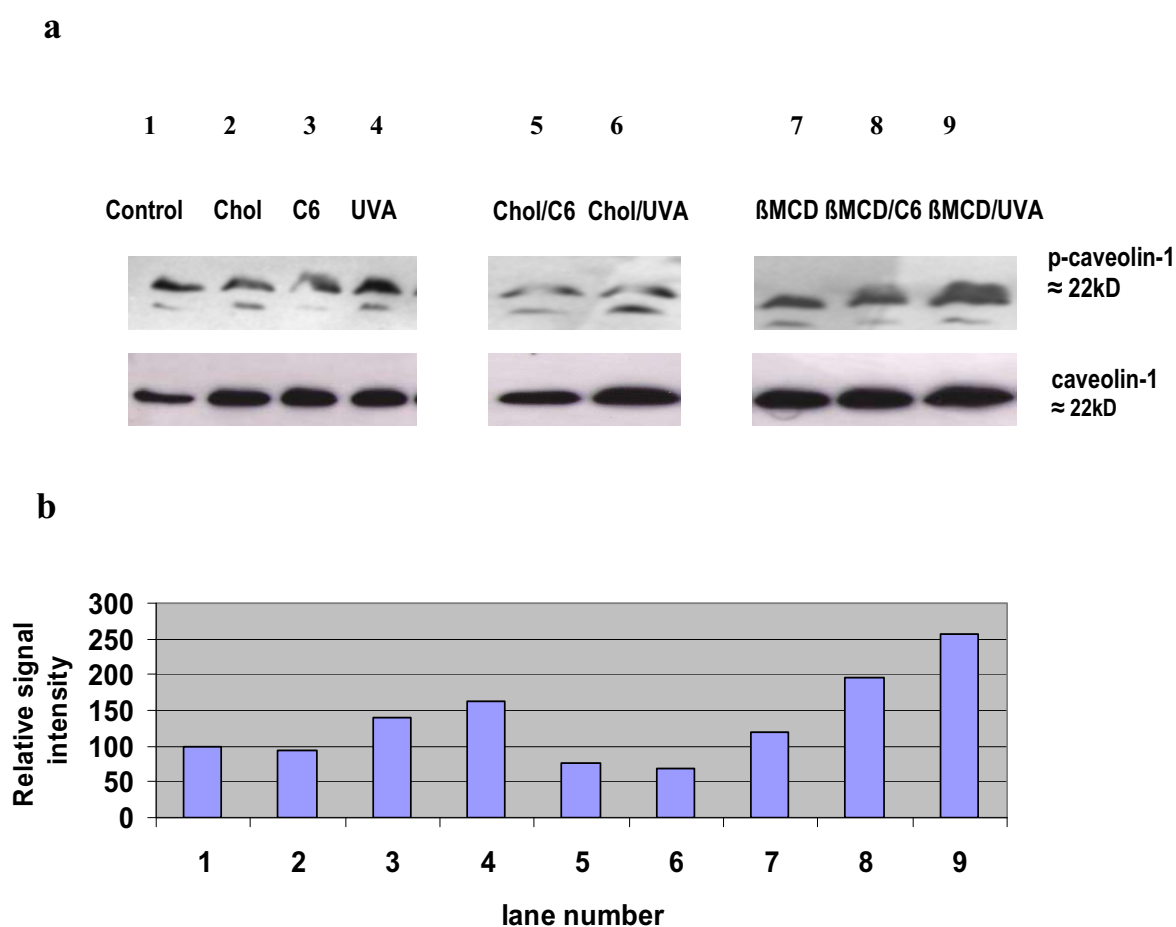


**Figure 3.23: Effect of cholesterol content on UVA radiation-induced and ceramide-induced caveolin-1 phosphorylation.** (a) Wild type HaCaT cells were left untreated (control, lane 1) or were treated with 30  $\mu$ M cholesterol for 24 h (chol, lane2), were irradiated with 30 J/cm<sup>2</sup> UVA and harvested after 30 min post exposure (UVA, lane 3), were treated with 10  $\mu$ M C6-ceramide and harvested after 30 min (C6, lane 4), were pretreated with 30  $\mu$ M cholesterol for 24 h prior to ceramide treatment (chol/C6, lane 5), were pretreated with 30  $\mu$ M cholesterol for 24 h prior to UVA irradiation (chol/UVA, lane 6), were pretreated with 5 mM  $\beta$ -methylcyclodextrin and harvested after 2 h ( $\beta$ MCD, lane7), were pretreated with 5 mM  $\beta$ -methylcyclodextrin for 2 h prior to ceramide treatment ( $\beta$ MCD/C6, lane8), or were pretreated with 5 mM  $\beta$ -methylcyclodextrin for 2 h prior to UVA irradiation ( $\beta$ MCD/UVA, lane 9). The immunoblotting was carried out using a specific antibody for p-caveolin-1 Y14. Reproducible results were obtained and representative data are presented. (b) the density of the signal is calculated using Image J program and is presented as % intensity change as compared to the control untreated sample (set 100%).



We wondered whether inhibition of caveolin-1 phosphorylation upon UVA by cholesterol pretreatment was also caused by concomitant decrease of Src kinase activity. For this purpose, we assessed UVA radiation-induced Src kinase activity in human keratinocytes, in which cholesterol content was altered in identical experimental conditions as above. In line with the previous findings, Src kinase activity was affected in a similar manner (Figure 3.24), indicating that in human keratinocytes, low cholesterol level favors UVA radiation-induced Src activation, whereas, high cholesterol level decrease it.

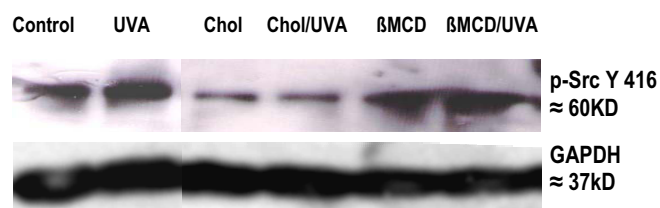


**Figure 3.24: Modulating cholesterol content affects UVA radiation-induced Src kinase activation.** Wild type HaCaT cells were either left untreated (control), were pretreated with cholesterol (Chol), or  $\beta$ -methylcyclodextrin ( $\beta$ MCD), were only UVA irradiated or were irradiated after pretreatments and harvested 30 min post UVA exposure time point. Conditions were as follows: UVA dose 30 J/cm<sup>2</sup>, 30  $\mu$ M cholesterol pretreatment for 24 h, 5 mM  $\beta$ -methylcyclodextrin pretreatment for 2 h.

The immunoblotting was carried out using a specific antibody for p-Src kinase Y416. GAPDH served as loading control. Reproducible results were obtained and representative data are presented.

### 3.5. Impact of ratio ceramide / cholesterol for signaling

Recently, we had shown that UVA-induced signaling occurred, when the ratio of ceramide versus cholesterol in rafts was  $> 1$  (Table 3.4, (Grether-Beck *et al.* 2008)).

**Table 3.4: Molar ratio of sphingomyelin, cholesterol and ceramide in rafts under various conditions and relation to signaling events such as ceramide formation and ICAM-1 upregulation.**

Stimulus	Cholesterol set to 1			Signaling	
	Sphingomyelin	Cholesterol	Ceramide	Ceramide Formation	ICAM-1 Induction
Control	0.38	1	0.5	-	-
UVA	0.6	1	2.6	++	++
Cholesterol	0.4	1	0.2	-	-
Cholesterol/UVA	0.42	1	0.2	-	-
$\beta$ MCD	1.15	1	2.6	++	++
$\beta$ MCD/UVA	0.92	1	3.8	+++	+++
Ceramide	0.38	1	2.3	++	++
Cholesterol/Ceramide	0.3	1	1.1	+	+

Abbreviations:  $\beta$ MCD,  $\beta$ -methylcyclodextrin; Chol, cholesterol; ICAM, intercellular adhesion molecule, UVA, ultraviolet A. +, slight induction; ++, induction; +++, strong induction. In detail: UVA (30J/cm<sup>2</sup>), Chol (30 $\mu$ M, 24 h),  $\beta$ MCD (5mM, 2 h).

In the wild type cells, the relative increase of ceramide formation and ICAM-1 expression had been calculated based on procedures setting the basal values equal to one.

In caveolin-1 knockdown cells, we had observed that no further ceramide formation and ICAM-1 upregulation could be achieved after UVA irradiation. Analysis of the ratio of ceramide / cholesterol indicates that untreated caveolin-1 knockdown cells already presented an increased ratio of ceramide / cholesterol being larger than one (Table 3.5).

**Table 3.5: Molar ratio of sphingomyelin, cholesterol and ceramide in rafts after UVA treatment (n=4) and relation to signaling events such as ceramide formation and ICAM-1 upregulation in caveolin-1 knockdown cells.**

<b>Caveolin-1 knockdown cells</b>	<b>Cholesterol set to 1</b>			<b>Signaling</b>	
	<b>Sphingomyelin</b>	<b>Cholesterol</b>	<b>Ceramide</b>	<b>Ceramide Formation</b>	<b>ICAM-1 Induction</b>
Control (1)	0.75	1	7.3	-	-
UVA (1)	0.65	1	1.8	-	-
Control (2)	0.7	1	6.7	-	-
UVA (2)	0.77	1	2.0	-	-
Control (3)	0.53	1	6.4	-	-
UVA (3)	0.56	1	2.5	-	-
Control (4)	0.6	1	7.2	-	-
UVA (4)	0.8	1	2.7	-	-

## **4. Discussion**

### **4.1. The role of lipid rafts in UVA radiation-induced signal transduction**

There is increasing evidence that longwave ultraviolet radiation (UVA; 320-400 nm) plays an important role in the pathogenesis of photodermatoses such as polymorphous light eruption as well as photoaging (Krutmann 2000). In order to fully understand these detrimental effects it is important to analyze the photobiological and molecular mechanisms by which UVA radiation affects the function of human skin cells. In attempt to further elucidate the molecular mechanisms involved in UVA radiation-induced gene expression, we have assessed the role of lipid rafts in UVA radiation-induced signal transduction in this thesis. For this purpose, human keratinocytes were exposed to 30 J/cm<sup>2</sup> of UVA radiation. This dose was equivalent to the amount of UVA radiation human skin may be exposed to on a summer day at approximately noon at the Northern latitude of 30°-35° during a 1- to 2-h period (Grether-Beck *et al.* 1996). In addition, a UVA radiation dose identical to the dose used in this study is capable of inducing skin lesions in patients suffering from polymorphous light eruption. The development of skin lesions in these patients after UVA radiation exposure is accompanied by a prolonged expression of proinflammatory genes such as ICAM-1 in keratinocytes. In previous studies in our laboratory, it has been shown that UVA radiation-induced gene expression is initiated by the generation of ceramide at the plasma membrane via non-enzymatic hydrolysis of sphingomyelin. Sphingomyelin hydrolysis upon UVA irradiation was found to be a result of reactive oxygen species generation at the plasma membrane of the irradiated cells (Grether-Beck *et al.* 2000). Direct evidence that reactive oxygen species affect raft signaling and function through their actions on many lipid raft components such as ceramide, cholesterol and related raft proteins has recently been presented (Dumitru *et al.* 2007; Morgan *et al.* 2007). Furthermore, we have recently shown that UVA radiation-induced gene expression and ceramide signaling are linked (Grether-Beck *et al.* 2008). Ceramide formation occurs upon UVA treatment within microdomains enriched in sphingolipids and cholesterol but display low protein content.

Resting lipid rafts are generally 50-100 nm in diameter and thus cannot be visualized directly. One approach used to study lipid rafts is the biochemical isolation of these structures. Based on their specific physicochemical properties, lipid rafts have been isolated as low density and detergent (Triton X-100)-resistant membrane fractions by fractionation of the cellular components through a discontinuous density gradient (Mishra & Jushi 2007). Using the method of Brown & Rose (1992) we were able to isolate lipid

rafts exhibiting no contamination by other non-raft plasma membranes or intracellular membranes.

#### **4.2. UVA radiation leads to decrease of the ganglioside GM3 content in rafts and total cell extracts of human keratinocytes via activation of neuraminidase 3 enzyme.**

We have demonstrated in the present study that UVA irradiation leads to GM3 degradation in total cell extracts and in rafts of primary human keratinocytes or HaCaT cells through the activation of neuraminidase 3. Our results also indicate that the extent of induction of the enzyme activity was slightly higher in total cell extracts than in rafts. This observation is consistent with our finding that the degree of GM3 decrease upon UVA irradiation was higher in total cell extract than in rafts. However, it was obvious that neuraminidase 3 is enriched within rafts, because the specific activity of neuraminidase 3 in rafts ( $5.6 \pm 0.7$  U/mg total protein; mean $\pm$ SD, n=3) was higher than in total cell extracts of unstimulated control HaCaT cells ( $3.1 \pm 0.2$  U/mg total protein; mean $\pm$ SD, n=3) (Table 1). Consistently, it has recently been shown using laser confocal microscopic analysis that neuraminidase 3 is also localized in intracellular structures (Zanchetti *et al.* 2007). Neuraminidase 3 mainly co-localizes with markers of lipid rafts including flotillins and Src kinase (Kalka *et al.* 2001). As shown in Figure 3.2, 30 min after UVA irradiation, the activity of neuraminidase3 in total extracts was increased by about 4-fold, whereas, the enzyme activity was increased by about 3-fold in rafts.

Accordingly, 24 h post UVA treatment UVA radiation-induced activation of neuraminidase 3 was markedly increased in total cell extracts (2.3-fold), whereas we could not observe any increased activity at this time point in rafts (1.0-fold). The 2.3-fold increase in neuraminidase 3 activity in total extracts was accompanied by a 1.6-fold increase in neuraminidase 3 (Neu3) mRNA expression at that time point. In addition, we demonstrated in this study that primary normal human keratinocytes exhibit lower neuraminidase 3 activity than the spontaneously immortalized keratinocyte derived HaCaT cell line (Table 3.1). Our findings are consistent with studies by Wada (Wada *et al.* 2007) where normal human keratinocytes possessed lower level of neuraminidase 3 mRNA than the epithelial HeLa cell line. In the cell line HeLa, neuraminidase 3 activity was about 3 U/mg total protein, while normal human keratinocytes had a basal neuraminidase 3 activity of 2.2 U/mg total protein.

Neuraminidase 3 is the plasma membrane-associated neuraminidase (Miyagi *et al.* 1999; Yamaguchi *et al.* 2006) exhibiting high substrate specificity towards GM3. GM3 degradation by neuraminidase 3 results in release of sialic acid (Ha *et al.* 2004; Miyagi *et*

*al.* 2008b; Oehler *et al.* 2000). It has previously been shown that sialic acid functions as a hydrogen peroxide scavenger under physiological conditions (Iijima *et al.* 2004). This observation could be of physiological relevance for UVA-induced activation of neuraminidase 3, because UVA radiation induced stress response in human keratinocytes is initiated by generation of reactive oxygen species in a photo-oxidative process (Grether-Beck *et al.* 1996). In the present work, we have demonstrated that pretreatment of human keratinocytes with 2-deoxy-2,3-didehydro-*N*-acetylneuraminic acid (DANA) strongly inhibits the UVA-induced neuraminidase 3 activity and its subsequent GM3 degradation (Figure 3.4 and Figure 3.7). DANA is a sialic acid analog which exhibits high structural similarity to the potent inhibitor of influenza virus neuraminidase zanamivir. The inhibitor DANA differs from the effective influenza drug 4-guanidino-2-deoxy-2,3-didehydro-*N*-acetylneuraminic acid (Zanamivir) simply by the substitution of the O<sub>4</sub>-hydroxyl moiety with a guanidine group as it could be seen in Figure 4.1 (Burmeister *et al.* 1993; Smith *et al.* 2001). Both inhibitors act by preventing the enzyme from cleaving sialic acid residues (Elliott 2001). Interestingly, DANA was detected as a normal component of human urine, serum and saliva (Haverkamp *et al.* 1976). Regarding specificity of DANA towards neuraminidase 3, the compound has been shown to inhibit neuraminidase 3 purified from human neurons *in vitro* with a IC<sub>50</sub> of 10 μM (Kopitz *et al.* 1997b; Oehler *et al.* 2000). In addition, it has previously been shown that DANA is a potent inhibitor specific for human neuraminidase 3 (Da Silva *et al.* 2005; Kopitz *et al.* 1997a; Usuki *et al.* 1988a; Woronowicz *et al.* 2007). Additional *in vivo* evidence from experiments in cell culture using metabolic labelling studies in SK-N-MC neuroblastoma cells, showing that presence of DANA in the culture medium results in specific inhibition of desialylation of the gangliosides lining the plasma membrane including GM3 (Kopitz *et al.* 1996). Analyzing substrate specificity of neuraminidase 3 in neuroblastoma cells revealed that brain neuraminidase 3 is highly specific for GM3 leading to formation of lactosylceramide (Kopitz *et al.* 1997a). Importantly, presence of DANA in the culture medium indeed affected solely the cell surface enzyme and not also a lysosomal sialidase, this was demonstrated in an experiment where the desialylation of exogenously added radioactive gangliosides was determined in absence and presence of DANA and NH<sub>4</sub>Cl, which is an inhibitor of lysosomal function (Kopitz *et al.* 1997b).

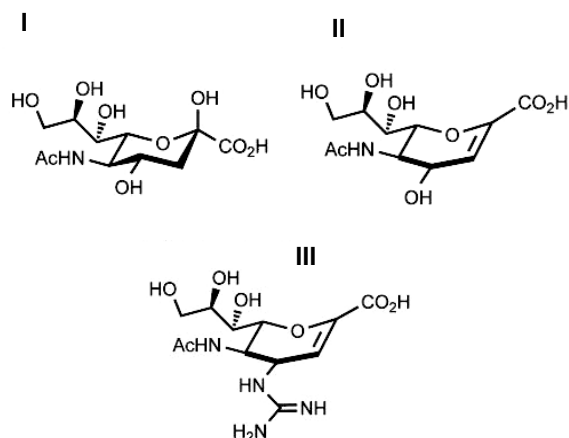


**Figure 4.1: Chemical structure of some sialidase inhibitors.** (I) *N*-acetylneuraminic acid (Sialic acid); (II) 2-deoxy-2,3-didehydro-*N*-acetylneuraminic acid (DANA); and (III) 4-guanidino-2-deoxy-2,3-didehydro-*N*-acetylneuraminic acid (Zanamivir), (Jeffrey & Carolyn 2008).

We have demonstrated that, DANA pretreatment also inhibits UVA radiation-induced neuraminidase 3 mRNA upregulation in human keratinocytes (Figure 3.5). The expression of mRNA encoding neuraminidase 3 gene (*Neu3*) was upregulated 8 h (2-fold) after UVA irradiation and was also elevated at 24 h (1.6-fold) post treatment. The differences observed with regards to percentage increase of mRNA level and enzyme activity are probably caused by involvement of posttranscriptional modification of neuraminidase 3 such as phosphorylation. It is known that the phosphorylation of Tyr 412 of the lysosomal form of neuraminidase regulates its distribution within the cell (Lukong *et al.* 2001).

It is worth mentioning that interleukin-6 (IL-6) treatment is capable of inducing neuraminidase 3 mRNA expression and activity in renal cell carcinomas (Ueno *et al.* 2006). Since UVA radiation rapidly induces the expression of interleukin-6 in human keratinocytes (Tebbe *et al.* 1997) and fibroblasts (Vielhaber *et al.*, 2006), the possible biological relevance of cytokine release upon UVA irradiation to neuraminidase 3 may be considered.

#### **4.3. UVA radiation-induced GM3 degradation partially contributes to UVA radiation-induced ceramide formation**

We have observed in the present study that a part of the ceramide formed 30 min post UVA irradiation is due to GM3 degradation by neuraminidase 3 (Figure 3.7), because complete inhibition of GM3 degradation by means of DANA resulted in about 30% decrease in lactosylceramide and ceramide formed in rafts and about 55 % decrease in the amount of ceramide seen in total cell extracts (Figure 3.9). In this regard, we recently

showed that (i) more than 60 % of the ceramide formed in rafts of human keratinocytes upon UVA irradiation originates from hydrolysis of sphingomyelin and that (ii) the amount of sphingomyelin hydrolysis was more pronounced in rafts than in total cell extracts (Grether-Beck *et al.* 2008), suggesting that the predominant mechanism of ceramide formation in rafts of irradiated cells is the non-enzymatic hydrolysis of sphingomyelin. It is worth mentioning that blocking GM3 degradation in irradiated cells by means of DANA had no effect on the sphingomyelin hydrolysis observed in rafts of these cells (Figure 3.11b).

Recently, formation of lactosylceramide and ceramide from GM3 at the plasma membrane of human fibroblasts, overexpressing neuraminidase 3 has been shown (Valaperta *et al.* 2006). In this study, lysosomal degradation of GM3 by neuraminidase 1 was excluded by treatment with chloroquine or ammonium chloride.

#### **4.4. Neuraminidase 3 partially contributes to UVA radiation-induced gene expression**

UVA radiation induces ICAM-1 gene transcription in human keratinocytes in a biphasic manner. The first peak was observed between 4-8 h after UVA exposure and the second was detected after 24 h post irradiation (Grether-Beck *et al.* 1996). The early increase of ICAM-1 mRNA upregulation was mediated via ceramide release at the plasma membrane that can be detected within the first two hours after irradiation. Ceramide formation during this period of time was shown to be mediated by a non-enzymatic hydrolysis of plasma membrane localized sphingomyelin via the generation of singlet oxygen. UVA treatment and also a singlet oxygen generating system were able to form ceramides from sphingomyelin-rich liposomes free of proteins *in vitro*. Moreover, addition of a singlet oxygen quencher such as vitamin E was shown to effectively prevent UVA radiation-induced ceramide formation (Grether-Beck *et al.* 2000). The second increase of ICAM-1 expression was again mediated via the second messenger ceramide detected 16 h after irradiation. In this case, the second messenger was formed as a result of an increased mRNA expression of serine palmitoyltransferase in response to the early ceramide release after UVA irradiation (autocrine loop). The second peak is a consequence of the first peak. Accordingly, inhibition of the first ceramide peak abolished the early and the late ICAM-1 upregulation seen upon UVA treatment (Grether-Beck *et al.* 2005b). In keeping with this concept, we have observed that partial inhibition of the first ceramide peak in human keratinocytes upon UVA treatment by means of the neuraminidase 3 inhibitor DANA



results in a subsequent partial inhibition of the first and the second ICAM-1 mRNA upregulation seen after 8 h and 24 h post irradiation (Figure 3.6).

The functional relevance of UVA radiation-induced neuraminidase 3 activation for UVA radiation-induced ICAM-1 expression is supported by the observation that modulating cellular cholesterol level affects UVA radiation-induced neuraminidase 3 activation in a similar manner as observed for UVA radiation-induced ICAM-1 mRNA expression (Figure 3.3). Increasing cellular cholesterol by cholesterol preloading has previously been shown to prevent UVA radiation-induced ICAM-1 upregulation, whereas, depleting cellular cholesterol by means of  $\beta$ -methylcyclodextrin ( $\beta$ MCD) enhanced UVA radiation-induced ICAM-1 upregulation.  $\beta$ -methylcyclodextrins are cyclic water-soluble heptasaccharides consisting of  $\beta$ (1-4) glucopyranose units, which contain a hydrophobic core capable of solubilizing sterols (Grether-Beck *et al.* 2008). Accordingly, increasing cellular cholesterol decreased UVA radiation-induced neuraminidase 3 activation, whereas, decreasing cholesterol enhanced UVA radiation-induced neuraminidase 3 activation. Modulating cholesterol content has been shown to affect ceramide release in lipid rafts ceramide formation. Increased cholesterol content can also diminish hydrolysis of sphingomyelin upon UVA treatment and thereby decrease the formation of ceramide. In contrast to our results, Wang and co-workers (Wang *et al.* 2002b) demonstrated a decrease of neuraminidase 3 activity after depletion of cholesterol by means of  $\beta$ -methylcyclodextrins in HeLa cells. In these studies, neuraminidase 3 co-fractionated with caveolin-1 probably due interaction to a caveolin-1 binding motif and accordingly overexpression of caveolin-1 also increased Neu 3 activity. Interestingly,  $\gamma$ -cyclodextrin could increase neuraminidase activity from *Arthrobacter ureafaciens* to effectively cleave the internal sialic acid residue from GM1 (Mitsumori *et al.* 2009).

Pretreatment with  $\alpha$ -tocopherol (vitamin E) a well known singlet oxygen quencher, markedly inhibited UVA radiation-induced neuraminidase 3 activation (Figure 3.3). UVA radiation-induced ICAM-1 mRNA expression was shown to be mediated through the generation of singlet oxygen (Grether-Beck *et al.* 1996). This effect was abolished by addition of vitamin E, because vitamin E effectively prevents UVA-induced ceramide formation (Grether-Beck *et al.* 2000).

#### **4.5. A link between caveolin-1 and neuraminidase 3 in UVA-induced gene expression**

Neuraminidase 3 functions as a caveolin-related signaling molecule within caveolin rich microdomains. Human neuraminidase 3 is enriched in caveolae of HeLa cells and closely

associates with caveolin-1 (Wang *et al.* 2002b). The residues 179-186 (YTYYPISW) within the hydrophobic stretch of the putative transmembrane domain sequence in Neu3 have been identified as binding motif to interact with the scaffolding domain of caveolin-1 (20 amino acids, residues 82–101) (Couet *et al.* 1997a). Most of caveolae-associated proteins (including Src kinase) contain such a binding motif in their amino acid sequence. As the caveolin region preferentially recognizes the inactive conformation of these molecules, it has been suggested that caveolae may function as subcellular compartments to store inactive signaling molecules for regulated activation. In case of neuraminidase 3, a mutation with a single amino acid change in the caveolin-binding motif led to inhibition of recruitment of the sialidase to caveolae accompanied by reduction of the enzyme activity (Wang *et al.* 2002b). In contrast, neuraminidase 3 was activated by increased caveolin-1 expression in HeLa cells (Wang *et al.* 2002b). A tight association of neuraminidase 3 with caveolin-1 was supported further by co-immunoprecipitation of neuraminidase 3 by anti-caveolin-1 antibody.

We have also demonstrated in this work that caveolin-1 depletion by means of retro-virus mediated RNA interference completely blocks UVA-induced ICAM-1 upregulation (Figure 3.12). Given that ceramide release upon UVA irradiation is an indispensable prerequisite for ICAM-1 upregulation, depletion of caveolin-1 also inhibited the sensitivity of human keratinocytes towards UVA-induced ceramide formation. (Figure 3.14b).

Caveolin-1-mediated neuraminidase 3 activity upon UVA exposure in human keratinocytes was of functional relevance for UVA-induced ICAM-1 mRNA upregulation. In this regard, caveolin-1 depletion has previously been shown to result in disappearance of caveolae from the cells, furthermore, electron microscopy analysis of cells derived from caveolin-1 null mice demonstrated a loss of caveolae (Drab *et al.* 2001; Razani *et al.* 2002; Zhao *et al.* 2002).

Although the level of sphingomyelin decreased in caveolin-1 knockdown cells upon UVA exposure, no detectable amount of ceramide could be observed (Figure 3.14b and Figure 14c). In this regard, it is attempting to speculate that the ceramide generated from sphingomyelin hydrolysis might rapidly be consumed, because we have observed a slight increase in GM3 and GM1 levels in rafts of caveolin-1 knockdown cells upon UVA irradiation (Figure 3.14a). This speculation needs further investigation. As GM1 can be generated from GM3 in stepwise reactions (Proia 2003) it is reasonable that GM1 levels increase as a consequence of GM3 formation.

These observations could also suggest that in caveolin-1 knockdown cells UVA-induced sphingomyelin hydrolysis does not occur to a similar extent as observed in wild types, because the raft compositions differ (Tables 3.4 and 3.5). In previous studies we had presented evidence that signaling occurred when the ratio of ceramide versus cholesterol was  $> 1$ . In the caveolin-1 knockdown cells this ratio was already larger than one in untreated cells. The corresponding neuraminidase 3 expression and the downstream elements of the signaling cascade (i) Src kinase activation, (ii) AP2- activation and (iii) ICAM-1 expression were elevated already and no further increase could be obtained upon UVA treatment.

The mechanisms by which cholesterol decrease enhances ceramide release have been discussed in detail in the study of Grether-Beck (Grether-Beck *et al.* 2008). However, it is worth mentioning, that cholesterol decrease might be a consequence of its displacement by UVA-induced ceramide formation from hydrolysis of sphingomyelin and from degradation of gangliosides by neuraminidase 3. Depletion of sphingomyelin due to enzymatic degradation e.g. due to addition of bacterial sphingomyelinase C has been shown to result not only in a decrease of sphingomyelin and formation of ceramide, but also leads to a rapid translocation of free cholesterol from the plasma membrane to intracellular sites, where it is esterified to cholesteryl esters. In case of sphingomyelinase D, not ceramide but ceramide phosphate is formed and translocation of free cholesterol to intracellular locations is diminished to 20%, indicating that the loss of cholesterol observed for sphingomyelinase C is mainly due to the formation of ceramide and not due to the decrease of sphingomyelin (Subbaiah *et al.* 2003). This findings are consistent with the concept that UVA-induced sphingomyelin decrease is not independent from UVA-induced cholesterol decrease (Grether-Beck *et al.* 2008). In difference to most biological phospholipids, the acyl-chains of sphingomyelin are mostly long and largely saturated. This acyl-chain structure allows a more dense and ordered packing of molecules likely to result in the formation of specialized functional microdomains like the sphingomyelin- and cholesterol rich structures called rafts (Brown & London 1998).

Biophysical studies showed that ceramides mix very poorly with cholesterol and spontaneously undergo lateral phase separation and formation of ceramide-enriched microdomains. In addition, the interaction of cholesterol with sphingomyelin occurs through hydrogen bonding of the C3-hydroxyl of cholesterol with sphingosine backbone of sphingomyelin. Although this structure is maintained in ceramide, the loss of the polar phosphocholine group during ceramide formation from sphingomyelin results in a

ceramide molecule having a very poor affinity for cholesterol (Yu *et al.* 2005). Moreover, treatment of immortalized Schwann cells with bacterial sphingomyelinase not only resulted in ceramide formation from sphingomyelin but also in a decrease of the cholesterol binding protein caveolin-1.

Consistently, we have observed a marked difference in the degree of UVA-induced cholesterol decrease in rafts of caveolin-1 knockdown cells and wild type cells. Caveolin-1 depletion attenuated UVA-induced cholesterol decrease. Previous experiments have clearly shown that UVA treatment does not result in formation of radical- or singlet oxygen mediated oxysterols (Grether-Beck *et al.* 2008). Therefore, it is reasonable to propose that caveolin-1 might play a role in the observed UVA-induced decrease of cholesterol within the rafts of human keratinocytes e.g. via caveolin-mediated trafficking mechanisms. Caveolin-1 is a cholesterol binding protein constitutively transporting cholesterol to the cell surface (Smart *et al.* 1996). Moreover, depletion of caveolin-1 from the plasma membrane by expression of a dominant negative mutant of caveolin-1, which still contains an intact scaffolding domain was accompanied with depletion of caveolae, as well as a reduced efflux of cellular cholesterol (Pol *et al.* 2001). In fact, the observed decrease of raft localized sphingomyelin in caveolin-1 knockdown cells (about 50 %) was slightly lower by trend than in wild type cells (about 60 %) upon UVA treatment.

We have recently shown that the ratio of ceramide versus cholesterol in rafts determines signaling. Therefore also the ratio of the two lipids were calculated in caveolin-1 knockdown cells (Table 3.5) In primary human keratinocytes as well as in wild type HaCaT signaling occurred when the ratio of ceramide versus cholesterol was found to be  $> 1$ . In our caveolin-1 knockdown cells, the ratio of ceramide to cholesterol was even in the untreated control cells  $>1$  and was associated with an increased basal neuraminidase activity (Table 3.2).

#### **4.6. Role of caveolin-1 in ceramide-induced ICAM-1 expression**

Strong inhibition of neuraminidase 3 activity in wild type cells by means of DANA results in a complete block of UVA-induced ICAM-1 upregulation (Figure 3.4 and Figure 3.12), possibly indicating that UVA-induced neuraminidase 3 activity is an indispensable prerequisite for ICAM-1 upregulation. We have addressed the question whether inhibition of ICAM-1 upregulation by caveolin-1 depletion is a consequence of impaired ceramide release or impaired neuraminidase 3 activation upon UVA irradiation. Stimulation of keratinocytes with exogenous ceramide can be considered as a substitute for ceramide

response occurring early after UVA exposure (Grether-Beck *et al.* 2005b). Additionally, recent evidence indicated that stimulation of unirradiated keratinocytes with ceramides induced ceramide dependent signal transduction. Ceramide-induced signaling is tightly associated with ceramide-induced changes in the composition and the function of rafts, because addition of ceramides led to marked decrease of cholesterol and sphingomyelin content within rafts (Grether-Beck *et al.* 2008).

We have observed that caveolin-1 depletion does not affect the uptake of exogenous ceramide into rafts, because the extent of ceramide increase in rafts of caveolin-1 knockdown cells did not differ from that of wild type cells (Figure 3.15a). However, addition of exogenous ceramide to caveolin-1 knockdown cells was not capable of inducing ICAM-1 upregulation (Figure 3.15c). Interestingly, we have observed that exogenous ceramide can activate neuraminidase 3 in rafts of wild type cells, whereas, in caveolin-1 knockdown cells, exogenous ceramide induced neuraminidase 3 activity to a lesser extent (Figure 3.15b).

In confluent HaCaT keratinocytes fluorescent labeled ceramides were rapidly incorporated into the plasma membrane, quickly moved to intracellular compartments, and were found to be concentrated in the Golgi stacks (Wanner *et al.* 2004). As a considerable fraction of added lipids was metabolized before being transported to intracellular compartments, rapid metabolic activities seem to be localized at the plasma membranes. It is of interest that ceramide is capable of inducing gene expression in human keratinocytes at concentrations that are several fold lower than those necessary to induce apoptosis. Although both effects are sharing same features e.g. the release of cytochrome *c* from mitochondria, the concentrations of ceramides required for regulating gene expression were lower than those needed to induce caspase 3 activation in primary keratinocytes (Grether-Beck *et al.* 2003).

Besides UVA and exogenous ceramide also addition of GM3 results in induction of both ceramide release and neuraminidase 3 activity (Figure 3.16 b and Figure 3.16c) in wild type cells. In contrast, inhibition of ICAM-1 upregulation by caveolin-1 depletion is also observed upon addition of exogenous GM3 to caveolin-1 knockdown cells (Figure 3.16d), further supporting our concept that UVA-induced activation of neuraminidase 3 is an indispensable prerequisite for a UVA response.

There is increasing evidence that gangliosides on the outer surface of mammalian cell membranes significantly contribute to a variety of cellular events such as proliferation, tumor progression or metastasis (Birklé *et al.* 2003). Since glycolipids are rapidly taken up

by cells from the culture medium (Spiegel *et al.* 1984) attempts were reported to supplement surface membrane glycolipids by incorporation of exogenous compounds. Incorporation of exogenous gangliosides into the plasma membrane has been extensively studied using radiolabelled as well as fluorescently labelled gangliosides. It is worth mentioning that incorporation and metabolism of the exogenous gangliosides are varying among the different cell types.

In our study, cellular GM3 content was transiently increased upon addition of the compound and also an increase in neuraminidase 3 activity was observed. Moreover, GM3-induced neuraminidase 3 activation was paralleled by an increase in ceramide content (Figure 3.16a, Figure 3.16b, and Figure 3.16c) suggesting that a considerable amount of the added GM3 was successfully incorporated into the cells. Remarkably, the amount of ganglioside GM3 in the cell culture medium when 10  $\mu$ M GM3 is added is, by calculation, more than 60 times that in keratinocytes cell membrane (Paller *et al.* 1993), suggesting exogenous GM3 to be a pharmacological modulator rather than a physiological modulator of neuraminidase 3 at the cell membrane.

Concerning GM3 degradation at the plasma membrane, it has been previously speculated that this ganglioside is actively degraded at the plasma membrane to lactosylceramide and free sialic acid by neuraminidase activity *in situ* on the outer surface of cultured human fibroblasts (Usuki *et al.* 1988b). Using radiolabelled compounds it has been shown that 35 % of the ganglioside GM3 at the cell surface are actively metabolized during a chase period of 24 h. The lactosylceramide formed then cycled to the Golgi apparatus where GM3 is synthesized by addition of sialic acid and the newly synthesized GM3 is returned to the plasma membrane (Usuki *et al.* 1988b).

Since increased concentrations of substrate are an obvious regulatory factor in many enzyme-catalyzed reactions, it is reasonable to speculate that increasing cellular GM3 content by addition of GM3 rapidly stimulates neuraminidase 3 activity leading to an increased formation of lactosylceramide.

In line with our findings, increasing endogenous levels of lactosylceramide resulted in induction of ICAM-1 mRNA upregulation in vascular endothelial cells and cell systems through the generation of reactive oxygen species (Bhunja *et al.* 1998; Yeh *et al.* 2001). As addition of exogenous GM3 to caveolin-1 knockdown cells did not induce ICAM-1 upregulation, presence of caveolin-1 in the cell is an essential prerequisite for GM3-induced ICAM-1 upregulation during the time course of our experiment (Figure 3.16d).

#### **4.7. Cross-talk involving Src kinase, caveolin-1 and neuraminidase 3 in UVA radiation-induced signal transduction**

Caveolae and caveolin-1 play an important role in the modulation of cell signal transduction (Quest A. *et al.* 2004; Simons & Toomre 2000). Biochemical analysis of isolated caveolae indicated that these structures contain a variety of signaling molecules such as Src-like kinases and heterotrimeric G proteins. Caveolin-1 interacts with a lot of lipid-anchored integral membrane and soluble signaling proteins recruited to caveolae during their activation cycles including Src kinase (Schlegel *et al.* 2000). The N- and C-termini of caveolin-1 face the cytoplasm with an intervening 33 amino acid hydrophobic segment predicted to reside within the membrane. The C-terminus of caveolin is attached to the lipid bilayer by three palmitoyl residues. The amino acids 82-101 of caveolin-1 immediately adjacent to the membrane insertion site are serving as scaffolding domain. In a model membrane, the scaffolding domain peptide consisting of amino acids 82-101 induced the formation of domains enriched in cholesterol and phospholipids (Wanaski *et al.* 2003). Moreover, the Src kinase binding region was co-localized in such domains (Ikonen *et al.* 2004). By interaction of the scaffolding domain with an aromatic amino acid based caveolin binding domain usually found in the active catalytic domain of a given caveolae associated protein caveolin-1 can render a molecule inactive within the caveolae e.g. by inhibition of EGF receptor autophosphorylation (Couet *et al.* 1997b) or can activate a pathway as shown for insulin signaling (Cohen *et al.* 2003). Environmental stressors such as high osmolarity but not heat shock resulted in a transient phosphorylation of caveolin-1 at tyrosine 14 mediated via p38 MAP kinase and c-Src. Upon phosphorylation, a partial redistribution of caveolin-1 occurs leading to co-localization of tyrosine 14-phosphorylated caveolin-1 and focal adhesions that are major sites of tyrosine kinase signaling. Similarly, oxidative stress such as H<sub>2</sub>O<sub>2</sub> but also UVC (360 J/m<sup>2</sup>) induced tyrosine 14-phosphorylation of caveolin-1 (Volonte *et al.* 2001).

UVA exposure of primary human keratinocytes (30 J/cm<sup>2</sup>) resulted in a transient phosphorylation of caveolin-1 at tyrosine Y14. This activation was mediated by Src family kinases Yes and Fyn activated by phosphorylation on Y418. Functional relevance of caveolin-1 for UVA signaling was demonstrated by retrovirus-mediated RNA interference resulting in prevention of UVA-induced gene expression in keratinocytes. Inhibition of Src kinase using inhibitor Su6656 prevented UVA-induced caveolin-1 phosphorylation. However, preincubation with Su6656 did not prevent UVA-induced ceramide formation and stimulation of unirradiated keratinocytes with cell-permeable ceramide induced Src

kinase phosphorylation, indicating that ceramide formation occurred upstream of Src kinase activation (Grether-Beck *et al.* 2005a).

Given that caveolin-1 depletion abolishes UVA-induced ceramide release, it would be consistent with this concept that UVA-induced Src kinase activation would also be inhibited by caveolin-1 knockdown (Figure 3.18). Interestingly, addition of exogenous ceramide could stimulate Src kinase phosphorylation in caveolin-1 knockdown cells (Figure 3.19a). This result indicates that in case of the caveolin-1 knockdown cells UVA-induced signaling is not blocked by the inability of Src kinase to undergo phosphorylation, but due to a lack of ceramide formation. In addition, this observation also indicates that activation of Src kinase can be achieved in the absence of caveolin-1 provided that sufficient ceramide is present in the cell. It has previously been shown that caveolin-1 knockdown does not alter the localization and the abundance of Src kinase within the cell (Gonzalez *et al.* 2004). In line with our observations Czarny and co-workers have shown that increased ceramide levels in caveolae of endothelial cells induce Src kinase activation (Czarny & Schnitzer 2004).

As ceramide release can also be achieved by incubation of cells with GM3 (Figure 3.16c), we have addressed the question whether GM3 can also induce Src kinase activation in caveolin-1 knockdown cells. We could demonstrate in the present work that in contrast to cell permeable ceramide, GM3 on its own did not activate Src kinase in caveolin-1 knockdown cells (Figure 3.19c). However, exogenous lactosylceramide, which is known to be generated upon degradation of GM3 by neuraminidase 3, was capable of activating Src kinase in caveolin-1 knockdown cells (Figure 3.19b). Taken together, these observations could suggest that GM3 induces Src kinase activity through the activation of neuraminidase 3 and the subsequent formation of lactosylceramide. Since further activation of neuraminidase 3 by GM3 might be inhibited by caveolin-1 depletion, GM3 on its own was not capable of inducing Src kinase activation in caveolin-1 knockdown cells. In line with our observation, exogenous lactosylceramide also activates Src kinase in other cell systems such as fibroblasts (Sharma *et al.* 2005). Addition of glycosphingolipids stimulates caveolar endocytosis mediated via Src kinase activation (Sharma *et al.* 2004).

Glycosphingolipids including GM3, have been implicated as modulators of signal transduction by influencing protein kinases associated with growth factor receptors (Hakomori 1990). Consistently, using antibodies that selectively interact with gangliosides it has been found that Src kinases co-localize with GM3-enriched microdomains. Furthermore, it has been shown that GM3-enriched microdomains in mouse melanoma



B16 cells display GM3-dependent cell adhesion and Src kinase activation (Iwabuchi *et al.* 1998). Similarly, GM3 has also been found to modulate cell growth by inhibiting EGF receptor phosphorylation (Bremer *et al.* 1986).

Endogenous accumulation of GM3 inhibits EGF receptor autophosphorylation through modulation of caveolin-1/ EGF receptor association in the keratinocyte-derived cell line SCC 12F2 (Wang *et al.* 2002a). Caveolin-1 and GM3 are expressed in low density, detergent insoluble fractions of the cellular membrane, while EGF receptor normally resides in noncaveolar membrane domains (Ringerike *et al.* 2002). Overexpression of GM3 (e.g. by treatment with antisense oligonucleotides to GM2 and GD2 synthase) shifts caveolin-1 from detergent-insoluble membrane microdomains into detergent-soluble membrane microdomains without affecting EGF receptor expression and distribution and results in (i) increased tyrosine phosphorylation of caveolin-1, and concurrently (ii) in inhibition of EGF receptor tyrosine phosphorylation and dimerization. Interaction of GM3 with other proteins involved extracellular carbohydrates. As caveolin-1 is not glycosylated and has no extracellular domain, direct interaction between GM3 and caveolin-1 therefore seems not possible. Alternatively, interaction with an adapter molecule having an own extracellular domain such as neuraminidase 3 could explain these results (Wang *et al.* 2002a). In line with this concept, neuraminidase 3 is enriched in caveolae and can interact with caveolin-1 via a caveolin-1 binding motif (Wang *et al.* 2002b). Given that GM3 is a substrate for neuraminidase 3, the binding of GM3 to neuraminidase 3 might compete with caveolin-1 binding to neuraminidase 3. Thus, the interaction between caveolin-1 and neuraminidase 3 depends also on the GM3 content in the cell. In line with this concept, we showed that neuraminidase 3 activity highly depends on the presence of caveolin-1. Inhibiting neuraminidase 3 activity by means of DANA was associated with decreased phosphorylation of (i) Src kinase and (ii) caveolin-1, this observation was not restricted to UVA irradiation because the same was observed upon treatment with ceramide or GM3 (Figure 3.17).

Src kinase activity and the subsequent caveolin-1 phosphorylation were identified as upstream events in UVA-induced activation of transcription factor AP-2, because we have observed that inhibition of Src kinase by means of PP2 inhibits AP-2 activation upon UVA irradiation. Similarly, depletion of caveolin-1 decreased AP-2 activation upon UVA irradiation (Figure 3.21). Transcription factor AP-2 binding site within the ICAM-1 promoter was identified as the UVA-responsive element of this gene (Grether-Beck *et al.* 1996), because deletion of this site in the ICAM-1 promoter resulted in loss of UVA-

induced reporter gene activity. In this regard, UVA-induced AP-2 activation has been found to be mediated through the release of cytochrome *c* from the mitochondria leading to oxidation of AP-2 protein. Oxidized AP2 was then transferred to the nucleus where it binds to the ICAM-1 promoter and activates ICAM-1 transcription.

As it has recently been shown that preloading of human keratinocytes with cholesterol results in prevention of UVA-induced AP-2 activation and the subsequent ICAM-1 gene upregulation (Grether-Beck *et al.* 2008), we have assessed the effect of modulating cellular cholesterol level on UVA radiation induced Src-kinase activation and its subsequent caveolin-1 phosphorylation. The results shown in Figure 3.23 and Figure 3.24 are further evidence that the cellular cholesterol level is affecting the UVA signaling cascade at the plasma membrane level where it alters the capacity of UVA radiation to release ceramide (Grether-Beck *et al.* 2008). Our results demonstrate that increased cholesterol level decreases Src kinase activity and the subsequent caveolin-1 phosphorylation, whereas, depleting cellular cholesterol by means of  $\beta$ -methylcyclodextrin ( $\beta$ MCD) promotes Src kinase activity upon UVA radiation. In line with our findings that modulation of the cholesterol content also modulates the UVA response at the level of ceramide formation, we were able to show that ceramide induced phosphorylation of caveolin-1 was also enhanced by decreasing cellular cholesterol content (Fig. 3.23) whereas increased cholesterol content diminished the capability of ceramide to induce caveolin-1 phosphorylation (Figure 3.24). Cholesterol depletion also diminishes caveolae from caveolin and increases its mobility outside of the raft and could explain the enhancing effects of  $\beta$ -methylcyclodextrin on UVA-induced signaling which is also accompanied by a cholesterol decrease (Parton & Simons 2007).

We have demonstrated in this work that caveolin-1 depletion attenuates UVA signaling at (i) neuraminidase 3 activation, (ii) Src kinase activation, (iii) transcription factor AP-2 activation, and finally at (iv) ICAM-1 upregulation. Taken together, our findings indicate that depletion of caveolin-1 is critical in maintaining a UVA response. These results were verified in caveolin-1 knockout animals (unpublished observation) where ICAM-1 expression did not increase in response to UVA irradiation. These studies also clearly demonstrate the pivotal role of raft-signaling in UVA radiation-induced gene expression in human keratinocytes *in vitro* (Grether-Beck *et al.* 2005a) and *in vivo*.

## **5. Summary**

Solar ultraviolet A (UVA; 320-400 nm) radiation in physiological doses is able to induce gene expression in human skin. There is increasing evidence that UVA radiation plays an important role in the pathogenesis of the most frequent photodermatoses, polymorphic light eruption as well as in photoaging and photocarcinogenesis. Human epidermal keratinocytes represent the primary cellular target for UVA radiation. Ceramide generation within membrane microdomains enriched in cholesterol and glycosphingolipids (lipid rafts) on the cell surface participate in the signal transduction pathway operative in UVA-induced gene expression. In this work we report that in addition to the degradation of sphingomyelin also the degradation of glycosphingolipids e.g. GM3 contributes to ceramide formation in rafts observed upon UVA treatment. The degradation of GM3, the main glycosphingolipid in keratinocytes, was found to be mediated via the raft associated, ganglioside specific sialidase called neuraminidase 3. Degradation of gangliosides was of functional relevance for UVA signaling and significantly contributed to the UVA response, because inhibiting neuraminidase 3 activation resulted in a subsequent inhibition of the downstream signaling elements which are (i) UVA-induced Src kinase activation, (ii) caveolin-1 phosphorylation, (iii) AP-2 activation, and (iv) finally ICAM-1 upregulation.

As expected for a raft associated enzyme, cholesterol loading decreased enzyme activity, whereas cholesterol decrease via beta-methylcyclodextrin treatment increased neuraminidase 3 activity. Furthermore, the singlet oxygen quencher vitamin E inhibited UVA-induced neuraminidase 3 activity. As neuraminidase 3 closely associates with caveolin-1, the caveolae stabilizing and cholesterol binding protein, we found that depletion of caveolin-1 by retrovirus-mediated RNA interference abolished the capacity of human keratinocytes to further increase neuraminidase 3 activity.

The composition of cholesterol, sphingolipids and glycosphingolipids critically controls the function of rafts. UVA responsiveness of the cells is determined by the ratio of these components in lipid rafts. In particular, the ratio of ceramide versus cholesterol determines the responsiveness towards UVA radiation. Our results indicate that depletion of caveolin-1 rendered keratinocytes resistant towards UVA-induced ceramide formation and the subsequent signaling events such as activation of Src kinase and AP-2, and upregulation of ICAM-1.

**6-Reference list**

- Abram, C. & Courtneidge, S. (2000). Src family tyrosine kinases and growth factor signaling. *Exp Cell Res.*, 254, 1-13.
- Alberts, B., Johnson, A., Lewis, J., Raff, A., Rober, K. & Walter, P. (2002). *Molecular biology of the cell*. 589-590. USA: Garland Science.
- Baier, J., Maisch, T., Maier, M., Landthaler, M. & Baumler, W. (2007). Direct detection of singlet oxygen generated by UVA irradiation in human cells and skin. *J Invest Dermatol.*, 127, 1498-1506.
- Bas, A., Forsberg, G., Hammarström, S. & Hammarström, M. (2004). Utility of the housekeeping genes 18S rRNA, beta-actin and glyceraldehyde-3-phosphate-dehydrogenase for normalization in real-time quantitative reverse transcriptase-polymerase chain reaction analysis of gene expression in human T lymphocytes. *Scand J Immunol.*, 59, 566-573.
- Beak, S., Lee, Y. & Kim, J. (2004). NADPH oxidase and cyclooxygenase mediate the ultraviolet B-induced generation of reactive oxygen species and activation of nuclear factor-kappaB in HaCaT human keratinocytes. *Biochimie.*, 86, 425-429.
- Bender, F., Reymond, M., Bron, C. & Quest, A. (2000). Caveolin-1 levels are down-regulated in human colon tumors, and ectopic expression of caveolin-1 in colon carcinoma cell lines reduces cell tumorigenicity. *Cancer Research.*, 60, 5870-5878.
- Bhunia, A., Arai, T., Bulkley, G. & Chatterjee, S. (1998). Lactosylceramide mediates TNF- $\alpha$ -induced intercellular adhesion molecule-1 (ICAM-1) expression and the adhesion of neutrophil in human umbilical Vein endothelial cells. *J Biol Chem.*, 273, 34349-34357.
- Bhunia, A., Schwarzmann, G. & Chatterjee, S. (2002). GD3 recruits reactive oxygen species to induce cell proliferation and apoptosis in human aortic smooth muscle cells. *J Biol Chem.*, 277, 16396-16402.
- Bickel, P., Scherer, P., Schnitzer, J., Oh, P., Lisanti, M. & Lodish, H. (1997). Flotillin and epidermal surface antigen define a new family of caveolae-associated integral membrane proteins. *J Biol Chem.*, 272, 13793-13802.
- Birklé, S., Zeng, G., Gao, L., Yu, R. & Aubry, J. (2003). Role of tumor-associated gangliosides in cancer progression. *Biochimie.*, 85, 463.
- Bonifacino, J., Dasso, M., Harford, J., Lippincott-Schwartz, J. & Yamada, K. (2003). *Short Protocols in Cell Biology*. 7-14. Wiley.
- Boukamp, P., Petrussevska, R., Breitkreutz, D., Hornung, J., Markham, A. & Fusenig, N. (1988). Normal keratinization in a spontaneously immortalized aneuploid human keratinocyte cell line. *The Journal of Cell Biology.*, 106, 761-771.
- Bradford, M. (1976). A rapid and sensitive method for the quantitation of microgram quantities of protein utilizing the principle of protein-dye binding. *Anal Biochem.*, 72, 248-254.

- Bremer, E., Schlessinger, J. & Hakomori, S. (1986). Ganglioside-mediated modulation of cell growth. Specific effects of GM3 on tyrosine phosphorylation of the epidermal growth factor receptor. *J Biol Chem.*, 261, 2434-2440.
- Brown, D. & Rose, K. (1992). Sorting of GPI-anchored proteins to glycolipid-enriched membrane subdomains during transport to the apical cell surface. *Cell.*, 533-544.
- Brown, D. & London, E. (1998). Functions of lipid rafts in biological membranes. *Annual Review of Cell and Developmental Biology.*, 14, 111-136.
- Bruls, W., van Weelden, H. & van der Leun, J. (1984). Transmission of UV-radiation through human epidermal layers as a factor influencing the minimal erythema dose. *Photochem Photobiol.*, 39, 63-67.
- Burek, C., Roth, J., Koch, H., Harzer, K., Los, M. & Schulze-Osthoff, K. (2001). The role of ceramide in receptor- and stress-induced apoptosis studied in acidic ceramidase-deficient Farber disease cells. *Oncogene.*, 20, -6493.
- Burmeister, W., Henrissat, B., Cusack, S., Bosso, C. & Ruigrok, R. (1993). Influenza B virus neuraminidase can synthesize its own inhibitor. *Structure.*, 1, 19-26.
- Callies, R., Schwarzmann, G., Radsak, K., Siegert, R. & Wiegandt, H. (1977). Characterization of the cellular binding of exogenous gangliosides. *Eur J Biochem.*, 80, 425-432.
- Cao, H., Courchesne, W. & Mastick, C. (2002). A phosphotyrosine-dependent protein interaction screen reveals a role for phosphorylation of caveolin-1 on tyrosine 14. Recruitment of c-terminal src kinase. *J Biol Chem.*, 277, 8771-8774.
- Capozza, F., Williams, T., Schubert, W., McClain, S., Bouzahzah, B., Sotgia, F. & Lisanti, M. (2003). Absence of caveolin-1 sensitizes mouse skin to carcinogen-induced epidermal hyperplasia and tumor formation. *American Journal of Pathology.*, 162, 2029-2039.
- Chavas, L., Tringali, C., Fusi, P., Venerando, B., Tettamanti, G., Kato, R., Monti, E. & Wakatsuki, S. (2005). Crystal Structure of the Human Cytosolic Sialidase Neu2. *J Biol Chem.*, 280, 469-475.
- Cohen, A., Combs, T., Scherer, P. & Lisanti, M. (2003). Role of caveolin and caveolae in insulin signaling and diabetes. *AJP - Endocrinology and Metabolism.*, 285, E1151-E1160.
- Coles, C., Forbes, P. & Davies, R. (1996). An action spectrum for photocarcinogenesis. *Photochem Photobiol.*, 43, 275-284.
- Couet, J., Okamoto, T., Ikezu, T. & Lisanti, M. (1997a). Identification of peptide and protein ligands for the caveolin-scaffolding domain. implications for the interaction of caveolin with caveolae-associated proteins. *J Biol Chem.*, 272, 6525-6533.
- Couet, J., Sargiacomo, M. & Lisanti, M. (1997b). Interaction of a receptor tyrosine kinase, egf-r, with caveolins. caveolin binding negatively regulates tyrosine and serine/threonine kinase activities. *J Biol Chem.*, 272, 30429-30438.

- Crennell, S., Garman, E., Graeme Laver, W., Vimr, E. & Taylor, G. (1993). Crystal structure of a bacterial sialidase (from *Salmonella typhimurium* LT2) shows the same fold as an influenza virus neuraminidase. *Proc Natl Acad Sci USA.*, 90, 9852-9856.
- Czarny, M. & Schnitzer, J. (2004). Neutral sphingomyelinase inhibitor scyphostatin prevents and ceramide mimics mechanotransduction in vascular endothelium. *AJP - Heart and Circulatory Physiology.*, 287, H1344-H1352.
- Da Silva, J., Hasegawa, T., Miyagi, T., Dotti, C. & Abad-Rodriguez, J. (2005). Asymmetric membrane ganglioside sialidase activity specifies axonal fate. *Nat Neurosci.*, 8, 606-615.
- De Gruijl, F. & van der Leun, J. (2000). Environment and health: 3. Ozone depletion and ultraviolet radiation. *CMAJ.*, 163, 851-855.
- De Gruijl, F., van Kranen, H. & mullenders, L. (2001). UV-induced DNA damage, repair, mutations, and oncogenic pathways in skin cancer. *J Photochem Photobiol B.*, 63, 19-27.
- Dignam, J., Martin, P., Shastry, B. & Roeder, R. (1983). Eukaryotic gene transcription with purified components. *Methods Enzymol.*, 101, 598.
- Dobrowsky, R. (2000). Sphingolipid signalling domains floating on rafts or buried in caves? *Cell Signal.*, 12, 81-90.
- Drab, M., Verkade, P., Elger, M., Kasper, M., Lohn, M., Lauterbach, B., Menne, J., Lindschau, C., Mende, F., Luft, F., Schedl, A., Haller, H. & Kurzchalia, T. (2001). Loss of caveolae, vascular dysfunction, and pulmonary defects in caveolin-1 gene-disrupted mice. *Science.*, 293, 2449-2452.
- Dumitru, C., Zhang, Y., Li, X. & Gulbins, E. (2007). Ceramide: a novel player in reactive oxygen species-induced signaling? *Antioxid Redox Signal.*, 9, 1535-1540.
- d'Azzo, A., Tessitore, A. & Sano, R. (2006). Gangliosides as apoptotic signals in ER stress response. *Cell Death Differ.*, 13, 404-414.
- Elias, P., Goerke, J. & Friend, D. (1977). Mammalian epidermal barrier layer lipids: composition and influence on structure. *J Invest Dermatol.*, 69,535-546.
- Elliott, M. (2001). Zanamivir: from drug design to the clinic. *Philos Trans R Soc Lond B Biol Sci.*, 356, 1885-1893.
- Elsner, P., Hölzle, E., Diepgen, T., Grether-Beck, S., Hönigsmann, H., Krutmann, J., Scharffetter-Kochanek, K., Schwarz, T. & Luger, T. (2007). Recommendation: daily sun protection in the prevention of chronic UV-induced skin damage. *J Dtsch Dermatol Ges.*, 5, 166-173.
- Epstein, J. (1983). Phototoxicity and photoallergy in man. *J Am Acad Dermatol.*, 8, 141-147.
- Feingold, K. (2007). Thematic review series: Skin Lipids. The role of epidermal lipids in cutaneous permeability barrier homeostasis. *Journal of Lipid Research.*, 48, 2531-2546.
- Folch, J., Lees, M. & Sloane, S. (1957). A simple method for the isolation and purification of total lipids from animal tissues. *J Biol Chem.*, 226, 497-509.

- Fried, M. & Crothers, D. (1981). Equilibria and kinetics of lac repressor-operator interactions by polyacrylamide gel electrophoresis. *Nucleic Acids Res.*, 9, 6505-6525.
- Fuchs, J. (1992). *Oxidative Injury in Dermatopathology*. 7-27. Springer Verlag.
- Garner, M. & Revzin, A. (1981). A gel electrophoresis method for quantifying the binding of proteins to specific DNA regions: application to components of the Escherichia coli lactose operon regulatory system. *Nucleic Acids Res.*, 9, 3047-3060.
- Gniadecki, R., Olszewska, H. & Gajkowska, B. (2001). Changes in the ultrastructure of cytoskeleton and nuclear matrix during HaCaT keratinocyte differentiation. *Exp Dermatol.*, 10, 71-79.
- Gong, N., Wei, H., Chowdhury, S. & Chatterjee, S. (2004). Lactosylceramide recruits PKC $\alpha$ /epsilon and phospholipase A2 to stimulate PECAM-1 expression in human monocytes and adhesion to endothelial cells. *Proc Natl Acad Sci U S A.*, 101, 6490-6495.
- Gonzalez, E., Nagiel, A., Lin, A., Golan, D. & Michel, T. (2004). Small Interfering RNA-mediated Down-regulation of Caveolin-1 Differentially Modulates Signaling Pathways in Endothelial Cells. *J Biol Chem.*, 279, 40659-40669.
- Greffard, A., Trabelsi, N., Terzidis, H., Bignon, J., Jaurand, M. & Pilatte, Y. (1997). Inhibition of acid sialidase by inorganic sulfate. *Biochim Biophys Acta*, 1334, 140-148.
- Grether-Beck, S., Bonizzi, G., Schmitt-Brenden, H., Felsner, I., Timmer, A., Sies, H., Johnson, J., Piette, J. & Krutmann, J. (2000). Non-enzymatic triggering of the ceramide signalling cascade by solar UVA radiation. *EMBO J.*, 19, 5793-5800.
- Grether-Beck, S., Felsner, I., Brenden, H. & Krutmann, J. (2003). Mitochondrial cytochrome c release mediates ceramide-induced activator protein 2 activation and gene expression in keratinocytes. *J Biol Chem.*, 278, 47498-47507.
- Grether-Beck, S., Olaizola-Horn, S., Schmitt, H., Grewe, M., Jahnke, A., Briviba, K., Sies, H. & Krutmann, J. (1996). Activation of transcription factor AP-2 mediates UVA radiation- and singlet oxygen-induced expression of the human intercellular adhesion molecule 1?gene. *Proc Natl Acad Sci U S A.*, 93, 14586-14591.
- Grether-Beck, S., Salahshour-Fard, M., Brammertz, D., Brenden, H., Felsner, I., Füllekrug, J. & Krutmann, J. (2005a). The raft associated protein caveolin-1 is critically involved in ultraviolet A radiation (UVA)-induced signaling in human keratinocytes. ESDR. Ref Type: Abstract
- Grether-Beck, S., Salahshour-Fard, M., Timmer, A., Brenden, H., Felsner, I., Walli, R., Füllekrug, J. & Krutmann, J. (2008). Ceramide and raft signaling are linked with each other in UVA radiation-induced gene
- Grether-Beck, S., Timmer, A., Felsner, I., Brenden, H., Brammertz, D. & Krutmann, J. (2005b). Ultraviolet A-induced signaling involves a ceramide-mediated autocrine loop leading to ceramide de novo synthesis. *J Invest Dermatol.*, 125, 545-553.
- Ha, K., Lee, Y., Cho, S., Kim, J. & Kim, C. (2004). Molecular characterization of membrane type and ganglioside-specific sialidase (Neu3) expressed in E. coli. *Mol Cells.*, 30, 267-273.

- Hakomori, S. (1990). Bifunctional role of glycosphingolipids. Modulators for transmembrane signaling and mediators for cellular interactions. *J Biol Chem.*, 265, 18713-18716.
- Hakomori, S. (2000). Cell adhesion/recognition and signal transduction through glycosphingolipid microdomain. *lycoconj J.*, 17, 143-151.
- Hamanaka, S., Hara, M., Nishio, H., Otsuka, F., Suzuki, A. & Uchida, Y. (2002). Human Epidermal Glucosylceramides are Major Precursors of Stratum Corneum Ceramides. *Journal of Investigative Dermatology*, 119, 416-423.
- Harder, T., Scheiffle, P., Verkade, P. & Simons, K. (1998). Lipid domain structure of the plasma membrane revealed by patching of membrane components. *The Journal of Cell Biology.*, 141, 929-942.
- Haverkamp, J., Schauer, R. & Wember, M. (1976). Neuraminic acid derivatives newly discovered in humans: N-acetyl-9-O-L-lactoylneuraminic acid, N,9-O-Diacetylneuraminic acid and N-acetyl-2,3-dehydro-2-deoxyneuraminic acid. *Hoppe Seylers Z Physiol Chem.*, 357, 1699-1705.
- Hirschberg, C., Goodman, S. & Green, C. (1976). Sialic acid uptake by fibroblasts. *Biochemistry.*, 15, 3591-3599.
- Hoath, S. & Leahy, D. (2003). The Organization of Human Epidermis: Functional Epidermal Units and Phi Proportionality. *Journal of Investigative Dermatology.*, 121, 1440-1446.
- Holleran, W., Takagi, Y., Menon, G., Legler, G., Feingold, K. & Elias, P. (1993). Processing of epidermal glucosylceramides is required for optimal mammalian cutaneous permeability barrier function. *The Journal of Clinical Investigation.*, 91, 1656-1664.
- Hoogeveen, A., Graham-Kawashima, H., d'Azzo, A. & Galjaard, H. (1984). Processing of human beta-galactosidase in GM1-gangliosidosis and Morquio B syndrome. *J Biol Chem.*, 259, 1974-1977.
- Hooper, N. (1998). Membrane biology: do glycolipid microdomains really exist? *Curr.Biol.*, 8, R114-R116.
- Huwiler, A., Kolter, T., Pfeilschifter, J. & Sandhoff, K. (2000). Physiology and pathophysiology of sphingolipid metabolism and signaling. *Biochim Biophys Acta.*, 1485, 63-99.
- Iijima, R., Takahashi, H., Namme, R., Ikegami, S. & Yamazaki, M. (2004). Novel biological function of sialic acid (N-acetylneuraminic acid) as a hydrogen peroxide scavenger. *FEBS Lett.*, 561, 163-166.
- Ikonen, E., Heino, S. & Lusa, S. (2004). Caveolins and membrane cholesterol. *Biochem Soc Trans.*, 32, 121-123.
- Iwabuchi, K., Handa, K. & Hakomori, S. (1998a). Separation of "Glycosphingolipid Signaling Domain" from caveolin-containing membrane fraction in mouse melanoma b16 cells and its role in cell adhesion coupled with signaling. *J Biol Chem.*, 273, 33766-33773.



- Iwabuchi, K., Yamamura, S., Prinetti, A., Handa, K. & Hakomori, S. (1998b). GM3-enriched microdomain involved in cell adhesion and signal transduction through carbohydrate-carbohydrate interaction in mouse Melanoma B16 cells. *J Biol Chem.*, 273, 9130-9138.
- Jeffrey D.Esko & Carolyn R.Bertozzi (2008). Chemical Tools for Inhibiting Glycosylation. In Varki, A., Cummings, R., Esko, J., Freeze, H., Hart, M. & Etzler, M. (Eds) *Essentials of Glycobiology*.705-722. Cold Spring Harbor Laboratory Press.
- Junqueira, L. & Carneiro, J. (2005). *Basic Histology*. 346-357. Appleton & Lange.
- Kaiser, S., Di Mascio, P., Murphy, M. & Sies, H. (1990). Quenching of singlet molecular oxygen by tocopherols. *Adv Exp Med Biol.*, 264, 117-124.
- Kakugawa, Y., Wada, T., Yamaguchi, K., Yamanami, H., Ouchi, K., Sato, I. & Miyagi, T. (2002). Up-regulation of plasma membrane-associated ganglioside sialidase (Neu3) in human colon cancer and its involvement in apoptosis suppression. *Proc Natl Acad Sci U S A.*, 99, 10718-10723.
- Kalka, D., von Reitzenstein, C., Kopitz, J. & Cantz, M. (2001). The plasma membrane ganglioside sialidase cofractionates with markers of lipid rafts. *Biochem Biophys Res Commun.*, 283, 989-993.
- Klotz, L., Pellieux, C., Briviba, K., Pierlot, C., Aubry, J. & Sies, H. (1999). Mitogen-activated protein kinase (p38-, JNK-, ERK-) activation pattern induced by extracellular and intracellular singlet oxygen and UVA. *Eur J Biochem.*, 260, 917-922.
- Kochevar, I., Pathak, M. & Parrish, J. (1999). *Fitzpatrick's dermatology in general medicine*. 220-229. New York, McGraw-Hill.
- Kolter, T., Proia, R. & Sandhoff, K. (2002). Combinatorial ganglioside biosynthesis. *J Biol Chem.*, 277, 25859-25862.
- Kopitz, J., von Reitzenstein, C., Sinz, K. & Cantz, M. (1996). Selective ganglioside desialylation in the plasma membrane of human neuroblastoma cells. *Glycobiology.*, 6, 367-376.
- Kopitz, J., Mühl, C., Ehemann, V., Lehmann, C. & Cantz, M. (1997a). Effects of cell surface ganglioside sialidase inhibition on growth control and differentiation of human neuroblastoma cells. *Eur J Cell Biol.*, 73, 1-9.
- Kopitz, J., Sinz, K., Brossmer, R. & Cantz, M. (1997b). Partial characterization and enrichment of a membrane-bound sialidase specific for gangliosides from human brain tissue. *Eur J Biochem.*, 248, 527-534.
- Krutmann, J. (2000). Ultraviolet A radiation-induced biological effects in human skin: relevance for photoaging and photodermatosis. *J Dermatol Sci.*, Suppl: S22-S6.
- Laemmli, U. (1970). Cleavage of structural proteins during the assembly of the head of bacteriophage T4. *Nature.*, 227, 680-685.
- Larouche, K., Bergeron, M., Leclerc, S. & Guérin, S. (1996). Optimization of competitor poly(dI-dC).poly(dI-dC) levels is advised in DNA-protein interaction studies involving enriched nuclear proteins. *Biotechniques.*, 20, 439-444.

- Le, P., Guay, G., Altschuler, Y. & Nabi, I. (2002). Caveolin-1 is a negative regulator of caveolae-mediated endocytosis to the endoplasmic reticulum. *J Biol Chem.*, 277, 3371-3379.
- Lee, H., Volonte', D., Galbiati, F., Iyengar, P., Lublin, D., Bregman, D., W., Campos-Gonzalez Boumediene Bouzahzah, R., Pestell, R., Scherer, P. & Lisanti, M. (2000). Constitutive and growth factor-regulated phosphorylation of caveolin-1 occurs at the same site (Tyr-14) in vivo: Identification of a c-Src/Cav-1/Grb7 signaling cassette. *Molecular Endocrinology.*, 14, 1750-1775.
- Leiter, U. & Garbe, C. (2008). Epidemiology of melanoma and nonmelanoma skin cancer--the role of sunlight. *Adv Exp Med Biol*, 89-103.
- Li, P. & Gulbins, E. (2007). Lipid rafts and redox signaling. *Antioxid Redox Signa.*, 9, 1411-1415.
- Li, R., Liu, Y. & Ladisch, S. (2001). Enhancement of epidermal growth factor signaling and activation of SRC kinase by gangliosides. *J Biol Chem.*, 276, 42782-42792.
- Li, S., Couet, J. & Lisanti, M. (1996). Src tyrosine kinases, G alpha subunits, and H-Ras share a common membrane-anchored scaffolding protein, Caveolin. *J Biol Chem.*, 271, 29182-29190.
- Livak, K. & Schmittgen, T. (2001). Analysis of relative gene expression data using real-time quantitative PCR and the 2(-Delta Delta C(T)) Method. *Methods.*, 25, 402-408.
- Lukong, K., Seyrantepe, V., Landry, K., Trudel, S., Ahmad, A., Gahl, W., Lefrancois, S., Morales, C. & Pshezhetsky, A. (2001). Intracellular distribution of lysosomal sialidase is controlled by the internalization signal in its cytoplasmic tail. *J Biol Chem.*, 276, 46172-46181.
- Madison, K. (2003). Barrier function of the skin: [ldquo]La Raison d'etre[rdquo] of the epidermis. *J Investig Dermatol.*, 121, 231-241.
- Madison, K., Swartzendruber, D., Wertz, P. & Downing, D. (1990). Sphingolipid metabolism in organotypic mouse keratinocyte cultures. *J Investig Dermatol.*, 95, 657-664.
- Masserini, M. & Ravasi, D. (2001). Role of sphingolipids in the biogenesis of membrane domains. *Biochim Biophys Acta.*, 1532, 149-161.
- Matsui, M. & Deleo, V. (1995). Mechanisms and human relevance. In Mukhtar H (Ed) *Skin Cancer*. 21-30. Ann Arbor, CRC Press.
- McCallum, F. & Maden, B. (1985). Human 18 S ribosomal RNA sequence inferred from DNA sequence. Variations in 18 S sequences and secondary modification patterns between vertebrates. *Biochem J.*, 15, 3-725.
- Merrill, A., Sullards, J., Wang, E., Voss, K. & Riley, R. (2001). Sphingolipid metabolism: roles in signal transduction and disruption by fumonisins. *Environ Health Perspect.*, 109, 283-289.
- Mishra, S. & Jushi, P. (2007). Lipid raft heterogeneity: an enigma. *J Neurochem.*, 103, 135-142.

- Mitsumori, R., Kato, T. & Hatanaka, K. (2009).  $\gamma$ -Cyclodextrin increases hydrolysis of gangliosides by sialidase from *Arthrobacter ureafaciens* : hydrolysis of gangliosides. *International Journal of Carbohydrate Chemistry* doi., 10, 398284.
- Miyagi, T., Wada, T., Iwamatsu, A., Hata, K., Yoshikawa, Y., Tokuyama, S. & Sawada, M. (1999). Molecular cloning and characterization of a plasma membrane-associated sialidase specific for gangliosides. *J.Biol.Chem.*, 274, 5004-5011.
- Miyagi, T., Wada, T., Yamaguchi, K., Hata, K. & Shiozaki, K. (2008b). Plasma membrane-associated sialidase as a crucial regulator of transmembrane signalling. *J Biochem.*, 144, 279-285.
- Miyagi, T., Wada, T. & Yamaguchi, K. (2008a). Roles of plasma membrane-associated sialidase NEU3 in human cancers. *Biochim Biophys Acta.*, 1780, 532-537.
- Miyagi, T., Wada, T., Yamaguchi, K., Shiozaki, K., Sato, I., Kakugawa, Y., Yamanami, H. & Fujiya, T. (2008c). Human sialidase as a cancer marker. *Proteomics.*, 16, 3303-33011.
- Monti, E., Bassi, M., Papini, N., Riboni, M., Manzoni, M., Venerando, B., Croci, G., Preti, A., Ballabio, A., Tettamanti, G. & Borsani, G. (2000). Identification and expression of NEU3, a novel human sialidase associated to the plasma membrane. *Biochemical Journal*, 349, 343-351.
- Monti, E., Preti, A., Venerando, B. & Borsani, G. (2002). Recent development in mammalian sialidase molecular biology. *Neurochem Res.*, 27, 649-663.
- Morgan, M., Kim, Y. & Liu, Z. (2007). Lipid rafts and oxidative stress-induced cell death. *Antioxid Redox Signal.*, 9, 1471-1483.
- Murata, M., Peränen, J., Schreiner, R., Wieland, F., Kurzchalia, T. & Simons, K. (1995). VIP21/caveolin is a cholesterol-binding protein. *Proc Natl Acad Sci U S A.*, 92, 10339-10343.
- Nöhle, U., Beau, J. & Schauer, R. (1982). Uptake, metabolism and excretion of orally and intravenously administered, double-labeled N-glycoloylneuraminic acid and single-labeled 2-deoxy-2,3-dehydro-N-acetylneuraminic acid in mouse and rat. *Eur J Biochem.*, 126, 543-548.
- Norkin, L. & Kuksin, D. (2005). The caveolae-mediated sv40 entry pathway bypasses the golgi complex route to the endoplasmic reticulum. *Virology*, 2, 38.
- Oehler, C., Kopitz, J. & Cantz, M. (2000). Substrate Specificity and Inhibitor Studies of a Membrane-Bound Ganglioside Sialidase Isolated from Human Brain Tissue. *Biol Chem.*, 383, 1735-1742.
- Okamoto, T., Schlegel, A., Scherer, P. & Lisanti, M. (1998). Caveolins, a family of scaffolding proteins for organizing "preassembled signaling complexes" at the plasma membrane. *J Biol Chem.*, 273, 5419-5422.
- Paerels, G. & Schut, J. (1965). The mechanism of the periodate-thiobarbituric acid reaction of sialic acids. *Biochemical Journal.*, 96, 787-792.
- Paller, A., Arnsmeier, S., Alvarez-Franco, M. & Bremer, E. (1993). Ganglioside GM3 inhibits the proliferation of cultured keratinocytes. *J Invest Dermatol.*, 100, 841-845.

- Paller, A., Arnsmeier, S., Robinson, J. & Bremer, E. (1992). Alteration in Keratinocyte Ganglioside Content in Basal Cell Carcinomas. *J Invest Dermatol.*, 98, 226-232.
- Papini, N., Anastasia, L., Tringali, C., Croci, G., Bresciani, R., Yamaguchi, K., Miyagi, T., Preti, A., Prinetti, A., Prioni, S., Sonnino, S., Tettamanti, G., Venerando, B. & Monti, E. (2004). The Plasma Membrane-associated Sialidase MmNEU3 Modifies the Ganglioside Pattern of Adjacent Cells Supporting Its Involvement in Cell-to-Cell Interaction. *J Biol Chem.*, 279, 16989-16995.
- Parton, R. & Simons, K. (2007). The multiple faces of caveolae. *Nat Rev Mol Cell Biol.*, 8, 185-194.
- Paschal, B. & Gerace, L. (1995). Identification of NTF2, a cytosolic factor for nuclear import that interacts with nuclear pore complex protein p62. *The Journal of Cell Biology.*, 129, 925-937.
- Patel, H., Murray, F. & Insel, P. (2008). G-Protein-Coupled Receptor-Signaling Components in Membrane Raft and Caveolae Microdomains. *Handb Exp Pharmacol.*, 186, 167-184.
- Pierce protein research products . Gel Shift Assays (EMSA). (2009). Ref Type: Catalog.
- Pike, L. (2004). Lipid rafts: heterogeneity on the high seas. *Biochemical Journal*, 378, 281-292.
- Pike, L. (2006). Rafts defined: a report on the Keystone symposium on lipid rafts and cell function. *Journal of Lipid Research.*, 47, 1597-1598.
- Platt, F. & Butters, T. (1998). New therapeutic prospects for the glycosphingolipid lysosomal storage diseases. *Biochem Pharmacol.*, 56, 421-430.
- Pol, A., Luetterforst, R., Lindsay, M., Heino, S., Ikonen, E. & Parton, R. G. (2001). A Caveolin Dominant Negative Mutant Associates with Lipid Bodies and Induces Intracellular Cholesterol Imbalance. *J. Cell Biol.*, 152, 1057-1070.
- Proia, R. (2003). Glycosphingolipid functions: insights from engineered mouse models. *Philosophical Transactions of the Royal Society of London. Series B: Biological Sciences*, 358, 879-883.
- Quest A., Leyton, L. & Parraga, M. (2004). Caveolins, caveolae and lipid rafts in cellular transport, signaling, and disease. *Biochem Cell Biol.*, 82, 129-144.
- Ravanat, J., Douki, T. & Cadet, J. (2001). Direct and indirect effects of UV radiation on DNA and its components. *J Photochem Photobiol B.*, 63, 88-102.
- Razani, B., Combs, T., Wang, X., Frank, P., Park, D., Russell, R., Li, M., Tang, B., Jelicks, L., Scherer, P. & Lisanti, M. (2002). Caveolin-1-deficient mice are lean, resistant to diet-induced obesity, and show hypertriglyceridemia with adipocyte abnormalities. *J Biol Chem.*, 277, 8635-8647.
- Reinehr, R., Becker, S., Eberle, A., Grether-Beck, S. & Häussinger, D. (2005). Involvement of NADPH oxidase isoforms and Src family kinases in CD95-dependent hepatocyte apoptosis. *J Biol Chem.*, 280, 27179-27194.

- Riboni, L. & Tettamanti, G. (1991). Rapid internalization and intracellular metabolic processing of exogenous ganglioside by cerebellar granule cells differentiated in culture. *J Neurochem.*, 57, 1931-1939.
- Ringerike, T., Blystad, F., Levy, F., Madshus, I. & Stang, E. (2002). Cholesterol is important in control of EGF receptor kinase activity but EGF receptors are not concentrated in Caveolae. *J Cell Sci.*, 115, 1331-1341.
- Rothberg, K., Heuser, J., Donzell, W., Ying, Y., Glenney, J. & Anderson, R. (1992). Caveolin, a protein component of caveolae membrane coats. *Cell.*, 68, 673-682.
- Sakarya, S., Rifat, S., Zhou, J., Bannerman, D., Stamatou, N., Cross, A. & Goldblum, S. (2004). Mobilization of neutrophil sialidase activity desialylates the pulmonary vascular endothelial surface and increases resting neutrophil adhesion to and migration across the endothelium. *Glycobiology*, 14, 481-494.
- Salahshour-Fard, M. Die Rolle von Membranlipiden in der UVA-induzierten Signaltransduktion in humanen Keratinozyten. 2006. Mathematisch-Naturwissenschaftlichen Fakultät der Heinrich-Heine-Universität Düsseldorf. Ref Type: Thesis/Dissertation.
- Sambrook, J., MacCallum, P. & Russell, D. (1989). Protein Interaction Technologies. *Molecular Cloning: A Laboratory Manual.*, Cold Spring Harbor laboratory Press.
- Sandhoff, K. & Kolter, T. (2003). Biosynthesis and degradation of mammalian glycosphingolipids. *Philos Trans R Soc Lond B Biol Sci.*, 358, 847-861.
- Sargiacomo, M., Scherer, P., Tang, Z., Kübler, E., Song, K., Sanders, M. & Lisanti, M. (1995). Oligomeric structure of caveolin: implications for caveolae membrane organization. *Proceedings of the National Academy of Sciences of the United States of America.*, 92, 9407-9411.
- Sasaki, A., Hata, K., Suzuki, S., Sawada, M., Wada, T., Yamaguchi, K., Obinata, M., Tateno, H., Suzuki, H. & Miyagi, T. (2003). Overexpression of plasma membrane-associated sialidase attenuates insulin signaling in transgenic mice. *J Biol Chem.*, 278, 27896-27902.
- Schauer, R. & Corfield, A. (1982). Colorimetry and Thin-layer Chromatography of sialic acids. In R. Schauer (Ed) *Sialic acids, chemistry, metabolism and functions* (pp. 77-83). Springer-Verlag.
- Schengrund, C., Lausch, R. & Rosenberg, A. (1973). Sialidase Activity in Transformed Cells. *J Biol Chem.*, 248, 4424-4428.
- Schieke, S., Schroeder, P. & Krutmann, J. (2003). Cutaneous effects of infrared radiation: from clinical observations to molecular response mechanisms. *Photodermatol Photoimmunol Photomed.*, 19, 228-234.
- Schlegel, A., Pestell, R. & Lisanti, M. (2000). Caveolins in cholesterol trafficking and signal transduction: implications for human disease. *Front Biosci.*, 5, 929-937.
- Schnitzer, J., McIntosh, D., Dvorak, A., Liu, J. & Oh, P. (1995). Separation of caveolae from associated microdomains of GPI-anchored proteins. *Science.*, 269, 1435-1439.

- Schuck, P. (2003). On the analysis of protein self-association by sedimentation velocity analytical ultracentrifugation. *Anal Biochem*, 320, 104-124.
- Schuck, S., Manninen, A., Honsho, M., Füllekrug, J. & Simons, K. (2004). Generation of single and double knockdowns in polarized epithelial cells by retrovirus-mediated RNA interference. *Proc Natl Acad Sci U S A.*, 101, 4912-4917.
- Sharma, D., Brown, J., Cheng, Z., Holicky, E., Marks, D. & Pagano, R. (2005). The Glycosphingolipid, Lactosylceramide, regulates  $\beta$ 1-Integrin clustering and endocytosis. *Cancer Research.*, 65, 8233-8241.
- Sharma, D., Brown, J., Choudhury, A., Peterson, T., Holicky, E., Marks, D., Simari, R., Parton, R. & Pagano, R. (2004). Selective Stimulation of Caveolar Endocytosis by Glycosphingolipids and Cholesterol. *Molecular Biology of the Cell.*, 15, 3114-3122.
- Sicheri, F. & Kuriyan, J. (1997). Structures of Src-family tyrosine kinases. *Curr Opin Struct Biol.*, 7, 777-785.
- Simons, K. & Ehehalt, R. (2002). Perspective: Cholesterol, lipid rafts, and disease. *J.Clin.Invest.*, 110, 597-603.
- Simons, K. & Ikonen, E. (1997). Functional rafts in cell membranes. *Nature.*, 387, 569-572.
- Simons, K. & Toomre, D. (2000). Lipid rafts and signal transduction. *Nat Rev Mol Cell Biol.*, 1, 31-39.
- Singer, S. & Nicolson, G. (1972). The fluid mosaic model of the structure of cell membranes. *Science.*, 175, 720-731.
- Smart, E., Graf, G., McNiven, M., Sessa, W., Engelman, J., Scherer, P., Okamoto, T. & Lisanti, M. (1999). Caveolins, liquid-ordered domains, and signal transduction. *Molecular and Cellular Biology.*, 19, 7289-7304.
- Smart, E., Ying, Y., Donzell, W. & Anderson, R. (1996). A role for caveolin in transport of cholesterol from endoplasmic reticulum to plasma membrane. *J Biol Chem.*, 271, 29427-29435.
- Smith, B., Colman, P., Von Itzstein, M., Danylec, B. & Varghese J. (2001). Analysis of inhibitor binding in influenza virus neuraminidase. *Protein Sci.*, 10, 689-696.
- Smith, P., Krohn, R., Hermanson, G., Mallia, A., Gartner, F., Provenzano, M., Fujimoto, E., Goeke, N., Olson, B. & Klenk, D. (1985). Measurement of protein using bicinchoninic acid. *Anal Biochem.*, 150, 76-85.
- Spiegel, S., Kassis, S., Wilchek, M. & Fishman, P. (1984). Direct visualization of redistribution and capping of fluorescent gangliosides on lymphocytes. *The Journal of Cell Biology.*, 99, 1575-1581.
- Stade, B., Messer, G., Riethmüller, G. & Johnson, J. (1990). Structural characteristics of the 5' region of the human ICAM-1 gene. *Immunobiology.*, 182, 79-87.

- Staunton, D., Marlin, S., Stratowa, C., Dustin, M. & Springer, T. (1988). Primary structure of ICAM-1 demonstrates interaction between members of the immunoglobulin and integrin supergene families. *Cell.*, 52, 925-933.
- Steinman, R., Mellman, I., Muller, W. & Cohn, Z. (1983). Endocytosis and the recycling of plasma membrane. *J Cell Biol.*, 96, 27.
- Subbaiah, P., Billington, S., Jost, B., Songer, J. & Lange, Y. (2003). Sphingomyelinase D, a novel probe for cellular sphingomyelin: effects on cholesterol homeostasis in human skin fibroblasts. *Journal of Lipid Research.*, 44, 1574-1580.
- Tebbe, B., Wu, S., Geilen, C., Eberle, J., Kodelja, V. & Orfanos, C. (1997). L-ascorbic acid inhibits UVA-induced lipid peroxidation and secretion of IL-1alpha and IL-6 in cultured human keratinocytes in vitro. *J Invest Dermatol.*, 108, 302-306.
- Thomas, S. & Brugge, J. (1997). Cellular functions regulated by Src family kinases. *Annual Review of Cell and Developmental Biology.*, 13, 513-609.
- Tjoelker, L., Seyfried, C., Eddy, R., Byers, M., Calderon, J., Schreiber, R. & Gray, P. (1994). Human, mouse, and rat calnexin cDNA cloning: identification of potential calcium binding motifs and gene localization to human chromosome 5. *Biochemistry.*, 33, 3229-3236.
- Tyrrell, R. (1995). Ultraviolet radiation and free radical damage to skin. *Biochem Soc Symp.*, 61, 47-53.
- Uchida, Y., Hara, M., Nishio, H., Sidransky, E., Inoue, S., Otsuka, F., Suzuki, A., Elias, P., Holleran, W. & Hamanaka, S. (2000). Epidermal sphingomyelins are precursors for selected stratum corneum ceramides. *Journal of Lipid Research.*, 41, 2071-2082.
- Ueno, S., Saito, S., Wada, T., Yamaguchi, K., Satoh, M., Arai, Y. & Miyagi, T. (2006). pPasma membrane-associated sialidase is up-regulated in renal cell carcinoma and promotes interleukin-6-induced apoptosis suppression and cell motility. *J.Biol.Chem.*, 281, 7756-7764.
- Usuki, S., Hoops, P. & Sweeley, C. (1988a). Growth control of human foreskin fibroblasts and inhibition of extracellular sialidase activity by 2-deoxy-2,3-dehydro-N- acetylneuraminic acid. *J Biol Chem.*, 263, 10595-10599.
- Usuki, S., Lyu, S. & Sweeley, C. (1988b). Sialidase activities of cultured human fibroblasts and the metabolism of GM3 ganglioside. *J Biol Chem.*, 263, 6847-6853.
- Valaperta, R., Chigorno, V., Basso, L., Prinetti, A., Bresciani, R., Preti, A., Miyagi, T. & Sonnino, S. (2006). Plasma membrane production of ceramide from ganglioside GM3 in human fibroblasts. *The FASEB Journal.*, 20, 1227-1229.
- Vielhaber, G., Grether-Beck, S., Koch, O., Johncock, W. & Krutmann, J. (2006). Sunscreens with an absorption maximum of > or =360 nm provide optimal protection against UVA1-induced expression of matrix metalloproteinase-1, interleukin-1, and interleukin-6 in human dermal fibroblasts. *Photochem Photobiol Sci.*, 5, 275-282.
- Volonte, D., Galbiati, F., Pestell, R. & Lisanti, M. P. (2001). Cellular stress induces the tyrosine phosphorylation of caveolin-1 (tyr14) via activation of p38 mitogen-activated protein kinase and c-src kinase. evidence for caveolae, the actin cytoskeleton, and focal adhesions as mechanical sensors of osmotic stress. *J.Biol.Chem.*, 276, 8094-8103.

- Wada, T., Hata, K., Yamaguchi, K., Shiozaki, K., Koseki, K., Moriya, S. & Miyagi, T. (2007). A crucial role of plasma membrane-associated sialidase in the survival of human cancer cells. *Oncogene.*, 2483-2490.
- Wada, T., Yoshikawa, Y., Tokuyama, S., Kuwabara, M., Akita, H. & Miyagi, T. (1999). Cloning, expression, and chromosomal mapping of a human ganglioside sialidase. *Biochem Biophys Res Commun.*, 261, 21-27.
- Wanaski, S., Ng, B. & Glaser, M. (2003). Caveolin-1 scaffolding region and the membrane binding region of SRC form lateral membrane domains. *Biochemistry.*, 42, 42-56.
- Wang, P., Zhang, J., Bian, H., Wu, P., Kuvelkar, R., Kung, T., Crawley, Y., Egan, R. & Billah, M. (2004). Induction of lysosomal and plasma membrane-bound sialidases in human T-cells via T-cell receptor. *Biochem J.*, 380, 425-433.
- Wang, X., Sun, P. & Paller, A. (2002a). Ganglioside induces caveolin-1 redistribution and interaction with the epidermal growth factor receptor. *J Biol Chem.*, 277, 47028-47034.
- Wang, Y., Satoh, A. & Warren, G. (2005). Mapping the functional domains of the Golgi stacking factor GRASP65. *J Biol Chem.*, 280, 4921-4928.
- Wang, Y., Yamaguchi, K., Wada, T., Hata, K., Zhao, X., Fujimoto, T. & Miyagi, T. (2002b). A close association of the ganglioside-specific sialidase Neu3 with caveolin in membrane microdomains. *J Biol Chem.*, 277, 26252-26259.
- Wanner, R., Peiser, M. & Wittig, B. (2004). Keratinocytes rapidly readjust ceramide-sphingomyelin homeostasis and contain a phosphatidylcholine-sphingomyelin transacylase. *J Invest Dermatol.*, 122, 773-782.
- Warren, L. (1959). The thiobarbituric acid assay of sialic acids. *J Biol Chem.*, 234, 1971-1975.
- Wertz, P. & Bergh, B. (1998). The physical, chemical and functional properties of lipids in the skin and other biological barriers. *Chemistry and Physics of Lipids.*, 91, 85-96.
- WHO (1994). Ultraviolet Radiation. *Environmental health Criteria 160*, <http://www.inchem.org/documents/ehc/ehc/ehc160.htm>.
- Wilkening, G., Linke, T., Uhlhorn-Dierks, G. & Sandhoff, K. (2000). Degradation of membrane-bound ganglioside GM1. Stimulation by bis(monoacylglycero)phosphate and the activator proteins SAP-B and GM2-AP. *J Biol Chem.*, 275, 35814-35419.
- Woods, J., Bethell, R., Coates, J., Healy, N., Hiscox, S., Pearson, B., Ryan, D., Ticehurst, J., Tilling, J. & Walcott, S. (1993). 4-Guanidino-2,4-dideoxy-2,3-dehydro-N-acetylneuraminic acid is a highly effective inhibitor both of the sialidase (neuraminidase) and of growth of a wide range of influenza A and B viruses in vitro. *Antimicrobial Agents and Chemotherapy.*, 37, 1473-1479.
- Woronowicz, A., Amith, S., De Vusser, K., Laroy, W., Contreras, R., Basta, S. & Szewczuk, M. (2007). Dependence of neurotrophic factor activation of Trk tyrosine kinase receptors on cellular sialidase. *Glycobiology.*, 17, 10-24.



- Yamaguchi K, Hata K, Wada T, Moriya S & Miyagi T. (2006). Epidermal growth factor-induced mobilization of a ganglioside-specific sialidase (NEU3) to membrane ruffles. *Biochem Biophys Res Commun.*, 346, 484-490.
- Yeh, L., Kinsey, A., Chatterjee, S. & Alevriadou, B. (2001). Lactosylceramide mediates shear-induced endothelial superoxide production and intercellular adhesion molecule-1 expression. *J Vasc Res.*, 38, 551-559.
- Young-Sun, L. & Gil-Ja, J. (1995). Studies on ganglioside GM3 and sialidase activity in human fetal liver. *J Biochem.Mol.Biol.*, 28, 432.
- Yu, C., Alterman, M. & Dobrowsky, R. (2005). Ceramide displaces cholesterol from lipid rafts and decreases the association of the cholesterol binding protein caveolin-1. *Journal of Lipid Research.*, 46, 1678-1691.
- Zanchetti, G., Colombi, P., Manzoni, M., Anastasia, L., Caimi, L., Borsani, G., Venerando, B., Tettamanti, G., Preti, A., Monti, E. & Bresciani, R. (2007). Sialidase NEU3 is a peripheral membrane protein localized on the cell surface and in endosomal structures. *Biochemical Journal.*, 408, 211-219.
- Zhao, Y., Liu, Y., Stan, R., Fan, L., Gu, Y., Dalton, N., Chu, P., Peterson, K., Ross, J. & Chien, K. (2002). Defects in caveolin-1 cause dilated cardiomyopathy and pulmonary hypertension in knockout mice. *Proceedings of the National Academy of Sciences of the United States of America.*, 99, 11375-11380.
- Zor, T. & Selinger, Z. (1996). Linearization of the Bradford protein assay increases its sensitivity: theoretical and experimental studies. *Anal Biochem.*, 236, 302-308.